ABSTRACT

STRUCTURAL AND PHASE INVESTIGATIONS

- I. CRYSTAL STRUCTURE OF LANTHANUM CARBONATE OCTAHYDRATE
- II. PHASE ANALYSES OF LANTHANIDE OXIDE FLUORIDES

by Dennis Burton Shinn

The crystal structure of lanthanum carbonate octahydrate $La_2(CO_3)_3 \cdot 8H_2O$, has been determined from an X-ray diffraction study of a single crystal specimen. Four formula units are contained in an orthorhombic unit cell (a = 8.984 \pm 0.004, b = 9.580 \pm 0.004, and c = 17.00 \pm 0.01 $\stackrel{\circ}{A}$). The space group is Pccn. The final R factor is 0.061 for three-dimensional counter data collected with CuK_{α} radiation (sin $\theta_{max} = 0.77$). La₂(CO₃)₃·8H₂O crystallizes in an irregular layer structure in which the basic layer is formed by alternate rows of carbonates and metals. Two distinctive 10-coordinate metal polyhedra occur in which coordination sites are occupied both by water molecules and by bidentate and unidentate carbonates. The symmetry of these polyhedra is similar to that of a dodecahedron except that bidentate carbonates occupy two of the normal ligand sites. One fourth of the water molecules are not bound to the metals and occupy holes between the layers. The average La-O(H2O) bond is 2.63 Å and the average La-O(CO₃) bond is 2.60 Å. Hydrogen bonding is apparent.

Lanthanide oxide fluorides, LnOF, have been studied with high temperature X-ray powder diffraction and differential thermal analysis techniques. They were found to

undergo reversible transitions from rhombohedral to cubic symmetry in the temperature range 495 to 608° . The enantiotropic transition occurred with a 0.7-1.0% increase in volume. Disordering of the oxygen and fluorine atoms apparently occurs as temperature is increased. At the transition point a displacive transformation of all atoms ensues. Neodymium oxide fluoride, NdOF, was observed to decompose at 1475° to the sesquioxide and the trifluoride which volatilized. Tetragonal phases $LnO_{1-x}F_{1+2x}$, $0.15 \lesssim x \lesssim 0.25$ and Ln = Nd, Gd, Dy and Er, were prepared by the reaction of the oxide and fluoride at 1050° . Unit cell parameters obtained for these phases range from $a = 3.999 \stackrel{O}{A}$ and c =5.704 Å for Nd(x = 0.25) to a = 3.907 Å and c = 5.385 Å for Er(x = 0.20). The tetragonal structure is a superlattice of fluorite in which the c/a ratio deviates from $\sqrt{2}$ according to the packing of the anions.

STRUCTURAL AND PHASE INVESTIGATIONS

- I. CRYSTAL STRUCTURE OF LANTHANUM CARBONATE OCTAHYDRADE
- II. PHASE ANALYSES OF LANTHANIDE OXIDE FLUORIDES

Ву

Dennis Burton Shinn

A THESIS

Submitted to
Michigan State University
in partial fulfillment of the requirements
for the degree of

DOCTOR OF PHILOSOPHY

Department of Chemistry

1968

649264

ACKNOWLEDGMENT

The author wishes to express his sincere thanks to Dr. Harry Eick for his encouragement and support throughout the pursuit of this work.

Appreciation is extended to Dr. Alexander Tulinsky for the use of equipment and his frequent advice.

The author is grateful to the E.I. duPont de Nemours
Company for a duPont Teaching Fellowship. Financial assistance from the Department of Chemistry and the United
States Atomic Energy Commission is also gratefully acknowledged.

TABLE OF CONTENTS

PART I	• CRYSTAL	STRUCT	URE C	F	LAI	TH	MUN	1 CA	RB	ONA	TE	OC	TA		DRATE age
I.	INTRODUCTI	on		•	•		•		•		•	•	•	•	1
II.	EXPERIMENT	AL		•			•		•		•	•	•	•	10
	Compositio			•			•		•			•	•		10
	Crystal Pr	operti	es .	•			•		•		•	•	•		11
	Unit Cell	and Sp	ace G	ro	up	Det	ern	nina	ti	on	•				13
	Lattice Pa	ramete	rs .				•								15
	Density an	d Mole	cules	P	er	Uni	it o	:e11	_		_	_	_	_	15
	Collection														16
	Absorption														19
	Computatio														22
	Computatio	ns	• •	•	•	•	•	• •	•	• •	•	•	•	•	22
III.	STRUCTURE	DETERM	ITANI	ON	•	• •	•		•	• •	•	•	•	•	24
	Patterson	Synthe	ses a	nd	Μe	ta1	Po	sit	io	ns	_				24
	Solution o														26
	Effect of													•	20
	the Stru													•	37
IV.	DESCRIPTIO	N OF T	HE ST	'RU	CTU	JR E			•		•	•	•	•	42
	Structure	as a W	hole												42
	Coordinati	on of	the M	· ·	• • • 1 e	•	• •	•	•	• •	•	•	•	•	49
	Carbonate														58
	Hydrogen B														59
	Observatio	ns Con	cerni	ng	Pr	evi	ous	In	ve	sti	gat	cic	ns	•	60
PART I	PHASE A	NALYSE	S OF	LΑ	NTH	IAN]	DE	OXI	DE	FL	UOF	RID	ES		
٧.	INTRODUCTI	on		•				•	•		•	•	•	•	62
	Literature														62
	Structures		 n+h nn	•	• •	•	· ·		•		•	•	•	•	66
	Purpose of	This	Resea	IC	n.	•	•	•	•	• •	•	•	•	•	72
VI.	EXPERIMENT	AL		•		•	•		•		•	•	•	•	73
	Preparatio	ns					•						•		73
	Analytical			•					•		•	•	•	•	74
	X-Ray Diff	ractio	n.						•						75
	High Tempe														75
	Differenti													_	80
	Thermal De											•	•	•	50
	Fluoride														82
	TILUUTIUE			•			• •		•		•	•	•	•	

TABLE OF CONTENTS (Cont.)

		Page
VII.	RESULTS	83
	Preparations and Phase Analyses	83
	Phase Transitions	85
	Decomposition of Neodymium Oxide Fluoride	95
VIII.	DISCUSSION	97
	The Phase Transition in Rhombohedral Oxide	
	Fluorides	97
	Observations on the Tetragonal Lanthanide Oxide Fluorides	104
IX.	SUGGESTIONS FOR FURTHER WORK	108
	REFERENCES	110
	APPENDICES	114
	I. Crystallographic Computer Programs	
	II. Diffraction Data for LnOF and LnOF	120

LIST OF TABLES

Table	I	?age
I.	Properties of space group No. 56, Pccn	14
II.	Positions of principal Patterson peaks	25
III.	Positions of the metal-metal Patterson peaks.	27
IV.	Parameters from least-squares refinement a) Atomic Coordinates	34 35
v.	Observed and calculated structure factors	36
VI.	Positional and thermal parameter changes due to absorption	41
VII.	Interatomic distances	46
VIII.	Bond angles	47
IX.	Corresponding reflections in LnOF phases	70
х.	Reported LnOF structural data	71
XI.	Analytical results	76
XII.	Structural data for tetragonal $LnO_{1-x}F_{1+2x}$.	8 6
XIII.	High Temperature X-ray diffraction data for LnOF	88
XIV.	NdOF high temperature structural data	89
xv.	Differential thermal analysis results	92
xvi.	X-Ray powder diffraction data for NdO.73F1.54	121
XVII.	X-Ray powder diffraction data for NdO $_{.85}F_{1.3}$	122
xvIII.	X-Ray powder diffraction data for GdO.72F1.5	123
xix.	X-Ray powder diffraction data for DyO.77F1.46	124
XX.	X-Ray powder diffraction data for ErO.85F1.3	125
XXI.	X-Ray powder diffraction data for ErO.80F1.4	126
XXII.	X-Ray powder diffraction data for LaOF and NdOF	127

LIST OF TABLES (Cont.)

Page						,	•		
128	EuOF	and	SmOF	for	data	diffraction	powder	X-Ray	xxIII.
129	TbOF	and	Gdof	for	data	diffraction	powder	X-Ray	xxiv.
130	YOF	and	DyOF	for	dat a	diffraction	powder	X-Ray	XXV.
131	ErOF	and	HoOF	for	data	diffraction	powder	X-Ray	xxvı.

LIST OF FIGURES

FIGURI	E		Page
1.	Crystal of $La_2(CO_3)_3 \cdot 8H_2O$	•	12
2.	Crystals of $La_2(CO_3)_3 \cdot 8H_2O$	•	12
3.	Representation of space group Pccn	•	14
4.	Stereoscopic illustration of $La_2(CO_3)_3 \cdot 8H_2O$ unit cell	•	43
5.	Stereoscopic illustration of $La_2(CO_3)_3 \cdot 8H_2O$ half cell	•	44
6.	Stereoscopic illustration of $La_2(CO_3)_3 \cdot 8H_2O$ half cell	•	44
7.	Stereoscopic illustrations of lanthanum coordination	•	45
8.	(a) Dodecahedraon, D_{2d} (b) Dodecahedral derivative, C_{2v}	•	54
9.	Lanthanide oxide fluoride structures		67
10.	Schematics of X-ray diffraction patterns of Er-O-F phases	•	84
11.	Thermal expansion of NdOF	•	90
12.	DTA curves for selected Gd-O-F stoichiometries		94

I. INTRODUCTION

Lanthanide carbonates have found limited application to date. One practical application is their use as starting materials for the preparation of water-soluble lanthanide complexes¹. The possibility of using the relative solubilities as a method of lanthanide separation has also been investigated². However, the carbonates have been studied frequently. Various methods of preparation, stoichiometries, thermal behavior, spectroscopy, X-ray diffraction and other miscellaneous properties have been reported. Unfortunately many of the results and their interpretations have been inconsistent, due in part to hydrolysis encountered in the preparation of pure materials in the pH range, 4.0-5.5, at which formation takes place. An equally important difficulty in the interpretation of results is the lack of knowledge of the various lanthanide carbonate crystal structures.

In order to demonstrate the inconsistencies of the reported results some of the pertinent recent investigations. will be reviewed. This review is not exhaustive; a more complete survey may be found in reference 3.

Lanthanide carbonates were once commonly prepared by carbonation of the hydroxide either with carbon dioxide or by addition of alkali carbonate to a solution of the metal salt saturated with CO₂. Unfortunately the products were often contaminated by alkali metals. Recently methods which

eliminate this problem have been developed. The most popular technique involves the hot hydrolysis of the lanthanide trichloroacetates first described by Salutsky and Quill4. The reaction is:

 $2 \text{Ln}(C_2 \text{Cl}_3 \text{O}_2)_3 + (3 + \underline{x}) \text{H}_2 \text{O} \rightarrow 3 \text{CO}_2 + 6 \text{CHCl}_3 + \text{Ln}_2 (\text{CO}_3)_3 \cdot \underline{x} \text{H}_2 \text{O}$ (1)

The stoichiometries of products obtained by this reaction vary from report to report. For lanthanum, neodymium and samarium, Salutsky and Quill reported $X \simeq 5.5$, 2.5 and 3.0 respectively. However, Charles⁵ suggested X = 8 for lanthanum and 2 for neodymium to holmium. Head and Holley⁶ reported the preparation of the carbonates of lanthanum to gadolinium under a pressure of CO_2 . With 200-300 psi the normal carbonates, Ln₂(CO₃)₃ ·XH₂O, were obtained where $X \simeq 8$ for La-Nd and 2-3 for Sm-Gd. With lower pressures a $\operatorname{Nd}_2(\operatorname{CO}_3)_3 \cdot 2\operatorname{H}_2\operatorname{O}$ was also obtained and at a CO_2 pressure of 1000 psi a $La_2(CO_3)_3 \cdot 6.4H_2O$ was found. In a later report⁷ they found $\underline{x} \simeq 2$ for terbium to ytterbium, and 5 for lutetium. Carbonate to metal ratios were less than 1.5 for preparations carried out in air. Strouth reported 3 or 4 waters for terbium, gadolinium and yttrium normal carbonates and 3-5 waters for the dysprosium to lutetium oxydicarbonates, $Ln_2O(CO_3)_2 \cdot XH_2O$, all prepared in air. Sastry, et al.⁸ have compared the products resulting from the older techniques with the trichloroacetate hydrolysis. In the latter technique the effect of using CO2-water or plain distilled water for washing was examined. Either

normal carbonate octahydrates or oxydicarbonate dihydrates were formed for praseodymium and neodymium depending on the method. Among the other methods of preparation is the reaction of warm, $45-60^{\circ}$, solutions of metal acetates with CO_2 at 900 psi reported by Head⁹. By this method the normal carbonates of La, Ce, Pr, Tb and Y were obtained with $\underline{X} \simeq 8$ for La-Pr and 2-3 for Y and Tb. To summarize, the reported stoichiometries may be divided into at least three general groups; $\operatorname{Ln}_2(CO_3)_3 \cdot \underline{X} \operatorname{H}_2O$ for La-Nd where $\underline{X} = 6-8$ but usually 8, $\operatorname{Ln}_2(CO_3)_3 \cdot \underline{X} \operatorname{H}_2O$ for Nd-Lu where $\underline{X} = 2-6$ but usually 2, and $\operatorname{Ln}_2O(CO_3)_2 \cdot \underline{X} \operatorname{H}_2O$ for Pr-Lu when the preparations are carried out with a limited source of CO_2 .

Nearly every investigator who has prepared a normal lanthanide carbonate has also studied its thermal decomposition. The reports of these investigations are in general agreement on two points: the first stage of decomposition is dehydration to the anhydrous carbonate and the second is decomposition with loss of carbon dioxide to form the lanthanide oxide. The existence and nature of any intermediate phases are matters of some disagreement. Consider the dehydration stage first. In thermogravimetric analyses(TGA) of La₂(CO₃)₃·8H₂O Charles⁵ observed inflections corresponding to the 6-, 3- and 2- hydrates. Pannetier, et al.¹⁰ observed no intermediates for this compound by TGA; however, in a differential thermal analysis (DTA) two endothermic peaks were observed which corresponded to dehydration. An

the first transition indicated it to be identical to the octahydrate whereas X-ray powder diffraction patterns of the completely anhydrous material were different. These authors believed the first DTA peak was due to adsorbed water, however, the peak seems too well defined for this type of reaction. Sastry, et al. claimed no inflections, corresponding to the formation of intermediate hydrates, occurred in the TGA curves of $Pr_2(CO_3)_3 \cdot 8H_2O$ and $Nd_2(CO_3)_3 \cdot 8H_2O$ in air or CO_2 . However, obvious inflections corresponding to the hexa-, diand mono-hydrate are observable in their reported praseodymium TGA curves. Head and Holley found no evidence of intermediate hydrates in the cases of La, Ce or Pr but did observe $Nd_2(CO_3)_3 \cdot 2H_2O$. Caro¹¹ has also observed this Nd phase.

Reports of intermediate phases occurring in the decomposition of the anhydrous carbonates are somewhat more consistent. Charles reported inflections in TGA curves corresponding to the dioxycarbonate, $\operatorname{Ln_2O_2CO_3}$, for La-Gd which were undetectable for Tb-Ho. Head and Holley^{6,7} also found the same approximate phase in thermal analyses of La, Pr-Yb carbonates under $\operatorname{CO_2}$ atmospheres. Another intermediate containing less carbonate was observed in the decompositions of the carbonates of Nd-Gd. The dioxycarbonate phase has also been reported by Sastry, et al.⁸ for the Nd case and by Pannetier, et al.¹⁰ in their DTA and TGA studies of $\operatorname{La}(\operatorname{CO_3})_3\cdot 8\operatorname{H_2O}$. Strouth³ observed oxydicarbonates and dioxycarbonates in the DTA of Y, Gd and Tb carbonates. Caro¹¹ observed the dioxycarbonate of Nd. In summary, from the

thermal decomposition of $\operatorname{Ln_2(CO_3)_3 \cdot XH_2O}$, evidence of intermediate hydrates is mixed and whereas $\operatorname{Ln_2O_2CO_3}$ is generally found in the decomposition other phases have also been observed.

The infrared spectra of the lanthanide carbonates have been reported^{3,5,8,11,12} but not interpreted in complete detail. Charles 5 commented that the spectra of $\operatorname{Ln_2(CO_3)_3 \cdot 2H_2O}$, Ln = Nd-Ho, differ significantly from that of Ln=La. He assigned absorptions at 3400 and 1650 cm⁻¹ to bound water molecules and stated that other observed absorptions may be due to coordinated water and various vibrational modes of the carbonate ions. Sastry, et al.⁸ noted that two CO stretching and two in-plane CO3 deformation bands are present in the spectra of the Pr, Nd and Tb carbonate hydrates and oxydicarbonate hydrates. They pointed out that such splitting occurs in basic carbonates and in compounds where the carbonate ion is a bidentate or unidentate ligand. suggested the C-O stretch splitting is similar to that of unidentate carbonates, but did not make an assertion of its existence. Caro¹¹ has attempted a more detailed analysis of the infrared spectra of the various carbonate phases. He believed the CO_3 vibrational spectrum in $Ln_2(CO_3)_3 \cdot 8H_2O$ is nearly identical to that in cobalt carbonate complexes such as $[Co(NH_3)_5CO_3]Br.^{13}$ This observation would indicate CO_3 is a unidentate ligand bonded to the lanthanide ion. Surprisingly, he postulated octahedral coordination of the metals by four water molecules, a unidentate carbonate and

another carbonate bonded to two metals. Caro found the spectrum of $\operatorname{Ln_2}(\operatorname{CO_3})_3 \cdot 2\operatorname{H_2O}$ more complex than that of the octahydrate and postulated the carbonates are in two types of sites. In summary, the interpretations of the infrared spectra of the normal carbonates are either vague or of doubtful value. Further analyses would seem to require crystal structure information.

Other spectroscopic studies have been made of the lanthanide carbonates. Barnes and $Pincott^{14}$ examined the electron transfer spectra of $Ln_2(CO_3)_3 \cdot 3H_2O$ and other salts, where Ln=La, Sm, Eu, and Yb. Lanthanum shows no electron transfer bands and was used to check against false assignment. The spectra were observed to be similar to those of other oxyanion salts of the lanthanides.

Brasseur¹⁵ has postulated on the relative orientation of the carbonate ions in various carbonates from the optical properties of the crystals. For $(La, Di, Ce)_2(CO_3)_3 \cdot 8H_2O$ he concluded that all the carbonates had parallel orientations on the basis of a comparison of calculated and observed indices of refraction.

No structure of any lanthanide carbonate phase has been determined by single crystal X-ray diffraction. With one exception 10 the X-ray powder diffraction photographs of $\operatorname{Ln}_2(\operatorname{CO}_3)_3 \cdot \operatorname{\underline{XH}}_2\operatorname{O}$ have been indexed by analogy to the unit cell observed in naturally occurring lanthanite, $(\operatorname{La}, \operatorname{Ce})_2(\operatorname{CO}_3)_3 \cdot \operatorname{BH}_2\operatorname{O}$. The studies of lanthanite crystals are summarized in "Dana's System of Mineralogy" 16 . From optical crystallography

these crystals were determined to have orthorhombic symmetry. dipyramidal -2/m 2/m. The parameters a = 9.50, b = 17.1 and c = 9.00Å were obtained by an unreported method. The unit cell contains four formula units but the space group was not determined. Sastry, et al. * reported similar lattice parameters from powder data for Ln₂(CO₃)₃·8H₂O of Pr and Nd. Caro¹¹ reports analogous results for Pr except that the b parameter is about one half the previous value. On this basis Strouth³ indexed X-ray powder diffraction patterns of $Ln_2(CO_3)_3 \cdot XH_2O$ of Tb, Gd and Y where X is 3, 4 and 3 respectively. However, only the first 9-12 lines of relatively complex powder patterns were indexed and the hk & values obtained are somewhat curious in that many common low index lines were not observed. Pannetier, et al. 10 indexed $La_2(CO_3)_3 \cdot 8H_2O$ on the basis of an orthorhombic unit cell in which a = 8.56, b = 5.78 and c = 8.89 and suggested a P222₁ space group from powder data. Although they gave no data, Head and Holley⁶, ⁷ reported on the basis of X-ray powder diffraction that the $Ln_2(CO_3)_3 \cdot 8H_2O$ for La-Nd are isomorphous but different from the lower hydrates of Nd-Yb and Y which are also isomorphous. $Lu_2(CO_3)_3 \cdot 5H_2O$ appeared to have a third structure. The powder pattern of lanthanum dioxycarbonate has been indexed by Pannetier, et al. 10 as hexagonal, a = 7.76 and c = 9.47 Å. In summary the compounds of the general formula Ln₂(CO₃)₃·8H₂O appear to crystallize with orthorhombic symmetry similar to that observed in lanthanite; for which the structure is unknown, and the lower hydrates

and the oxycarbonates have different but also unknown structures.

The intent of the preceding historical survey was to indicate the need for the determination of lanthanide carbonate structures. A complete structure analysis of the various carbonates should allow the interpretation of the following experimental observations.

- 1. The normal carbonates, $\operatorname{Ln_2}(\operatorname{CO_3})_3 \cdot \operatorname{\underline{X}H_2O}$, appear to be classified into at least two different groups on the basis of stoichiometry. Within each group a modest range of water content is possible without changing the general structure, at least as observed by powder X-ray diffraction. The observed stoichiometries are undoubtedly a reflection of the trend in metal ion size and the ability of the metals to accommodate ligands of various sizes. It is to be expected that the lighter lanthanides will have the maximum coordination numbers for a specific ligand. The observed change in stoichiometries from $\operatorname{Ln_2}(\operatorname{CO_3})_3 \cdot \operatorname{8H_2O}$ for La-Nd to $\operatorname{Ln_2}(\operatorname{CO_3})_3 \cdot (2-3)_{\operatorname{H_2O}}$ may result from one of two structural differences:
 - a. The coordination number of the metal is high 9-12, for the lighter members and is less for the heavier (and smaller) metal ions. This decrease in coordination number might be accomplished by removing water molecules from the coordination sphere, decreasing the water content.

- b) The coordination number may remain unchanged if the effective size of the ligands is decreased. This could occur if a carbonate were to act as a bidentate or tridentate ligand replacing two or more water molecules in the coordination sphere of the metal.
- 2. In the thermal decomposition of $\operatorname{Ln_2}(\operatorname{CO_3})_3 \cdot 8\operatorname{H_2O}$ the evidence for the presence of intermediate hydrates is contradictory. In one instance at least X-ray powder diffraction photographs of a suspected intermediate were identical to those of the octahydrate. Knowledge of the way the water molecules are bound in the crystal should explain these observations. The course of decomposition should also be explicable on the basis of structural changes.
- 3. The infrared spectra of the carbonates are very complex. Without knowledge of the nature of the bonding of the carbonate to the metals and the coordination of the metals there appears to be little hope of properly interpreting absorption spectra.

In view of the indicated usefulness of a structural examination of the lanthanide carbonates it was fortunate that $\operatorname{Ln_2}(\operatorname{CO_3})_3.\underline{X}\operatorname{H_2O}$ crystals of La, Pr and Nd were available in this laboratory. In this study the structure of $\operatorname{La_2}(\operatorname{CO_3})_3.8\operatorname{H_2O}$ has been determined by single crystal X-ray diffraction. The results of this structural determination should aid in the interpretation of lanthanide carbonate chemistry.

II. EXPERIMENTAL

Crystals of lanthanum carbonate hydrate, La₂(CO₃)₃·XH₂O and Pr₂(CO₃)₃·XH₂O were obtained from Prof. L. L. Quill of this department. They had been prepared according to equation (1) by slow hydrolysis of lanthanide trichloroacetate solutions at room temperature. Crystallization of the precipitated carbonates had been allowed to continue undisturbed for several years. The crystals, still in the reaction media when they were obtained for this investigation, were filtered, washed repeatedly first with distilled water and finally with acetone. Those specimens which were to be used for X-ray diffraction intensity measurements were coated quickly with Canada balsam in an effort to minimize possible dehydration. Other crystals were air-dried 1-2 hours, and then stored in capped vials.

Composition

Lanthanum carbonate hydrate was analyzed for carbon and hydrogen by Spang Microanalytical Laboratory, Ann Arbor, Michigan. Metal content was determined by ignition of airdried samples in platinum boats at approximately 900° . Anal. Calculated for La₂(CO₃)₃·8H₂O: La, 46.15; C, 5.98; H, 2.69. Found: La, 46.32±0.10; C, 6.0±0.1; H, 2.7±0.1. Errors listed are the standard deviation of four metal determinations and the probable error of duplicate carbon and hydrogen analyses.

The observed analytical results support the formation of the octahydrate reported^{5,6,9,10} and not the hexahydrate⁴. The apparent high lanthanum content may suggest a small impurity of another lanthanide. Ignition of a sample exposed to the atmosphere for approximately two weeks indicated an increase in the lanthanum content to 46.49%. If the experimental increase in metal percentage is assumed to result from a decrease in the water content of $\text{La}_2(\text{CO}_3)_3 \cdot 8\text{H}_2\text{O}$, the stoichiometry is $\text{La}_2(\text{CO}_3)_3 \cdot 7.9\text{H}_2\text{O}$. Thus although the stoichiometry will be referred to as octahydrate, the water content in individual samples may vary below this value.

Crystal Properties

Crystals of La₂(CO₃)₃·8H₂O and Pr₂(CO₃)₃·8H₂O were examined with a Spencer AO polarizing microscope and with a Bausch and Lomb Dynazoom metallograph to aid in the selection of an orientation for structure analysis. As Figures 1 and 2 indicate, the lanthanum crystals were observed to be colorless and transparent. Although the large faces appear rectangular, the face angles are 86.0±0.5° and 94.0±0.5°. Observation of these crystals under crossed polarizers indicated extinction directions coincident with the diagonals of the large face and with the face normal. These directions correspond to the observed crystallographic axes a, b and c. Cleavage was observed to be micaceous along (001). Attempts to cleave along planes normal to (001) led to complete disintegration of the crystal.

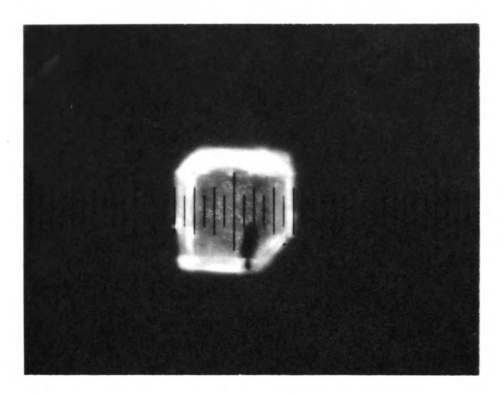


Figure 1. Crystal of La₂(CO₃)₃·8H₂O.



Figure 2. Crystals of $La_2(CO_3)_3 \cdot 8H_2O$.

Unit Cell and Space Group Determination

Preliminary Weissenberg photographs established the orthorhombic symmetry. Precession photographs of the hkO and Okl levels confirmed this. Weissenberg photographs were made with a Charles Supper Co. camera mounted on a North American Philips X-ray generator. Exposures, using copper radiation (45 kilovolts and 20 milliamperes) with a nickel filter, were taken for two crystal orientations. Exposure times varied from 8 to 72 hours. Reflections were present for the following conditions.

hoo, Oko, Oo ℓ only when h, k, ℓ = 2n Ok ℓ , ho ℓ only when ℓ = 2n hko only when h + k = 2n with no regular extinctions.

These conditions are satisfied unambiguously by space group $P2_1/c$ $2_1/c$ 2/n (No. 56) which will be referred to as Pccn. In addition to the above restrictions it was noted that hk ℓ reflections with $\ell=2n+1$ were in general very weak or absent. Ignoring the weak reflections would lead to assignment of the space group Pmmn (No. 59). Weissenberg photographs of $Pr_2(CO_3)_3 \cdot 8H_2O$ indicated it to be isomorphous with the lanthanum compound. The conditions governing possible reflections and coordinates of equivalent positions for the general and special position sets of Pccn are found in Table I. Schematics of the symmetry of the space group are illustrated in Figure 3.

Table I. Properties of space group No. 56, (Pccn).

	Point Symmetry	Co-ordinates of Equivalent Positions	Conditions for Non-extinction
8e	1	$\pm (x,y,z; 1/2-x,1/2-y,z;$ $1/2+x,\overline{y},1/2-z;$ $\overline{x},1/2+y,1/2-z)$	hk ℓ : no cond. Ok ℓ , hO ℓ : ℓ =2n hkO: h+k = 2n hOO,OkO,OO ℓ : (h,k, ℓ = 2n)
4 d	2	$\pm (1/4,3/4,z; 1/4,3/4,1/2+z)$	as for 8e, plus
4 c	2	$\pm (1/4,1/4,z; 1/4,1/4,1/2+z)$	$hk \ell : \ell = 2n$
4 b	ī	0,0,1/2; 1/2,1/2,1/2; 0,1/2,0; 1/2,0,0	as for 8e, plus $hk\ell: h+k, k+\ell,$
4a	ī	$\left.\begin{array}{c} 0,0,0;\ 1/2,1/2,0;\\ 0,1/2,1/2;\ 1/2,0,1/2 \end{array}\right\}$	$(h+\ell) = 2n$

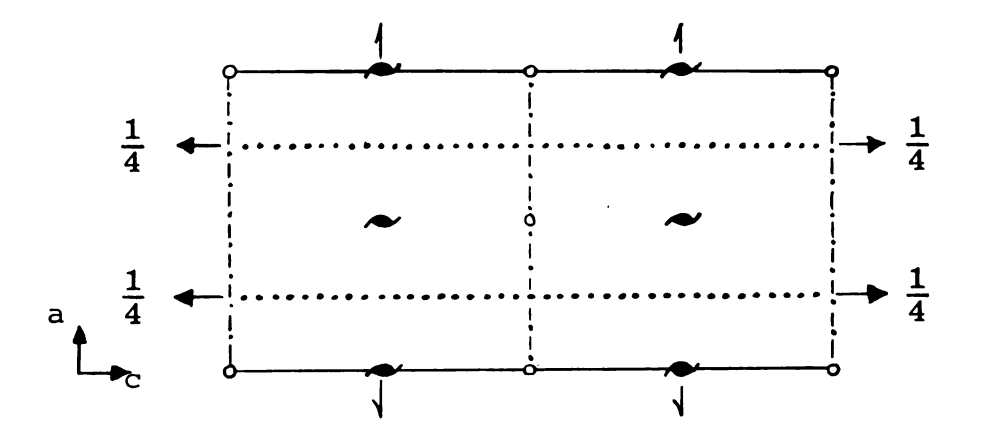


Figure 3. Representation of space group Pccn.

Lattice Parameters

Lattice parameters of lanthanum carbonate octahydrate were determined from calibrated X-ray powder diffraction data. The crystals were ground, mixed with potassium bromide powder (Baker Analyzed Reagent, 99.4% KBr) and applied to a glass plate in a thin layer using Canada balsam as binder. Diffraction patterns were obtained for this sample with a Siemens diffractometer mounted on a Siemens Crystalloflex IV X-ray generator using copper radiation (35 kilovolts and 20 milliamperes), nickel filter, proportional counter and one-eithth degree per minute scan. The resulting diffraction patterns were calibrated by comparing the observed positions of potassium bromide peaks with those calculated on the basis of a KBr lattice parameter, 17 a = 6.5966 Å. In the 2θ range utilized, $0-65^{\circ}$, the maximum correction was 0.010. The carbonate lattice parameters were calculated from twenty-one reflections which could be indexed unambiquously using a least squares program written by Vogel and Kempter 18. The refined parameters, expressed on the basis of space group Pccn, are: $a = 8.984 \pm 0.004 \text{ Å}$, $b = 9.580 \pm 0.004 \text{ Å}$, and $c = 17.00 \pm 0.01 \text{ Å}$. For the space group Pmmn, $c = 8.50 \pm 0.005 \text{ A}$.

Density and Molecules Per Unit Cell

The density of $\text{La}_2(\text{CO}_3)_3 \cdot 8\text{H}_2\text{O}$ was derived by the pycnometric method with water as a medium. At 26^0 a value 2.72 ± 0.01 g/cm³ was obtained. Based on the lattice

parameters observed for space group Pccn and a stoichiometry $La_2(CO_3)_3 \cdot 8H_2O$, this density corresponds to four molecules per unit cell. Under these conditions the theoretical density is 2.73 g/cm^3 .

Collection of Intensity Data

Two sets of intensity data were collected with copper radiation ($\lambda_{\overline{\Omega}}$ = 1.5418 $\overset{O}{A}$) on separate crystals using film and counter techniques, respectively.

The preliminary set of data was obtained on a crystal with (001) face dimensions $0.167 \text{ mm} \times 0.150 \text{ mm}$ and thickness 0.055 mm. The crystal was mounted on a glass fiber and aligned with the b-axis as the axis of rotation. X-Ray alignment was accomplished with oscillation photographs of the zero-layer line. Equi-inclination Weissenberg photos were taken of the hK ℓ levels, K = 0 - 6. Intensities were collected by the multiple film technique. Film packs, composed of three or four sheets of Ilford Industrial type G X-ray film, were exposed for 60 hours at 40 kilovolts and 20 milliamperes, Intensities were estimated visually by comparison with a calibrated intensity strip, prepared using the (202) reflection of the crystal under investigation. The intensities of each layer were then correlated and scaled to those of the most heavily exposed film in the pack. On the average the inter-film correlation factor was about 2.6. The values for each reflection were averaged and scaled linearly according to the time of exposure. A total of 705 non-equivalent reflections were measured.

The set of intensities used in the final refinement of parameters was measured with a General Electric XRD-5 goniostat equipped with scintillation counter. A crystal of approximate dimensions 0.160 x 0.152 x 0.110 mm, Figure 1. was mounted on a glass fiber. The b-axis of the crystal was aligned parallel, visually and by X-ray, with the qoniometer ϕ -axis. X-Ray alignment was accomplished at a 20 take-off angle by maximizing intensity of the (040) reflection. At $\chi = 90.0^{\circ}$ the two arcs of the goniometer, set parallel to the X-ray beam, were adjusted to produce maximum equal intensities at $\phi = 0^{\circ}$ and 180° and $\phi = 90^{\circ}$ and 270° The value of 2θ was also maximized. The ϕ settings corresponding to (h00) and (00 ℓ) reflections were determined by maximizing ϕ and 2θ at χ = 0° for the (400) and (008) reflections. The values of 2θ of the (h00), (Ok0), and (OO ℓ) reflections, h, k, $\ell = 4$, 6 and 8 were measured carefully. From these values the following lattice parameters were calculated: a = 8.976 Å, b = 9.563 Å, c = 17.00 Å. These parameters were used for the generation of χ , ϕ and 2θ values for other reflections.

The quality of the crystal was examined both as an aid in the selection of the best quadrant for data collection and as insurance that integrated intensities would be obtained. At χ = 0° the (400), ($\overline{4}$ 00), (008) and (00 $\overline{8}$) reflection intensities were counted versus ϕ at 0.04° intervals. At χ = 90° the (040) reflection intensity was measured as a function of ω at 0.04° intervals. Four scans were

made with the direct beam normal to [100], $[\overline{100}]$, [001] and $[00\overline{1}]$. The eight scans obtained were plotted and the quadrant to be used in data collection was chosen on the basis of the symmetry and narrow peak width of the plots.

The settings of χ , ϕ and $2\theta (0 \leq 2\theta \leq 100^{\circ})$ were generated using a program written by J. Gvildys, Argonne National Laboratory. Intensities of 749 independent reflections were measured with stationary-crystal, stationary-counter tech-These measurements were made with a 40 take-off angle. The χ , ϕ and 2θ values were set and the reflection was counted for 10 seconds with a nickel filter. The background was measured by replacing the Ni filter with a balanced Co filter and counting for 10 seconds. In principle the absorption of the Co and Ni filters matches at all wavelengths other than those which lie between the two absorption edges (1.608 A for Co and 1.488 A for Ni). If intensity measurements are made properly with each filter, the intensity difference between the two measurements results only from radiation whose wave length is within the narrow band between the absorption edges. In the case in question, this is principally $\operatorname{CuK}_{_{\operatorname{CY}}}$ radiation. Therefore the difference in count was recorded as the intensity of the reflection. Intensities of 116 reflections were recorded as zero, of these 108 had ℓ = 2n + 1. Similarly 94 of 125 reflections with intensities less than 2 had $\ell = 2n + 1$. The maximum intensity observed was 1547 cps for (002). Only 5 reflections with $\ell = 2n + 1$ produced intensities of greater than 30 cps

whereas for 29 reflections with ℓ = 2n the count was above 300 cps.

During collection of the data the alignment of the crystal was checked periodically by measuring the intensities of the (040), (060), (400), (600) and (008) reflections. These intensities were checked ten times during the data collection procedure, and no significant deviations were observed during the period of data collection; 13 hours of exposure at 40 kilovolts and 40 milliamperes over a 100 hour period.

Absorption Correction

The linear absorption coefficient, μ, for La₂(CO₃)₃·8H₂O is 444 cm⁻¹. This value was calculated from tabulated mass absorption coefficients and the experimental density. The crystals employed in the collection of intensity data were relatively large. In the case of the crystal used on the goniostat it was estimated that the path length of diffracted radiation through the crystal could differ as much as 0.004 cm for the two reflections. Use of this difference in conjunction with the intensity-absorption equation indicates that corrections as high as 5X would be required to put all intensities on the same relative scale. An approximate method for absorption correction was not used for two reasons: 1) the complicated external form of the crystal and 2) the magnitude of the corrections involved. Thus, the FORTRAN absorption correction program written by Coppens,

Leiserowitz and Rabinovich 19 was used to effect the corrections. The program is a modification of one written by Busing and Levy²⁰. The calculation involves evaluation by the method of Gauss of the integral: correction = $\int 1/V \exp[-\mu(r_i + r_d)] dV$, where $V = \text{crystal volume and } r_i$ and r_d are the path lengths of incident and diffracted radiation, respectively. In Coppens, Leiserowitz and Rabinovich's program an axial system dependent on both diffraction geometry and crystal orientation is established within the crystal. The volume of the crystal is determined and a grid of sampling points is constructed within it using distances measured from an internal origin to the crystal boundary planes. The incident and diffracted radiation path lengths between the crystal faces and each sampling point are then calculated for every reflection of interest. An absorption factor is calculated for each sampling point and the total absorption is computed as a weighted average over all sampling points.

The diffractometric intensities were corrected using the following data:

- a) orientation b-axis coincident with Φ-axis
- b) number Gaussian points 1440 (12, 12, 10 along
 a, b, c)
- c) number boundary planes 8.

distance from	estimated
chosen origin	possible error
(cm)	(cm)
.0058	.0003
.0058	.0003
.0080	.0002
.0088	.0002
.0076	.0002
.0076	.0002
.'p079	.0002
.0079	.0002
	chosen origin (cm) .0058 .0058 .0080 .0088 .0076 .0076

d) Linear absorption coefficient, $\mu = 444$ cm⁻¹

The correction factors varied from a maximum value of 64.1, for (002), to a minimum value of 12.0, for (14, 15). In general the correction factor decreased in a zone of reflections as the Miller indices increased. Based on a limiting stoichiometry $La_2(CO_3)_3 \cdot 7.5H_2O$ and a corresponding density, $d = 2.75 \text{ g/cm}^3$, the uncertainty in the absorption coefficient was estimated as 11 cm⁻¹. For the limiting value of $\mu = 456 \text{ cm}^{-1}$ it was found that relative intensities differed from those calculated with μ = 444 cm⁻¹, by less than 3%. On the other hand, the effect on the absorption coefficient resulting from an uncertainty in the crystal dimensions is more significant. For instance, an alteration of the dimensions of the $\{001\}$ faces by -0.0003cm and the other faces by +0.0002 cm introduced relative intensity differences of as much as 8%. In addition, a number of less prominent crystal faces (e.g. {112}) were not included in the description of the crystal on the assumption that the effect of their inclusion should be small. The validity of the absorption correction calculation was verified by comparison of experimentally determined and

and calculated absorption effects on (OkO) reflections. Intensities of reflections measured at χ = 90°, (OkO) reflections, have a ϕ -dependence which is a function of absorption only. Over a 90° range in ϕ , absorption decreased the intensity of the (040) and (080) reflections by factors of 0.51 and 0.47 respectively. The corresponding factors derived from the correction program were 0.47 and 0.45. However, even though the effect of absorption has been reduced significantly it still introduces a great limitation on the final results.

Computations

Calculations were performed on a CDC 3600 computer equipped with 64K memory. The programs for the least-squares calculation of lattice parameters, for generation of diffractometer settings, and for absorption correction have been mentioned previously. The programs used for intensity data reduction, Fourier functions, and distance and angle calculations were obtained from A. H. Zalkin who wrote them. The first of these programs is described in Appendix I. The full matrix least-squares program is a version of the Sparks, Gantzell and Trueblood program (ACA no. 317) as modified by Zalkin. This program is also described in Appendix I. The function minimized was $\Sigma W(|F_0| - |F_C|)^2$ where W is the weighting and $|F_0|$ and $|F_C|$ are respectively observed and calculated structure factors. Scattering factors used were those computed by Cromer and Waber²¹ for La³⁺

and carbon and that computed by Tokonami²² for 0^{2-} , the scattering factor for La³⁺ was corrected for anomalous dispersion in the final stages of least-squares refinement. The corrections, used, $\Delta f' = -2.10$ and $\Delta f'' = 8.90$, were those given by Cromer²³.

The stereo drawings of the structure were made using a CDC 6600 digital computer and a cathode ray plotter with a program written by A. C. Larson.

III. STRUCTURE DETERMINATION

Patterson Syntheses and Metal Positions

A three-dimensional Patterson function was calculated from film intensity data which had been corrected for Lorentz; polarization and velocity effects, but not for absorption. The positions and relative peak heights of the larger Patterson peaks observed are given in Table II. The corresponding peaks obtained from absorption corrected diffractometric data are also found in the table.

The locations of the eight lanthanum atoms in the unit cell were determined in the following manner. According to the notation of Table I, the possible lanthanum positions include: 8 La in Wyckoff set 8e, or 4 La in set 4a, 4b, 4c, or 4d and 4 additional La in a non-identical set 4a, 4b, 4c, or 4d. Use of the eight-fold positions was eliminated as incompatible with the Patterson results. Furthermore the low intensity of reflections for which $\ell = 2n + 1$ indicated that the metals were situated in one of the combinations of four-fold sets 4c-4c, 4d-4d, or 4c-4d. In these sets the only variable parameter is z. Analysis of the Patterson excluded the placement of all the lanthanum atoms in either of the sets 4c or 4d. Such a situation would result in the appearance of nine Patterson peaks along [OOz] -- only a peak at 0, 0, 1/2 is observed. Therefore four lanthanum atoms must be in each of the sets 4c and 4d:

Table II. Positions and heights of principal Patterson peaks

x	У	z	Relative Height *	Relative Height **
0.00	0.00	0.000	999	999
0.00	0.00	0.500	935	926
0.00	0.50	0.465	450	483
0.00	0.50	0.535	450	483
0.00	0.50	0.965	425	460
0.00	0.50	0.035	425	460
0.50	0.00	0.465	422	458
0.50	0.50	0.000	422	439
0.50	0.00	0.965	418	462
0.50	0.00	0.035	418	462
0.50	0.50	0.500	413	443
0.50	0.50	0.425	206	270
0.50	0.50	0.575	206	270
0.50	0.50	0.930	198	268
.50	0.50	0.070	198	268
0.06	0.25	0.500	41	26
0.00	0.00	0.250	41	108
0.00	0.00	0.750	41	108
0.02	0.00	0.935	_	154
0.02	0.00	0.435	_	142
0.12	0.00	0.985	_	138
0.12	0.00	0.485	_	136
0.48	0.50	0.630	_	120
0.48	0.50	0.130	_	112
.50	0.50	0.375	_	110
0.06	0.25	0.000	34	23
.22	0.25	0.000	28	26
0.50	0.00	0.870	2 5	95
0.50	0.00	0.130	2 5	95
.22	0.25	0.500	2 5	24
0.02	0.50	0.395	_	108
0.48	0.00	0.100	_	107
0.50	0.50	0.875	_	103
0.02	0.50	0.895	_	102
0.02	0.50	0.360	15	101
0.48	0.00	0.600	-	101

^{*} From diffractometer data corrected for absorption.

^{**} From film data uncorrected for absorption.

4c
$$\pm$$
 (1/4,1/4,z), \pm (1/4,1/4,1/2 + z)
4d \pm (1/4,3/4,z'), \pm (1/4,3/4,1/2 + z')

In order to determine the z-parameters in the two sets all the inter-atom vectors were calculated and the number of identical vectors summed. These data are tabulated in Table III. A comparison with the observed Patterson peaks disclosed two possible solutions:

Solution 1:
$$z = 0.000$$
, $z' = 0.033$
Solution 2: $z = 0.250$, $z' = 0.283$.

Originally only solution 1 was recognized. This oversight severely delayed the final solution of the structure. The full sets of coordinates for the two solutions are:

Solution 1: La(1) at
$$\pm(1/4,1/4,0)$$
, $\pm(1/4,1/4,1/2)$ and La(2) at $\pm(1/4,3/4,0.033)$, $\pm(1/4,3/4,0.533)$.

Solution 2: La(1) at
$$\pm(1/4,1/4,1/4)$$
, $\pm(1/4,1/4,3/4)$ and La(2) at $\pm(1/4,3/4,0.283)$, $\pm(1/4,3/4,0.783)$.

Solution of the Light Atom Structure

The heavy atom method was used to solve the light atom structure. In this method it is assumed that the atoms with predominant scattering factors, the lanthanum atoms in this case, will determine the phase of most structure factors. These phases may then be used to give a Fourier synthesis which is a close approximation of the actual structure. In the case of $\text{La}_2(\text{CO}_3)_3 \cdot 8\text{H}_2\text{O}$ the structure factor of a particular reflection may be written as:

Table III. Positions of the metal - metal Patterson peaks

Peak Positions- Unknown z Parameters	Wts ^b	Peak Positions- Known z Parameters	Wts	Relative Peak Heights	Relative Peak Height s
0,0,0	8	0,0,0	8	999	999
0,0,1/2	8	0,0,1/2	8	926	935
0,1/2,±(z - z')	4	$0,1/2,\pm v$	4	460	425
$1/2,0,\pm(z + z')$	4	$1/2$,0, $\pm v$	4	462	418
0,1/2,1/2±(z - z')	4	$0,1/2,1/2,\pm v$	4	483	450
1/2,0,1/2±(z + z')	4	$1/2$,0, $1/2 \pm v$	4	458	422
$1/2$, $1/2$, $\pm 2z$	2	1/2,1/2,0	4	439	422
$1/2$, $1/2$, $1/2 \pm 2z$	2	1/2,1/2,1/2	4	443	413
$1/2$, $1/2$, $\pm 2z$ '	2	1/2,1/2±2v	2	268	198
$1/2$, $1/2$, $1/2\pm 2z$ '	2	1/2,1/2,1/2,±2v	2	270	206

^aOne metal in each equivalent position of the Wyckoff sets 4c and 4d.

bweights equal the number of identical interatom vectors.

 $^{^{}C}v = z - z' = 0.033.$

 $^{^{\}rm d}$ From film data.

eFrom diffractometer data.

$$F(hkl) = \sum_{La=1}^{8} f_{La} \exp[2\pi i (hx_{La} + ky_{La} + \ell z_{La})]$$
$$+ \sum_{n} f_{n} \exp[2\pi i (hx_{n} + ky_{n} + \ell z_{n})]$$

where f_{La} and f_{n} are the scattering factors of lanthanum and the light atoms respectively and x, y, and z are the fractional coordinates of the respective atoms in the unit cell. Since f_{La} is much greater than any f_n , the magnitude of the first term will be much greater than that of the second for values of $hk \ell$ in which $\ell = 2n$, but the first term will vanish for values of $hk \ell$ in which ℓ = 2n + 1 because of the special positions of the metals. Lipson and Cochran²⁴ point out that if the scattering factor of the heavy atom is too large the Fourier synthesis will tend to show only this atom and the lighter atom positions will be very inaccurate. The best results are obtained if $\sum f_{La}^2 = \sum_n f_n^2$. But for $La_2(CO_3)_3 \cdot H_2O$: $2f_{La}^2 = 6498$ and $\sum_{n} f_{n}^{2}$ = 1196, excluding hydrogens and assuming the appropriate atomic number for f. Thus the light atoms should not be located very accurately by Fourier techniques. However, the method was used and approximate light atom parameters obtained by Fourier synthesis were refined by least-squares analysis. Such a Fourier-least-squares procedure of refinement permits faster location of atoms than that obtained by a Fourier technique alone.

The solution of the light atom structure commenced using the film data uncorrected for absorption. The metal positions, solution 1 above, the isotropic thermal parameters

and over-all scale factor were refined by least-squares. All data were included with unit weighting. The refinement yielded R = 0.264 (R = $\Sigma W \mid |F_0| - |F_C| \mid /\Sigma W \mid F_0 \mid$) and thermal parameters which were non-positive, approximately -0.5. It was surmised that the negative thermal parameters were due to the effect of absorption. Subsequently the same result was observed when refinement of diffractometeric data was initiated. Justification for the use of the negative thermal parameters in refinement will be discussed further in a later section. An electron density difference function, (1/V) $\Sigma\Sigma\Sigma$ $(|F_0| - |F_C|)$ $\exp -2\pi i(hx + ky + \ell z)$, was calculated using only ℓ = 2n data. Because the metal structure has Pmmn symmetry the difference Fourier showed duplicate images mirrored across the xz and yz planes containing the metal atoms. To locate the light atoms, various peaks in the Fourier were selected as trial atoms and the behavior of their thermal parameters was tested in leastsquares calculations. In this manner a 4-fold carbonate, symmetric about the 2-fold axis, was located near La(2). After several more cycles of least-squares refinement three 8-fold water molecules displaying orientations similar to those of the carbonate were recognized. At this point R was still 0.21 and all but one thermal parameter was still negative. An 8-fold carbonate and an 8-fold water remained to be located. The principal peaks remaining in the difference Fourier were of two types; near the xy plane of the metals or along the 2-fold axis. The positions of the

latter peaks, which were the largest, were physically unreal --that is they were superimposed over what would be normally considered the volume of the metal atoms. Attempts to refine atoms assigned to the other peaks near the metal xy planes met with some success, reducing R to 0.19. However, the problem of atom overlap was encountered again. That this overlap resulted from the choice of lanthanum atom positions will be discussed later. In the belief that part of the difficulties encountered resulted from imprecise data, attempts to solve the structure from film data were discontinued.

The solution of the structure was then attempted with diffractometer data uncorrected for absorption. After lanthanum atoms had been assigned and refined in the manner described previously, the value of R was 0.28 when all hk & data were included and the thermal parameters were approximately -2.0\AA^2 . Use of only $\ell=2\text{n}$ data produced R = 0.18. Employment of the techniques described earlier yielded a 4-fold carbonate and three 8-fold waters in the previously obtained positions (R = 0.19 for all data). The difference function again indicated the presence of atoms, apparently carbonate groupings, near the metal xy plane in seemingly unreal positions. At this time the importance of the alternative solution of metal positions was recognized. With the original choice of metal positions the carbonate groupings were located at an inversion center. Since the carbonate has no center of symmetry, duplicate overlapping groups

were required to fulfill the symmetry condition. Use of the metal position, z=0.250 and z'=0.283, and subsequent shift of z parameters of established atoms by +0.250 removed the overlap of carbonate groups. The process of atom location was continued producing the essentially correct placement of all but an 8-fold water and an R value of 0.16.

Before the complete structure had been solved the program for absorption correction became available. This correction was applied and the resulting data were entered in the least-squares refinement of the previously obtained parameters. After location of all atoms, except hydrogen, R was reduced to 0.08 and the isotropic thermal parameters had shifted to positive values.

In an effort to improve the fit by deleting the less precise intensity data the 125 reflections with intensities of less than 2 cps and 10 reflections in which the background intensity was greater than the peak intensity were given zero weight in the least-squares calculation. This procedure eliminated possible adverse effects of a large proportion (20%) of low reliability data. Subsequently, zero weight was assigned to 8 of the 29 most intense reflections in which the observed structure factors were significantly lower than the calculated values. Although extinction may have caused this discrepancy a direct relationship was not observed between intensity and the deviation. An alternative cause of the deviation may be inadequate absorption

correction. In any event, exclusion of these latter reflections produced a measurable effect on the thermal parameters of some of the light atoms even though the positional parameters were not shifted significantly. All other observed data were given unit weight. An anomalous dispersion correction to the scattering factor of lanthanum was included in succeeding calculations. After several least-squares cycles using isotropic thermal parameters R was reduced to 0.063. If no data were deleted and unit weighting was assigned the R would have been 0.076. The thermal parameters were allowed to refine anisotropically using $B_{ij} = 4b_{ij}/a_{i}^{*}a_{j}^{*}$ where a_{i}^{*} is the ith reciprocal cell length and the temperature correction is of the form:

$$\exp\big(-b_{11}h^2-b_{22}k^2-b_{33}\ell^2-2b_{12}hk-2b_{13}h\ell-2b_{23}k\ell\,\big)\,.$$

Using a technique described by Levy²⁵ the symmetry relations among coefficients were evaluated. For the two lanthanum atoms, one carbon atom and one oxygen atom, all of which were located on the 2-fold axis, B_{13} and $B_{23}=0$. When refinement was initiated it was found that several of the light atom coefficients changed non-positive definite, although the aqueous oxygens and metal parameters refined satisfactorily. This difficulty is due to the overall inaccuracies associated with the light atom structure—even the light atoms which refined properly had very large standard deviations. The principal causes of this inaccuracy are the dominance of the metal contribution to most observed reflections

and the low reliability of that data to which it does not contribute. In addition specific absorption effects may still be present in the data. As a result of the difficulty described above only the anisotropic coefficients of metal and aqueous oxygens were refined. The final R factor was 0.061 in contrast to the 0.063 value obtained with isotropic thermal parameters. The shift of any parameter in the last cycle of refinement was less than 0.1% of its standard deviation.

Final coordinates and their standard deviations are listed in Table IVa, thermal parameters and their deviations are found in Table IVb and the observed and calculated structure factors are given in Table V. Water molecules are designated by Aq, the 4-fold carbonate by C(1)-O(1)-O(2) and the 8-fold carbonate by C(2)-O(3-5). The standard deviations in the positional parameters of the light atoms range from 0.019 to 0.038 Å, while those of the thermal parameters are in some cases actually greater than of the anisotropic coefficients.

It was noted that the thermal parameters of O(2) and Aq(4) were abnormally large, isotropic B=5.9 and $6.1\ R^2$, respectively. For O(2) this parameter indicates only a large vibrational amplitude for a non-coordinating oxygen. However for Aq(4), the non-coordinating aqueous oxygen in the structure, all possible sites may not be occupied. Recall the discussion of stoichiometry, that the water content may be less than eight per formula. The assumption

Table IV. Parameters from least-squares refinement

a. Atomic coordinates

Atom	x	У	z
La (1)	0.250	0.250	0.2500
${\tt La(2)}$	0.250	0.750	0.2829(1)
Aq(1)	0.310(2)*	0.385(2)	0.117(1)
Aq(2)	0.113(2)	0.323(2)	0.380(1)
Aq(3)	0.121(2)	0.649(3)	0.409(1)
Aq(4)	0.382(4)	0.393(4)	0.492(2)
c(1)	0.250	0.750	0.110(3)
0(1)	0.320(2)	0.660(2)	0.148(1)
0(2)	0.250	0.750	0.034(3)
c(2)	0.456(3)	0.497(3)	0.282(2)
0(3)	0.019(2)	0.384(2)	0.208(1)
0(4)	0.018(2)	0.618(2)	0.240(1)
o(5)	0.317(2)	0.492(2)	0.296(1)

^{*}Standard deviations in parenthesis.

Parameters from least-squares refinement. Table IV.

b. Thermal parameters

La(1) 0.52(0.10)* 0.83(0.11) 0.68(0.11) 0.06(0.16) (0) (1) La(2) 0.64(0.10) 0.71(0.11) 0.43(0.11) -0.09(0.17) (0) (1) Aq(1) 0.8(0.9) 1.3(1.0) 1.5(1.0) 0.4(0.8) 0.3(0.7) 0.1(Aq(2) 1.2(1.0) 2.6(1.1) 2.2(1.1) -0.3(0.9) -1.0(0.9) -0.6(Aq(3) 1.5(1.1) 4.2(1.5) 1.5(1.2) 0.0(1.1) 0.2(0.8) 0.7(Aq(4) 5.2(1.8) 10.2(2.7) 4.6(1.9) 0.2(1.8) 2.7(1.5) -1.6(C(1) 2.4(0.9) 0.1 1.2(0.4) O(2) 5.9(1.0) C(2) 0.4(0.5) O(3) 1.5(0.4) O(4) 1.8(0.5) O(5) 1.1(0.4)		(B or B ₁₁)**	B22	Взз	B ₁₂	B ₁₃	B23
0.64(0.10) 0.71(0.11) 0.43(0.11) -0.09(0.17) (0) 0.8(0.9) 1.3(1.0) 1.5(1.0) 0.4(0.8) 0.3(0.7) 1.2(1.0) 2.6(1.1) 2.2(1.1) -0.3(0.9) -1.0(0.9) 1.5(1.1) 4.2(1.5) 1.5(1.2) 0.0(1.1) 0.2(0.8) 5.2(1.8) 10.2(2.7) 4.6(1.9) 0.2(1.8) 2.7(1.5) - 2.4(0.9) 1.2(0.4) 5.9(1.0) 0.4(0.5) 1.5(0.4) 1.5(0.4) 1.5(0.5) 1.1(0.4)	La(1)	0.52(0.10)*	0.83(0.11)	0.68(0.11)	0.06(0.16)	(0)	(0)
0.8(0.9) $1.3(1.0)$ $1.5(1.0)$ $0.4(0.8)$ $0.3(0.7)$ $1.2(1.0)$ $2.6(1.1)$ $2.2(1.1)$ $-0.3(0.9)$ $-1.0(0.9)$ $1.5(1.1)$ $4.2(1.5)$ $1.5(1.2)$ $0.0(1.1)$ $0.2(0.8)$ $2.4(0.9)$ $1.2(0.4)$ $5.9(1.0)$ $0.4(0.5)$ $1.5(0.4)$ $1.8(0.5)$	La(2)	0.64(0.10)	0.71(0.11)	0.43(0.11)	-0.09(0.17)	(0)	(0)
1.2(1.0) $2.6(1.1)$ $2.2(1.1)$ $-0.3(0.9)$ $-1.0(0.9)$ $-1.5(1.1)$ $4.2(1.5)$ $1.5(1.2)$ $0.0(1.1)$ $0.2(0.8)$ $2.4(0.9)$ $10.2(2.7)$ $4.6(1.9)$ $0.2(1.8)$ $2.7(1.5)$ $-1.2(0.4)$ $5.9(1.0)$ $0.4(0.5)$ $1.5(0.4)$ $1.8(0.5)$	Aq(1)	(6.0)8.0	1.3(1.0)	1.5(1.0)	0.4(0.8)	0.3(0.7)	0.1(0.8)
$\begin{array}{cccccccccccccccccccccccccccccccccccc$	Aq(2)	1.2(1.0)	2.6(1.1)	2.2(1.1)	-0.3(0.9)	-1.0(0.9)	(6.0)9.0-
5.2(1.8)10.2(2.7)4.6(1.9)0.2(1.8)2.7(1.5)2.4(0.9)1.2(0.4)5.9(1.0)0.4(0.5)1.5(0.4)1.8(0.5)1.1(0.4)	Aq(3)	1.5(1.1)	4.2(1.5)	1.5(1.2)	0.0(1.1)	0.2(0.8)	0.7(1.0)
	Aq(4)	5.2(1.8)	10.2(2.7)	4.6(1.9)	0.2(1.8)	2.7(1.5)	-1.6(1.7)
	c(1)	2.4(0.9)					
	0(1)	1.2(0.4)					
_	0(2)	5.9(1.0)					
	c(2)	0.4(0.5)					
	0(3)	1.5(0.4)					
	0(4)	1.8(0.5)					
	0(2)	1.1(0.4)					

* Standard deviations in parenthesis.

All parameters in units of \mathbb{A}^2 . * œ ** $B_{ij} = 4B_{ij}/a_{i}^{*}$

factors structure #aimmadillamudicimbadikmimadimbenambenintan amammadumbenintan amammadumbenintan amammadillik calculated a%pcunaeaussuudeäsauuuääsuussissevasuuuseusuuseaaääääääsaastookkuuseaasuunnakkuu and Observed 4 ##wwgilidatasiasiawgangangilitasilitasiyasilitasiyasiyasiyasiyasiyasiyasiyasi > 4 5 5 8 8 9 5 7 3 7 7 8 9 7 7 8 9 7 7 8 9 7 7 8 9 7 7 7 8 9 7 7 7 8 7 7 7 8 7 7 7 8 7 7 8 7 7 8 7 7 8 7 7 8 7 8 7 8 7 8 7 8 7 8 7 8 7 8 7 8 7 8 7 8 7 8 7 8 7 8 7 8 7 8 7 8 7 8 7 8 7 8 7 8 7 8 7 8 7 8 7 8 7 8 7 8 7 8 7 8 7 8 7 8 7 8 7 8 7 8 7 8 7 8 7 8 7 8 7 8 7 8 7 8 7 8 7 8 7 8 7 8 7 8 7 8 7 8 7 8 7 8 7 8 7 8 7 8 7 8 7 8 7 8 7 8 7 8 7 8 7 8 7 8 7 8 7 8 7 8 7 8 7 8 7 8 7 8 7 8 7 8 7 8 7 8 7 8 7 8 7 8 7 8 7 8 7 8 7 8 7 8 7 8 7 8 7 8 7 8 7 8 7 8 7 8 7 8 7 8 7 8 7 8 7 8 7 8 7 8 7 8 7 8 7 8 7 8 7 8 7 8 7 8 7 8 7 8 7 8 7 8 7 8 7 8 7 8 7 8 7 8 7 8 7 8 7 8 7 8 7 8 7 8 7 8 7 8 7 8 7 8 7 8 7 8 7 8 7 8 7 8 7 8 7 8 7 8 7 8 7 8 7 8 7 8 7 8 7 8 7 8 7 8 7 8 7 8 7 8 7 8 7 8 7 8 7 8 7 8 7 8 7 8 7 8 7 8 7 8 7 8 7 8 7 8 7 8 7 8 7 8 7 8 7 8 7 8 7 8 7 8 7 8 7 8 7 8 7 8 7 8 7 8 7 8 7 8 7 8 7 8 7 8 7 8 7 8 7 8 7 8 7 8 7 8 7 8 7 8 7 8 7 8 7 8 7 8 7 8 7 8 7 8 7 8 7 8 7 8 7 8 7 8 7 8 7 8 7 8 7 8 7 8 7 8 7 8 7 8 7 8 7 8 7 8 7 8 7 8 7 8 7 8 7 8 7 8 7 8 7 8 7 8 7 8 7 8 7 8 7 8 7 8 7 8 7 8 7 8 7 8 7 8 7 8 7 8 7 8 7 8 7 8 7 8 7 8 7 8 7 8 7 8 7 8 7 8 7 8 7 8 7 8 7 8 7 8 7 8 7 8 7 8 7 8 7 8 7 8 7 8 7 8 7 8 7 8 7 8 7 8 7 8 7 8 7 8 7 8 7 8 7 8 7 8 7 8 7 8 7 8 7 8 7 8 7 8 7 8 7 8 7 8 7 8 7 8 7 8 7 8 7 8 7 8 7 8 7 8 7 8 7 8 7 8 7 8 7 8 7 8 7 8 7 8 7 8 7 8 7 8 7 8 7 8 7 8 7 8 7 8 7 8 7 8 7 8 7 8 7 8 7 8 7 8 7 8 7 8 7 8 7 8 7 8 7 8 7 8 7 8 7 8 7 8 7 8 7 8 7 8 7 8 7 8 7 8 7 8 7 8 7 8 7 8 7 8 7 8 7 8 7 8 7 8 7 8 7 8 7 8 7 8 7 8 7 8 7 8 7 8 7 8 7 8 7 8 7 8 7 8 7 8 7 8 7 8 7 8 7 8 7 8 7 8 7 8 7 8 7 8 7 8 7 8 7 8 7 8 7 8 7 8 7 8 7 8 7 8 7 8 7 8 7 8 7 8 7 8 7 8 7 8 7 8 7 8 7 8 7 8 7 8 7 8 7 8 7 8 7 8 7 8 7 8 7 8 7 8 7 8 7 8 7 8 7 8 7 8 7 8 7 8 7 8 7 8 7 8 7 8 7 8 7 8 7 8 7 8 7 8 7 8 7 8 7 8 7 8 7 8 7 8 7 8 7 8 7 8 7 8 7 8 7 8 7 8 7 8 7 8 7 8 7 8 7 8 7 8 7 8 7 8 7 8 7 8 7 8 7 8 7 8 7 8 7 8 7 8 7 8 7 8 7 8 7 8 7 8 7 8 7 8 7 8 7 8 7 8 7 8 7 8 7 8 7 8 7 8 7 8 7 8 7 8 7 8 7 8 7 8 7 8 7 8 7 8 7 8 7 8 7 8 7 8 7 8 7 8 7 8 7 8 7 8 7 8 7 8 7 8 7 8 7 8 7 8 7 8 7 8 7 8 7 8 7 8 7 8 7 8 7 8 7 8 7 8 7 8 7 8 7 8 7 8 7 8 7 8 7 8 7 8 7 8 7 8 7 8 7 8 7 8 7 8 7 8 7 8 7 8 7 8 Table

that only 3/4 of the Aq(4) sites are occupied corresponding to a formula of La₂(CO₃)₃·7.5H₂O produces B = 3.3 $\frac{Q_2}{A}$.

Difference density maps were calculated using both isotropically and anisotropically refined data. In all cases the largest residual peaks were associated with the metals. The approximate numbers of electrons associated with these peaks were estimated using the height of lanthanum peaks in a Fourier of F(calculated) to scale the relative heights. The largest peak heights corresponded to one to two electrons. All other peaks in the difference function were about one electron or less. Some of these residual peaks were identified later as probable hydrogen peaks. Attempts to refine H atom parameters by the method of least-squares were completed with very limited success. The most reasonable results will be discussed in a later section.

Effect of Absorption on the Determination of the Structure

It was mentioned previously that least-squares refinement using film data uncorrected for absorption produced negative thermal parameters. This effect was found to be even more pronounced using diffractometric data similarly uncorrected. At that time we postulated the phenomenon resulted from absorption, as the effect would be more marked for the larger crystal used in the diffractometric work.

The first attempts to correct for absorption using the program of Coppens $\underline{\text{et}}$ $\underline{\text{al.}}^{19}$ did not eliminate the negative parameters since an undetected error occurred when the

program was reproduced. To support the conjecture of large absorption effects a Wilson plot of $ln(|F_0|^2/\frac{\sum_i f_i^2}{\sum_i f_i^2})$ versus $\sin^2 \theta$ was constructed. The term $\left|\overline{F_0}\right|^2$ is the average value of the observed structure factor for a $\sin^2 \theta$ interval and $^0\,\mathrm{f}_{\,\mathrm{i}}$ is the atomic scattering factor of atom $_{\dot{1}}$. The slope of a Wilson plot equals $-2B/\lambda^2$ where B is an overall temperature coefficient. The arithmetic average $(\Sigma |\mathbf{F_0}|^2)/n$ was evaluated including both observed and absent reflections in five equal intervals of $\sin^2 \theta$ between 0.05 and 0.55. Boundary points were assigned half weight. The $\left|\mathbf{F_0}\right|^2$ were diffractometric intensities corrected for Lorentz and polarization effects. The quantity $\sum_{i=0}^{\infty} f_{i}$, excluding H atoms, was determined for the median value in each 2θ interval. From the slope of the Wilson plot a physically impossible value, B =-1.2 $^{\circ}$, was obtained. To prove that this negative temperature coefficient resulted from absorption rather than some other physical factor, intensities were collected using molybdenum radiation $(\lambda_{\mathbf{K}}$ - 0.7107 $\hat{\mathbf{A}})$. The linear absorption coefficient for $\text{La}_2(\text{CO}_3)_3 \cdot 8\text{H}_2\text{O}$ is only $22~\text{cm}^{-1}$ with this radiation in contrast to the value of 444 cm⁻¹ for copper radiation. Intensities were obtained for the $(Ok \ell)$ level, with the Weissenberg multiple film method, on a crystal of approximate dimensions; 0.18 x 0.18 x 0.10 mm. After intensities had been corrected for Lorentz and polarization effects, a Wilson plot was prepared. From this slope the value B = 2.0Å² was calculated. This positive value obtained with weakly

absorbed molybdenum radiation seemed to verify that absorption caused the negative coefficients. An average B, \overline{B} , was calculated from the final refined isotropic parameters by weighting each individual B according to the number of electrons in that atom. The result, \overline{B} = 1.7 R^2 , substantiated further the original postulate.

The effect of absorption on crystal structure refinement has been discussed in two recent papers. Werner²⁶ noted that failure to correct for absorption in BiOF approximately doubled the R value and altered thermal parameters significantly. However, positional parameters were not changed substantially, but their standard deviations increased. Srivastava and Lingafelter²⁷ made a study of the influence of absorption on a variety of parameters. They found that thermal parameters decrease to negative values with increasing size of regular parallelopiped crystals. They stated that this effect should be anticipated since the amount of absorption is related to the crystal volume and the observed structure factors will show the slope of the absorption correction line. In the case of large crystals they observed for B changes much larger than the corresponding standard deviation. Changes in positional parameters were generally within the standard deviations and the R values were higher.

My observations regarding the effects of absorption are in agreement with those discussed above. Not only did R decrease dramatically during refinement when the data

were corrected for absorption but the thermal parameters changed from non-positive, definite, to positive. To obtain an estimate of the effect of absorption on positional parameters a least-squares refinement was performed using uncorrected data. All data (633 reflections) were given unit weighting and refinement continued until all parameter shifts were less than 0.3% of the standard deviation. The resulting parameters were compared with those refined similarly with absorption corrected data. The positional and thermal parameter differences are listed in Table VI. Twenty-three of the positional parameter changes are less than the corresponding standard deviations and none is greater than 2 sigma of the corrected data. The largest change is 0.04 Å. Surprisingly, the increase in R was small, less than 0.01.

This discussion may be concluded by observing that even with serious absorption errors the $\text{La}_2(\text{CO}_3)_3\cdot 8\text{H}_2\text{O}$ structure could be solved with some accuracy. To do this, however, negative thermal parameters had to be refined. Such a procedure, of course, has little general applicability if facilities are available to eliminate or correct for absorption.

Table VI. Positional and thermal parameter changes due to absorption.

	∆x(x10 ⁺⁴)	∆y(x10⁺⁴)	$\triangle z (x10^{+4})$	ΔΒ
La(1)	(0)	(0)	(0)	-2.0
La(2)	(0)	(0)	- 2	-2.0
c(1)	(0)	(O)	-14	-2.3
0(2)	(0)	(0)	+23	-4.4
0(1)	+6	-45	0	-2.1
C(2)	-32	- 4	+ 8	-2.3
0(3)	+23	+39	+ 8	-1.8
0(4)	+ 4	-32	+ 1	-2.0
o(5)	-11	+ 1	- 8	-2.2
Aq(1)	- 8	+ 1	+ 8	-2.0
Aq(2)	-48	+ 6	- 8	-2.0
Aq(3)	-44	+11	+ 6	-1.8
Aq(4)	+19	+69	+12	-2.4

IV. DESCRIPTION OF THE STRUCTURE

Structure as a Whole

Stereoscopic illustrations of the complete and partial structure, which may be viewed in 3-D with a standard steroscope, are shown in Figures 4-7. The letter designations for the atoms used in the illustrations are given in Figure 4. Interatomic distances and angles are listed in Tables VII and VIII. As is evident in Figures 4-6, $La_2(CO_3)_3 \cdot 8H_2O$ crystallizes in a layer structure. The primary components of the layers are alternating rows of metals and 8-fold carbonates parallel to the x-axis. The carbonates, designated by C, N, O and P in the illustrations, are situated so that each oxygen is bonded to two metals. Every carbonate occupies a total of six coordination sites on the four neighboring metals in the layer. Similarly each metal is bonded to four carbonates to produce an irregular La-CO3 layer. The carbonates are tilted 170 out of the x-y plane with one bond, C-P, nearly parallel to the x-axis. In adjoining rows of carbonates the C-P bonds have opposite orientations. One oxygen-oxygen distance, O(3)-O(4)=2.72 Å, between adjacent carbonates is smaller that that normally expected for non-bonded oxygens. This short distance may imply that the negative charge on each oxygen is distributed to two metals and one carbon thereby reducing the effective oxygen size. The four remaining coordination sites of the

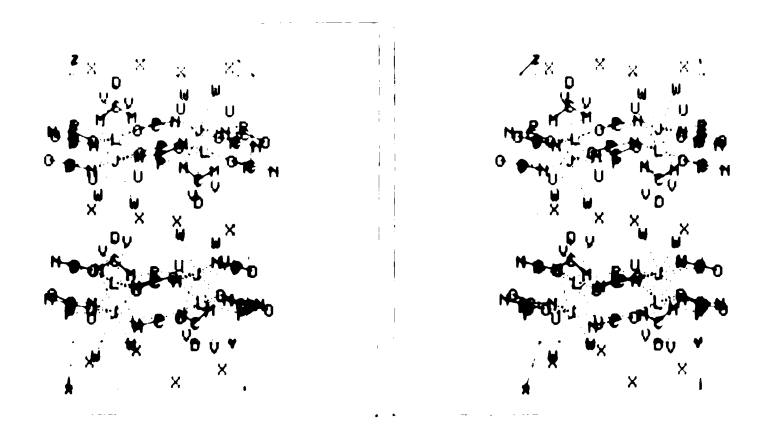


Figure 4. Stereoscopic illustration of $La(CO_3)_3 \cdot 8H_2O$ unit cell.

Atom Identification for Figures 4-8.

L - La(1)	c - c(1) or c(2)
J - La(2)	D - O(2)
U - Aq(1)	M - O(1)
V - Aq(2)	N - O(3)
W - Aq(3)	0 - 0(4)
X - Aq(4)	P - O(5)

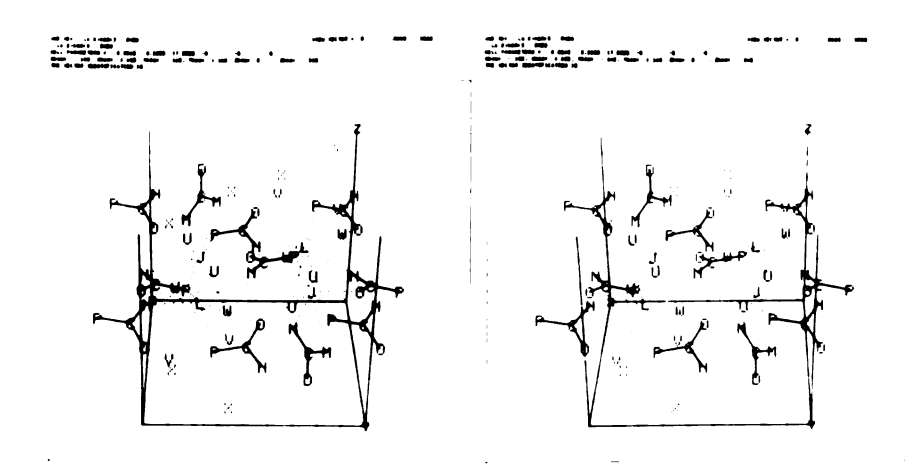


Figure 5. Stereoscopic illustration of $La_2(CO_3)_3 \cdot 8H_2O$ half cell.

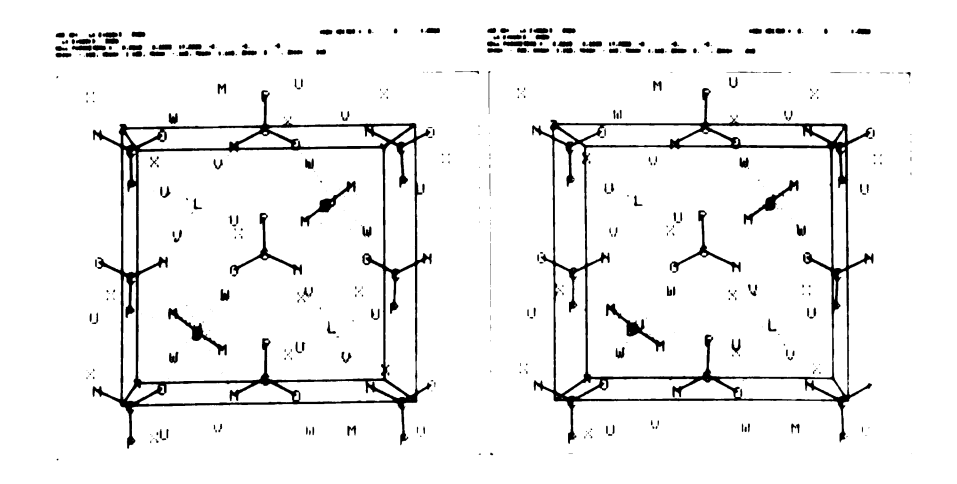
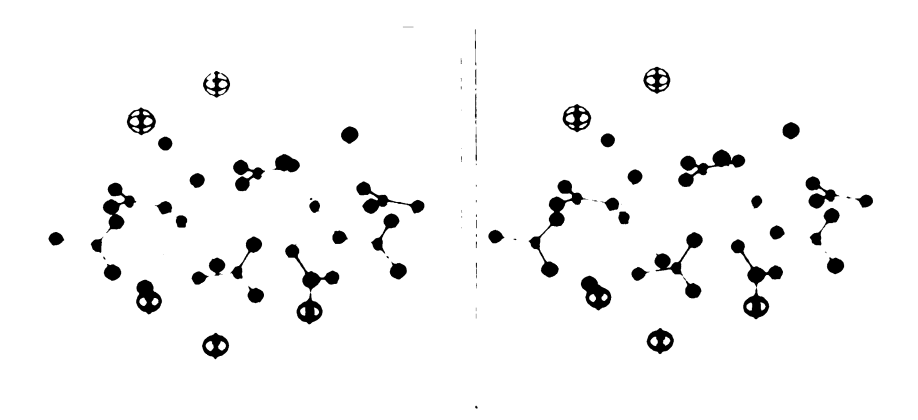


Figure 6. Stereoscopic illustration of $La_2(CO_3)_3 \cdot 8H_2O$ half cell



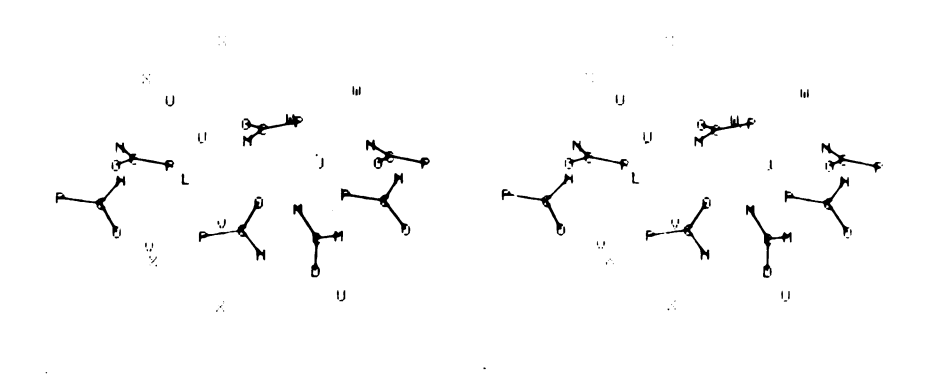


Figure 7. Stereoscopic illustrations of lanthanum coordination in $\text{La}_2(\text{CO}_3)_3 \cdot 8\text{H}_2\text{O}$.

Table VII. Interatomic distances*

Atom (1)	Atom (2)	Distance (R)	Atom (1)	Atom (2)	Distance (A)
A. Coordi	nation Sph	ere La(1)			
La(1) - 2 2 2 2 2	0(5) 0(5) Aq(2) Aq(1)	2.52(2) 2.54(2) 2.62(2) 2.66(2)	0(3) -	Aq(1) Aq(1) Aq(2) O(4)	3.04(3) 3.38(3) 3.09(3) 2.72(3)
Aq(1) - Aq(2) - O(5) -	O(4) Aq(1) Aq(2) Aq(1) Aq(2)	2.73(2) 2.81(4) 2.82(4) 3.22(3) 2.82(3)	0(4)	O(5) Aq(1) Aq(2) O(5)	3.24(3) 3.07(3) 3.06(3) 2.18(3)
B. Coordi	nation Sph				
La(2) - 2 2 2 2 2 2	O(1) O(4) O(5) Aq(3) O(3)	2.53(2) 2.55(2) 2.55(2) 2.62(2) 2.74(2)	0(4) -	Aq(3) O(1) O(1) O(3) O(5)	3.04(3) 3.01(3) 3.15(3) 2.72(3) 3.10(3)
Aq(3) - O(1) - O(3) -	Aq(3) O(1) Aq(3) O(1)	3.02(5) 2.14(4) 3.26(3) 3.05(3)	o(5) -	Aq(3) O(1) O(3)	3.00(3) 2.99(3) 2.17(3)
C. Carbon	ates				
C(1) - 2 C(2) -	0(1) 0(2) 0(3) 0(4) 0(5)	1.25(3) 1.30(6) 1.29(4) 1.28(4) 1.28(3)	o(1) - o(3) - o(4) -	O(1) O(2) O(4) O(5) O(5)	2.14(4) 2.21(4) 2.30(3) 2.17(3) 2.18(3)
D. Aqueou	s 0 - 0				
Aq(1) -	O(1) Aq(4) Aq(1) Aq(3)	2.68(3) 2.74(4) 2.81(4) 2.85(3)	Aq(2) -	O(1) O(5) Aq(4) Aq(2)	2.68(3) 2.82(3) 2.82(4) 2.82(4)
Aq(3) -	O(2) Aq(1) O(5)	2.61(4) 2.85(3) 3.00(3)	Aq(4) -	Aq(1) Aq(2) Aq(4)	2.74(4) 2.82(4) 2.95(7)

^{*}Standard deviation of the last digit is indicated in parenthesis.

Table VIII. Bond angles

Atom (1)	Atom (2)	Atom (3)	Angle
A. Coordina	ation Sphere La(1)	
Aq(1) Aq(1) Aq(1) Aq(1) Aq(2) Aq(2) Aq(2) Aq(2) Aq(2) O(3) O(3) O(3) O(4) Aq(1) Aq(1) Aq(1) Aq(1) Aq(1) Aq(1) O(5) Aq(2) Aq(1) O(5) Aq(1) O(5)	La(1) Aq(1) Aq(1) Aq(1) Aq(2) O(4) O(5) Aq(2) O(3) Aq(1)	Aq(1) 0(3) 0(4) 0(5) Aq(2) 0(3) 0(4) 0(5) 0(4) 0(5) 0(3) 0(5) 0(4) Aq(2) 0(5) 0(4) Aq(1) Aq(2) 0(3) Aq(2) 0(5)	63.9(0.9)* 71.6(0.6) 69.4(0.6) 76.7(0.6) 65.3(1.0) 73.6(0.7) 69.9(0.7) 66.5(0.7) 62.0(0.7) 79.5(0.7) 147.6(1.0) 48.9(0.6) 103.1(0.8) 106.2(0.9) 107.5(0.5) 106.0(0.9) 107.2(0.9) 96.6(0.8) 80.1(0.7) 99.4(0.8) 78.5(0.7)
B. Coordina	ation Sphere La(2)	
Aq(3) Aq(3) Aq(3) O(1) O(1) O(1) O(1) O(3) O(4) O(4) O(4) O(3) Aq(3) Aq(3) O(5) O(1) Aq(3) O(4) O(3)	La(2) Ca(2) Ca(2) Ca(3) Ca(3) Ca(4) Ca(3) Ca(4) Ca(3) Ca(4) Ca(3)	Aq(3) 0(4) 0(5) 0(1) 0(3) 0(4) 0(5) 0(4) 0(5) 0(4) 0(5) 0(1) 0(1) Aq(3) 0(1) 0(3) 0(4)	70.3(1.0) 72.0(0.7) 70.8(0.7) 50.0(0.9) 70.6(0.7) 76.9(0.7) 72.7(0.7) 72.2(0.7) 61.9(0.7) 48.3(0.6) 146.4(1.0) 74.7(0.8) 117.2(0.8) 100.5(0.8) 106.0(0.9) 115.2(0.8) 99.6(0.8) 105.0(0.9) 95.2(0.8) 78.2(0.7)

^{*}Standard deviation.

Table VIII (Cont.)

Atom (1)	Atom (2)	Atom (3)	Angle
Heom (1)	Acom (2)		
C. Carbonate	es		
0(1)	c(1)	0(2)	121.0(2.0)
o(1)	c(1)	o(1)	118.0(4.0)
o(3)	c(2)	$\mathbf{o}(4)$	127.4(2.5)
o(3)	c(2)	o(5)	115.6(2.6)
o(4)	c(2)	0(5)	117.1(2.7)
D. Possible	Hydrogen Bonds		
$\mathtt{Aq}(1)$	$\mathtt{Aq}(1)$	Aq(3)	105.8(1.1)
Aq(1)	$\mathbf{Aq}(1)$	$\mathbf{A}\mathbf{q}(4)$	77.4(1.0)
Aq(1)	$\overline{Aq}(1)$	$\bar{\mathbf{o}}(1)$	156.6(1.1)
$\mathtt{Aq}(3)$	Aq(1)	o(1)	96.3(1.1)
$\mathtt{Aq}(\mathtt{3})$	$\mathtt{Aq}(1)$	$\mathtt{Aq}(4)$	120.1(1.1)
Aq(4)	$\mathbf{Aq}(1)$	o(1)	98.3(1.1)
Aq(2)	Aq(2)	0(1)	152.1(1.4)
$\mathbf{Aq}(2)$	$\operatorname{Aq}(2)$	$\mathbf{Aq}(4)$	68.0(1.0)
Aq(2)	Aq(2)	0(5)	73.8(0.9)
Aq(4)	Aq(2)	o(1)	100.2(1.1)
Aq(4) `O(1)	Aq(2)	0(5)	138.8(1.2)
- } {	$\operatorname{Aq}(2)$	O(5) O(2)	120.9(1.0)
$egin{array}{l} \mathtt{Aq}(1) \ \mathtt{Aq}(1) \end{array}$	Aq (3) Aq (4)) _ ($egin{array}{c} 127.2 (1.0) \ 120.9 (1.4) \end{array}$
Aq(1) $Aq(1)$	$egin{array}{l} \mathtt{Aq}\left(oldsymbol{4} ight) \ \mathtt{Aq}\left(oldsymbol{4} ight) \end{array}$	$egin{array}{l} \mathtt{Aq}\left(2 ight) \ \mathtt{Aq}\left(4 ight) \end{array}$	113.8(1.7)
Aq(1) $Aq(2)$	$\begin{array}{c} Aq(4) \\ Aq(4) \end{array}$	Aq(4)	124.0(1.7)
$\mathbf{Aq}(3)$	O(2)	Aq(3)	70.7(1.5)
c(1)	o(2)	Aq(3)	144.7(0.8)

10-coordinate metals are completed by four water molecules in one case and by two water molecules and the 4-fold carbonate acting as a bidentate in the other case. These molecules and ions project out from the primary layer described above. The metals and coordinated ligands form a series of widely spaced layers. No direct bonding between the layers is apparent except for a probable hydrogen bond between the terminal oxygen of the 4-fold carbonate and the water molecules in the next layer. The remaining water molecules, X in the illustrations, are situated between the layers and probably furnish additional hydrogen bonding. The weakness of the bonding between layers is supported by the facile cleavage observed along (001).

Much of the structure as illustrated in Figure 4 nearly repeats with a translation of c/2. The longer repeat distance of course results from the c-axis glide. In order to describe the structure in terms of space group Pmmn, in which the glide planes are replaced by mirror planes, distorder phenomena would have to be invoked. A random orientation of carbonate (2), of water molecules and of O(1) would be necessary. In the crystals observed in this study, no evidence of disorder, such as film streaking or appropriate residual peaks in the difference synthesis, was found.

Coordination of the Metals

The lanthanum atoms in $La_2(CO_3)_3 \cdot 8H_2O$ are situated in two somewhat different environments as is indicated in

Figure 7. The pertinent La-O distances uncorrected for thermal motion are listed in Table VIII. La(1) is coordinated by four water molecules, two unidentate and two bidentate carbonates. In La(2) the bidentate 4-fold carbonate replaces two water molecules in the coordination sphere. The bidentate oxygens from the 8-fold carbonates are O(4)and O(5) for La(1) and O(3) and O(5) for La(2). The unidentate oxygens are O(3) and O(4) for La(1) and La(2) respectively. The average lanthanum to oxygen distances are 2.61 $\stackrel{\circ}{A}$ (La(1)) and 2.60 $\stackrel{\circ}{A}$ (La(2)). The average La-O(CO₂) distance is 2.60 Å, but two of the distances are appreciably greater (2.73 and 2.74 A) for each metal. Each of these larger La-O(CO₃) distances involves one oxygen of a bidentate carbonate. The average La-O(CO3) distance is 2.63 A. The observed La-O distances seem consistent with the interatomic distances reported for other lanthanum compounds. In hexagonal La₂O₃, in which lanthanum is 7coordinate, distances range from 2.42-2.69 A. Hunt, Rundle and $Stosick^{28}$ reported both 9- and 12-coordination in $La_2(SO_4)_3 \cdot 9H_2O$. The metal-oxygen distances calculated were: $La-O(SO_4) = 2.70 \text{ Å}$, La-O(Aq) = 2.74 Å for 9-coordination and La-O(SO₄) = 2.60 or 2.74 $\stackrel{\circ}{A}$ for 12-coordination. Recently Carter²⁹ reported for the layer structure of La(OH)₂Cl distances between 2.47 and 2.63 Å for 8-coordinate lanthanum. Hoard, Lee and Lind³⁰ report for KLaZ·8H₂O, where Z is the ethylenediamminetetraacetate ion a 9-coordinate La with distances: La-O(carboxylate) = 2.507 Å and La-O(Aq) =

2.580 Å. Of greatest pertinence are the distances reported by Lind, Lee and Hoard³¹ for the 10-coordinate $\text{HLaZ} \cdot 7\text{H}_2\text{O}$; La-O(Aq) = 2.592 Å, La-O(carboxylate) = 2.537 Å and La-O(carboxylic acid) = 2.609 Å. The bond distances, La-O(Aq) and $\text{La-O}(\text{CO}_3)$, observed for $\text{La}_2(\text{CO}_3)_3 \cdot 8\text{H}_2\text{O}$ fall within the range of literature values for similar cases. However, the average distance for $\text{La-O}(\text{CO}_3)$, 2.60 Å, appears slightly high in comparison to Hoard's analogous 10-coordinate case. However, if the longer bonds are excluded the average drops to 2.54 Å, a value which is in good agreement with the cited work.

The characteristics of high (7-12) coordination have recently been investigated vigorously. Hoard and coworkers made important contributions, and Muetterties and Wright32 have prepared a comprehensive review. The various lanthanide compounds offer a wide range of high-numbered coordination polyhedra for study. Two factors are of necessity important in a correlation of the various structures in this series. These are the size of the metal ion, which decreases with increasing atomic number for a constant oxidation state, and the stereochemical requirements of the coordinated ligands, that is, the number and spatial requirements of coordination sites on the ligand. The importance of metal size is emphasized in a statement by Hoard, et al.30 that the average hydration number approaches nine for La^{3+} (e.g., $Nd(OH_2)_9(BrO_3)_3^{33}$) and eight for Lu^{3+} . Analogously the tribromides (LaBr₃-GdBr₃) are also

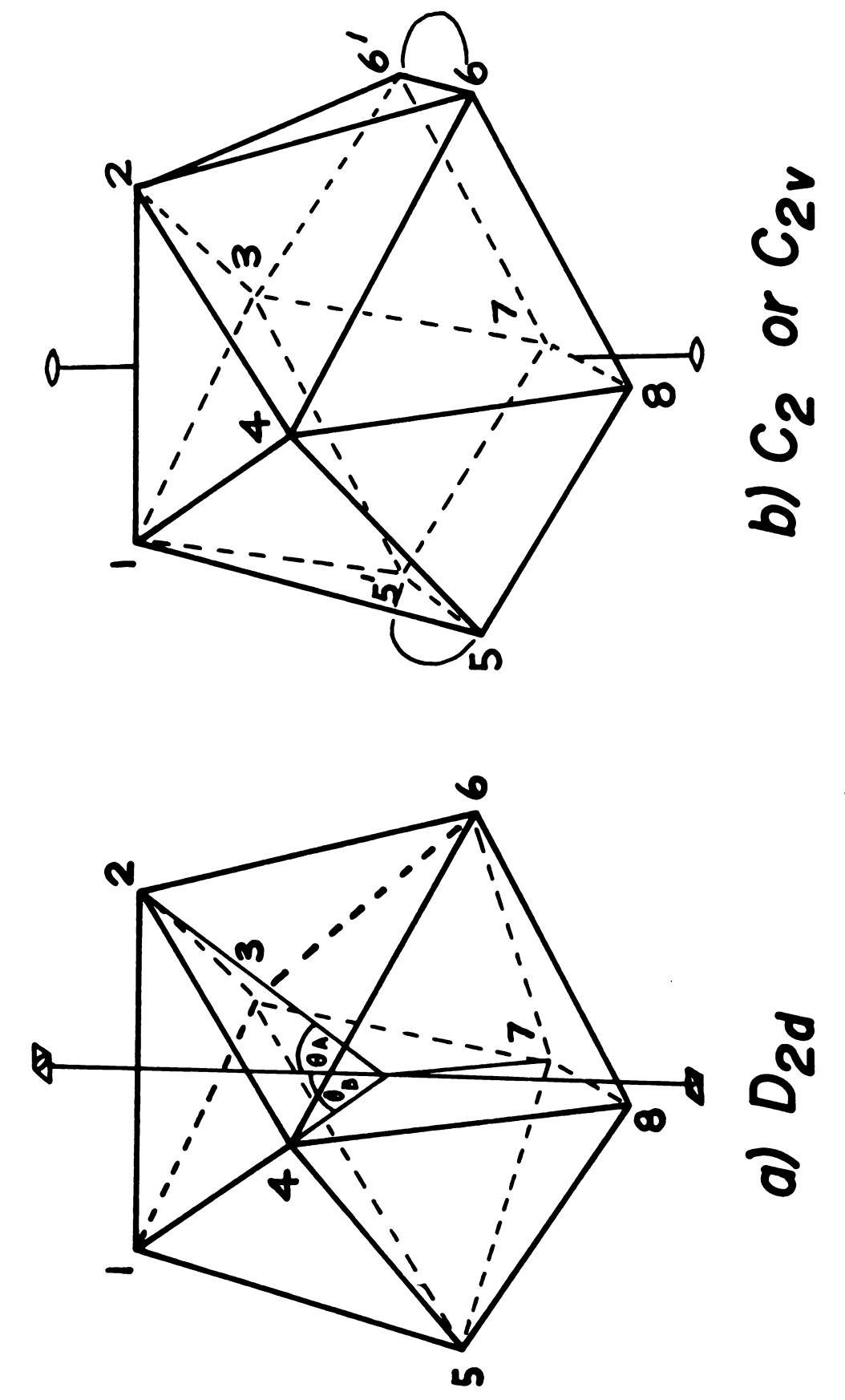
nonacoordinate whereas the series $DyBr_3-LuBr_3$ are hexacoordinate. The importance of the ligands in determining the coordination number is supported by the lack of examples of unidentate coordination greater than nine (possible exception: $YbSb_2^{34}$), however, with bi- or higher dentate ligands, coordination numbers up to 12 have been observed for the lanthanides. For example in $Ce_2Mg_3(NO_3)_{12}\cdot 24H_2O$, an irregular icosahedral $Ce(NO_3)_6^{3-}$ has been observed. In $La_2(SO_4)_3\cdot 9H_2O$ where both 9- and 12-coordination occur, sulfate acts as a tridentate in one coordination sphere.

Decacoordination is quite rare--it seems restricted to only lanthanide and actinide metal compounds. In fact no example of 10-coordination had been established until the HLaZ·7H₂O structure was reported. Other 10-coordinate species characterized by X-ray structural analysis include tetrakisacetatouranium(IV) 36 , in which the oxygens are arrayed at the corners of a bicapped square antiprism, and YbSb₂³⁴ in which two antimony atoms are above one face of a nearly square antiprism formed by the other eight antimony atoms. The tropolone anion, $O_2C_7H_5^-$, is reported³⁷ to form ten-coordinate complexes with Th⁴⁺ and U⁴⁺. Other species in which decacoordination is suspected are the salts of $Th(CO_3)_5^{6-38}$ and $Mo(CO_3)_5^{6-39}$. The coordination polyhedra for decacoordination have not been studied effectively Muetterties and Wright³² suggest the symmetrically bicapped square antiprism (D_{4d}) or a bicapped dodecahedron (C_2) are of proper symmetry for a sp3d5f hybrid model. However, since a decacoordinate complex with unidentate ligands is

unknown, the ground state configuration for 10-coordination is uncertain. A bicapped square antiprism can be used to describe the structure of the acetate complex of U(IV), however. Also part of the stereochemistry of HLaZ·7H₂O has been related to the dodecahedron, but the entire polyhedron has not been described in terms of either decacoordinate polyhedron.

The coordination sphere of the lanthanum atoms in $La_2(CO_3)_3$ $\dot{8}H_2O$ is of low symmetry (C_2) . Consequently the description of the polyhedra must be considered in terms of distortions or modification of such idealized polyhedra as the pentagonal pyramid (C_{5V}) , the pentagonal bipyramid (D_{5h}) , the bicapped square antiprism (D_{4d}) and dodecahedron (D_{2d}) .

One of the simplest models useful in describing the $\operatorname{La_2(CO_3)_3} \cdot 8\operatorname{H_2O}$ structure is that of two identical pentagonal pyramids sharing one edge, 1-2 in Figure 8b, with bidentate carbonates bridging the equatorial sites next to the shared edge. For the $\operatorname{La}(1)$ coordination sphere two $\operatorname{Aq}(1)$ would form the shared edge, $\operatorname{O}(4)$, $\operatorname{Aq}(2)$ and $\operatorname{O}(5)$ would complete the pentagonal planes and $\operatorname{O}(3)$ are at the apices. For $\operatorname{La}(2)$, the bidentate $\operatorname{O}(1)$ forms the common edge, $\operatorname{O}(3)$, $\operatorname{Aq}(3)$ and $\operatorname{O}(5)$ complete the pentagonal planes and $\operatorname{O}(4)$ are at the apices. The 2-fold rotation-axis passes through the centers of the shared edge and the edge opposite. All five atoms assigned to the pentagon lie within $\operatorname{O.38}$ Å of the average pentagonal plane for $\operatorname{La}(1)$ coordination and the sum



Dodecahedral derivative. **Q** a) Dodecahedron. Figure 8.

of the plane angles is 531° versus 540° for an ideal pentagonal plane. The individual angles range from 103 to 1070. For the La(2) coordination all five atoms are within 0.13 $^{\circ}$ of the average plane and the sum of plane angles is 5380, with individual angles ranging from 100 to 1170. The pentagonal pyramid model seems to fit the La(2) coordination somewhat better than that of La(1), that is, the pentagons are closer to being planar. In the case of La(2) the principal distortion of the pentagonal plane is the out of the plane bend of Aq(3) which is opposite the shared edge. The five angles within the pentagonal plane of La(2) are unequal largely because of the shortness of the shared bidentate edge, 2.14 Å, compared to the average length of 3.10 Å of the other edges. Thus the angles associated with the shared edge are increased with respect to the others which are decreased.

The polyhedral arrangement just described also may be derived from the pentagonal bipyramid. Using the numbering rules given by Muetterties and Wright³², in which 1 and 7 designate apical positions, the 4, 6 and 5 sites are split into two sites each by occupation by two bidentate carbonates and two waters respectively.

The presence of a bicapped square antiprism is difficult to detect in $\text{La}_2(\text{CO}_3)_3 \cdot 8\text{H}_2\text{O}$. Definitely no 4-fold inversion axis is coincident with the crystallographic twofold axis. However, distorted polyhedra which approach the necessary symmetry requirements can be discerned. For

t) Sj

L

٥f

Cā:

La(1) the "square faces" consist of Aq(1)-O(5)-Aq(2)-O(3)with O(4) at the caps. The four atoms in the "square face" are within $0.26\ \text{A}$ of the average plane and the face angles are 97, 80, 99 and 79^{0} for a total of 355^{0} . The O(4)-La(1)-O(4) angle is 173° , with La(1)-O(4) making about an 84° angle with the plane. In the analogous La(2) polyhedron, Aq(3), $\mathrm{O}(4)$, $\mathrm{O}(1)$ and $\mathrm{O}(3)$ form the "square" and $\mathrm{O}(5)$ are at the apices. All the atoms of the "square" fall within 0.21 Å of the average plane. The O(5)-La(2)-O(5) angle is 169° and the La(2)-O(5) line makes about a 74° angle with the average plane. The sum of the "square" angles, however, is 379°, indicative of a more highly distorted bicapped square antiprism arrangement about La(2) than La(1). The greater distortion for La(2) might be expected since two of the equatorial sites have a short separation due to bidentate coordination by the 4-fold carbonate. One feature of the bicapped square antiprism model which corresponds to the experimental geometry is that the cap sites should be more distant from the metal than the others. In the $La_2(CO_3)_3 \cdot 8H_2O$ the oxygens in these sites are 0.1 to 0.2 Å further from the metals than the other ligands.

A useful model for the coordination polyhedra in $\operatorname{La_2(CO_3)_3\cdot 8H_2O}$ may be derived from the dodecahedron. Using the numbering rules suggested by Muetterties and Wright as shown in Figure 8a, sites 5 and 6 are occupied by bidentate carbonates which split each site, Figure 8b. The splitting of the sites alone lowers the model symmetry to $C_{2\,V}$. The

polyhedra symmetries are actually lower in the lanthanum carbonate structure since the orientation of the carbonates as well as that of the other ligands prohibits the presence of mirror planes, thereby further reducing the symmetry to C2. An ideal dodecahedron may be visualized as two interpenetrating orthogonal trapezoids. In the present cases the trapezoids are neither quite planar nor orthogonal. The planes of the two trapezoids about each metal were calculated by the least-squares technique using the appropriate carbon coordinates as the positions of substituted bidentates. The standard deviations of these planes are 0.04 and 0.27 Å for the two La(1) planes and 0.16 and 0.01 Å for those of La(2). The angles between the planes are 86 and 87^{0} respectively for the La(1) and La(2) coordinations. Normally a dodecahedron is described by two angles $\boldsymbol{\theta}_{\mathbf{A}}$ and $\boldsymbol{\theta}_{\mathbf{R}}$ as is indicated in Figure 8a. The predicted values of $\theta_{\mathbf{\lambda}}$ and $\theta_{_{\rm D}}$ for a hard sphere dodecahedral model are about 37^{0} and 70° respectively. On the basis of energy considerations, Hoard and Silverton⁴⁰ calculated values of 35.2 and 73.5^{0} . The corresponding angles in the present case compare favorably with these values if only the angles involving unidentate ligands are considered. In the La(2) polyhedra $heta_{ extbf{A}}$ is 35^{0} and θ_{R} is 73^{0} . For La(1) the corresponding angles are 33° or 32° and 74° . Thus the polyhedra in question, although distorted from $C_{2\,V}$, approximate the symmetry of the suggested dodecahedral derivative model.

Which of the models just described is most appropriate for this structure? An examination of the various structural models indicates the ease with which they may be interconverted without significantly changing individual atom environ-The bicapped square antiprism and dodecahedron modifications are in fact special cases of the model based on the pentagonal pyramid. In the bicapped square antiprism the two opposite edges containing the 2-fold axis are oriented about 600 apart and in the dodecahedron the angle is 90° . The model from the pentagonal pyramid permits any angle between 0 and 90° . The observed angles are 87° for the La(2) case and 83° for the La(1) case. On this basis the best description of the polyhedra is probably as dodecahedral models distorted slightly towards a bicapped square antiprismatic arrangement. However, such a description should be regarded only as a conceptual tool since the polyhedra are of low symmetry.

Carbonate Ions

The geometries obtained for the two carbonate ions indicate they are somewhat distorted. The 4-fold carbonate is planar due to symmetry requirements but one bond length is apparently longer than the others, 1.30 ± 0.06 Å versus 1.25 ± 0.03 Å. The bond, to the terminal uncoordinated oxygen, has an unusually large thermal parameter. This bond is expected to be shorter than those to coordinated oxygens. For example, in the nitrate ions of the species

Ce₂Mg₃(NO₃)₁₂·24H₂O ³⁵ and Th(NO₃)₄·5H₂O ⁴¹ the terminal oxygens have the shortest bond lengths and large thermal parameters. Because of the high standard deviation of these lengths, further conjecture seems unwarranted. In the case of the 8-fold carbonate the atoms are planar within experimental error and the bond lengths are approximately equal, 1.28 Å. The C-O distances reported in other carbonate structures range from 1.23 Å in Na₂CO₃·2H₂O ⁴² to 1.31 Å in Na₂Ca₂(CO₃)₃ ⁴³, however, the often-cited value for calcite is 1.294 Å. ⁴⁴ The O-C-O angles do not equal 120°, and only for the 4-fold carbonate is deviation from 120° within the limits of experimental error. Interestingly, the angles are less than 120° if both oxygens are coordinated to the same metal and greater if they are not.

Hydrogen Bonding Evidence

The distances observed for many of the 0-0 bonds involving water molecules strongly suggest the existence of hydrogen bonds. In the final electron density difference map several residual peaks appeared in positions appropriate for bonding hydrogens. The attempts to refine some of these parameters met with only limited success. The most reasonable results were obtained for hydrogens located between the terminal carbonate oxygen, O(2), and the water molecules, Aq(3). But even here the calculated parameters were somewhat improbable. Unfortunately the location of the hydrogen atoms will require more accurate data.

Observations Concerning Previous Investigations

Knowledge of the $La_2(CO_3)_3 \cdot 8H_2O$ structure allows interpretation of some of the reported results of the lanthanide carbonate systems reviewed in the introduction. The lighter lanthanide carbonates should normally occur as octahydrates isomorphous to this lanthanum compound. Preliminary work indicates this is true for the praseodymium analogue. However, two of the water molecules are so loosely bound that stoichiometries as low as the hexahydrate will be observed occasionally4,6. The hexahydrate should be observed in thermal decomposition of octahydrate as a stable intermediate although it has not always been reported. Observations of dihydrates in thermal studies suggest they too are structurally similar to the octahydrate. The infra-red data reported for $Ln_2(CO_3)_3 \cdot 8H_2O$ should be interpretable from the structure. The spectral assignments of the carbonate ions may be complicated since carbonate oxygens are involved in both bidentate and unidentate bonding and also are hydrogen bonded to water molecules. The symmetry of the ion is $\textbf{C}_{2\,\textbf{V}}$ for the 4-fold carbonate and $\textbf{C}_{\textbf{c}}$ for the 8-fold ion, although the site symmetries are lower, C_2 and C₁ respectively. These symmetries will cause splitting of the fundamental frequencies corresponding to the free ion. More accurate atomic parameters are required for a quantitative analysis of the carbonate ion spectra. The expected assignment of spectral bands to water molecules bound to

the metals have been reported. Although the structures of the dihydrate and anhydrous carbonate cannot be predicted it is possible that the basic layer structure observed in the lanthanum compound also would be found in these cases. It is also probable that the metal coordination numbers in these structures are either less than ten or that they remain the same by substitution of carbonate oxygens for water molecules in the coordination sphere. Neodymium seems to represent the borderline in stability between the octahydrate and dihydrate. The structure determination of crystals of $\mathrm{Nd}_2(\mathrm{CO}_3)_3$ - $\mathrm{XH}_2\mathrm{O}$ should be of great interest.

V. INTRODUCTION

Lanthanide oxide fluorides are often encountered as contaminants in investigations of the metal trifluorides. The stoichiometric phases, LnOF, have been studied most frequently, but the number of reported investigations is still small—about twelve. Undoubtedly the sparsity of data reported for these oxide fluorides results from the variability of the anion composition. This variability, which is extensive in some instances, makes the attainment of accurate property data difficult. The significance of this variability problem appears evident in the lack of agreement of reported structural parameters and even structural types for nominally identical stoichiometries.

Literature

Klemm and Klein⁴⁵ studied the phases in the lanthanum-oxygen-fluorine system using X-ray powder diffraction. They prepared a series of samples of the composition $\text{LaO}_{1-x}F_{1+2x}$, $-0.5 \leq x \leq 1.0$ by heating appropriate mixtures of LaF_3 and La_2O_3 at 900° in vacuum. In the region $0.0 \leq x \leq 0.5$ they observed an apparently face-centered cubic phase of the CaF_2 type. Samples with a value of x > 0.5 contained both the cubic phase and LaF_3 . For $x \simeq -0.02$ the authors observed another phase, which they thought to be tetragonal. Both this phase and La_2O_3 coexisted for x < -0.02. Zachariasen⁴⁶

has made the most prominent contribution to lanthanide oxide fluoride crystal chemistry. Employing X-ray powder diffraction techniques he investigated the hydrolysis products of lanthanum and yttrium fluoride as a function of their molecular weight. In both of these systems he observed a rhombohedral phase for the stoichiometric LnOF. This was apparently the same phase identified as tetragonal by Klemm and Klein. For lower fluoride content, x < 0.0, both the rhombohedral oxide fluoride and the oxide were present. composition range $0.0 \le x \le 0.3$ a tetragonal phase was observed. The dimensions of this unit cell increased with increasing fluorine content. For higher fluoride content, x > 0.3, the tetragonal phase and the trifluoride were present. Both the rhombohedral and tetragonal structures are superstructures derived from fluorite. The superstructures result from ordering of the oxygen and fluorine atoms into These structures will be discussed in detail special sites. in the next section. Zachariasen also studied the tetragonal PuOF and cubic AcOF phases. In the cubic phase it was assumed that the oxygen and fluorine atoms were statistically distributed over the 8-fold anion sites. Zachariasen postulated that the disordered cubic phase should exist at high temperature for all lanthanide oxide fluorides. However, his attempts to prepare cubic samples of LaOF and YOF by quenching were unsuccessful, although the intensity of the superstructure lines was decreased.

At approximately the time of Zachariasen's publication other somewhat contradictory reports appeared. Hund^{47,48}

a tetragonal phase by cooling approximately stoichiometric mixtures of Y2O3 and YF3 slowly from 900°. However, when samples with a slight fluoride excess were quenched from 1200° the product diffraction patterns were typical of a fluorite structure. Disordering of oxygen and fluorine atoms was postulated for the cubic phase. Mazza and Iandelli reported the possible formation of solid solutions between oxide fluorides and fluorides. The increase of fluoride content increased the lattice parameters of the cubic cells for PrOF, NdOF and SmOF. These workers also reported reflection spectra of these and related phases. Zalkin and Templeton reported a cubic HoOF phase formed in attempt to prepare NaHoF4. This report must be regarded with some doubt since the product was a mixture of two phases.

More recent investigations of the lanthanide oxide fluorides, are in agreement with Zachariasen's results. Templeton and Dauben⁵¹ found the pyrohydrolysis product of TbF₄ to be rhombohedral TbOF. Popov and Knudsen⁵² prepared the rhombohedral LnOF, Ln = lanthanum to terbium, by the pyrohydrolysis of the corresponding trifluorides. In the cases of PrOF, CeOF, and TbOF the hydrolysis was carried out with moist hydrogen. The authors noted the oxide fluorides are soluble only in hot sulfuric or perchloric acids. Rhombohedral lattice parameters for these preparations were given in a later report⁵³. Vorres and Riviello⁵⁴ prepared rhombohedral LaOF and YOF by heating the sesquioxide

an: of

> at th fo

7.0

I (

We

we se

ti ti

0)

0: 0: 0: 1

cs a

p.

and trifluoride at 1000°. They prepared isomorphous phases of Y, Dy, Er, Tm, Yb and Lu by hydrolysis of the trifluorides at 500°. These authors also observed tetragonal phases on the exterior of pellets used in the preparation of LiLnF4 for Ln = europium to ytterbium. Batsanova and co-workers⁵⁵, ⁵⁶ have prepared the stoichiometric oxide fluorides (La, Pr, Nd, Sm, Gd, Dy, Ho, Er, and Yb). Two methods of preparation were used; hydrolysis of the trifluoride at 800-900° and reaction of Ln2O3 and LnF3 at 1000-1100°. All preparations were rhombohedral except LaOF and NdOF prepared by the second method which were cubic. The authors reported densities, refractive indices and infrared spectra for many of these phases and rhombohedral lattice parameters of the Dy to Yb phases.

The recent report of the crystal structure of scandium oxide fluoride by Holmberg⁵⁷ is also of interest. ScoF crystallizes in a monoclinic space group isotypic with that of monoclinic ZrO₂. Each scandium is surrounded by four oxygen and three fluorine atoms. The structure analysis confirmed that the oxygen and fluorine atoms are situated in specific sites. In contrast Kutek⁵⁸ has prepared a cubic ScOF by a slightly different method. Apparently the oxygen and fluorine atoms were disordered in this fluorite-type phase.

Structures of the Lanthanide Oxide Fluorides

Three crystal structure modifications have been observed for the lanthanide oxide fluorides; rhombohedral, tetragonal, and cubic. Each of these structures may be related to that of fluorite, CaF2. In the fluorite structure, Figure 9a, each metal is at the center of eight anions situated at the corners of a cube and each anion has a tetrahedron of metal ions about it. The resulting symmetry is cubic, space group Fm3m, with four molecules per unit cell. It is common to place the metals at 000 plus F.C. (face-centered translations) and the anions at $\pm (\frac{1}{4}, \frac{1}{4}, \frac{1}{4})$ plus F.C. Alternatively, by choosing a different origin the anions are placed at 000 and $\frac{1}{2} \frac{1}{2} \frac{1}{2}$ plus F.C. and the metals at $\frac{1}{4} \frac{1}{4} \frac{1}{4}$ plus F.C. The radius ratio requirement for fluorite type structures is $r(M)/r(X) \ge 0.73$. The fluorite structure occurs only with relatively large metal ions. The ionic radii of the lanthanides⁵¹ range from 1.061 Å for La³⁺ to 0.848 Å for Lu³⁺. Assuming an anion radius of $1.38 \stackrel{\circ}{A}$ in the oxide fluorides, a radius ratio range of 0.77 to 0.61 is calculated for the trivalent lanthanides. Thus not all the lanthanide oxide fluorides should be stable with an undistorted fluorite lattice.

In the cubic lanthanide oxide fluorides, in which the cations occupy the normal metal sites in fluorite, one of two possible anion arrangements may exist. The first of these possibilities is that the oxygen and fluorine atoms

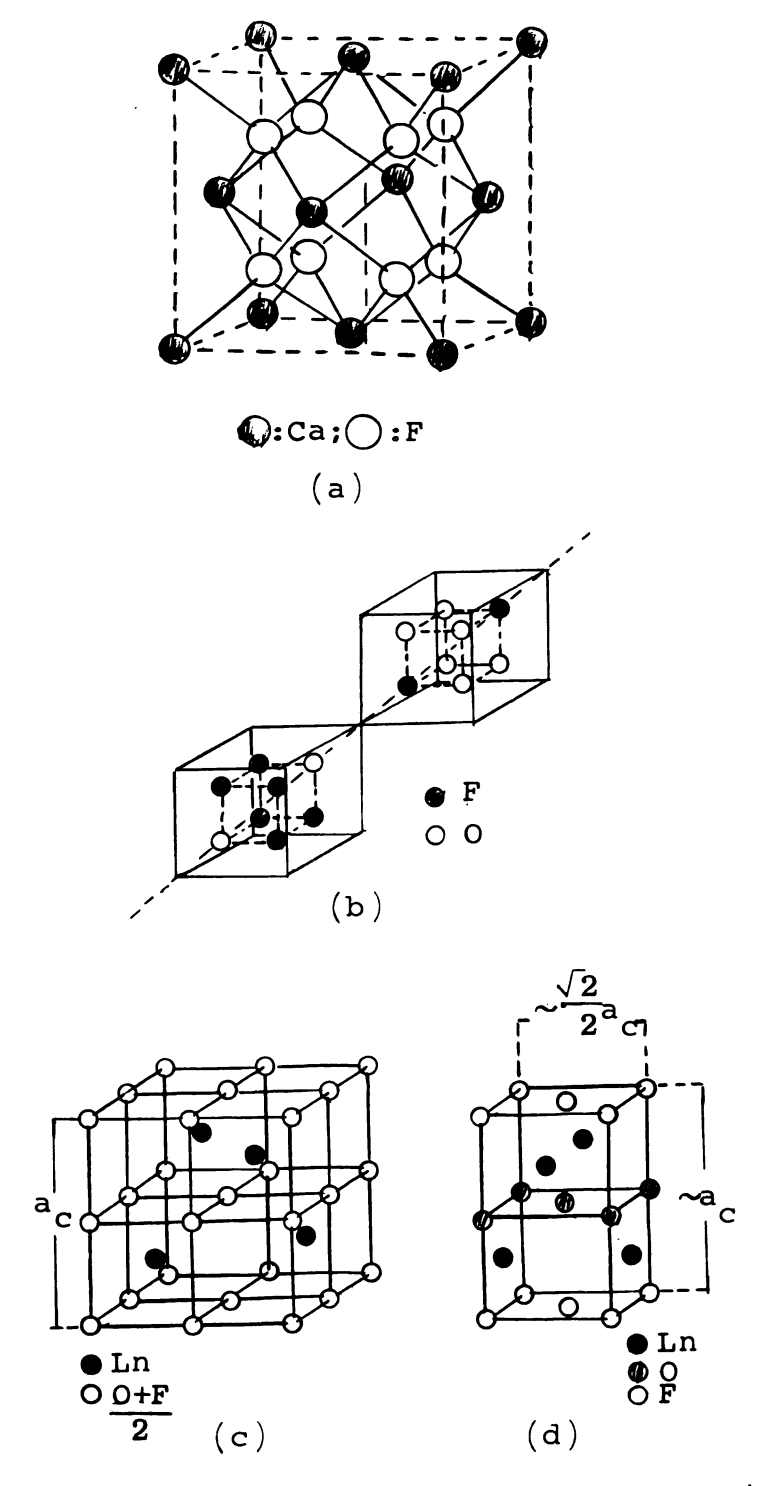


Figure 9. Lanthanide oxide fluoride structures. (a) Fluorite structure. (b) Ordering of oxygen and fluorine in rhombohedral LnOF. (c) and (d) Disordered cubic and ordered tetragonal LnOF structures.

are distributed statistically in the 8-fold sites of space group Fm3m. The second is that the oxygen atoms occupy one of the 4-fold sets of space group $F\overline{4}3m$ ($\underline{i}.\underline{e}.$ $\frac{1}{4}$ $\frac{1}{4}$ $\frac{1}{4}$ plus F.C.) and the fluorine atoms the other 4-fold set. Such a structure would consist of alternate layers of oxygen and fluorine atoms parallel to (111). The possibility of an ordered cubic structure has hardly been considered in the literature. These two possible cubic structures would be indistinguishable by normal X-ray diffraction techniques because of the similar magnitude of the oxide and fluoride ion scattering factors in comparison with those of the lanthanides.

The cubic fluorite structure may be referred to a rhombohedral unit cell. The transformation matrix is:

$$\begin{array}{c|cccc} 1 & \frac{1}{2} & \frac{1}{2} \\ \frac{1}{2} & 1 & \frac{1}{2} \\ \frac{1}{2} & \frac{1}{2} & 1 \end{array}$$

This places the endpoints of the rhombohedral translations at the most distant face-centers of a cubic cell. The rhombohedral lattice parameter, a_r , equals $\sqrt{1.5}$ a_c and the angle α is 33.56° . In the bimolecular rhombohedral unit cell observed by Zachariasen and others for LnOF, α varies between 33.0 and 33.2° . This variation suggests a small distortion from the cubic cell. The atoms all occupy the special positions of space group R3m, \pm (xxx). For LaOF; \times (La) = 0.242, \times (F) = 0.122 and \times (0) = 0.370. For perfect

respectively. Zachariasen's distinction between oxygen and fluorine atom sites was based on symmetry and size considerations. As is shown in Figure 9b the ordering of oxygen and fluorine atoms permits 3-fold symmetry about only one body diagonal of the original cube. The anions are arranged in alternating pairs of layers, -F-F-O-O-F-F-, normal to this 3-fold axis.

The cubic fluorite lattice may also be referred to a bimolecular tetragonal unit cell. The transformation matrix is:

$$\begin{vmatrix} -\frac{1}{2} & \frac{1}{2} & 0 \\ \frac{1}{2} & \frac{1}{2} & 0 \\ 0 & 0 & 1 \end{vmatrix}$$

As is indicated in Figures 4c and 4d the tetragonal lattice parameters would be $a_t = \frac{\sqrt{2}}{2} a_c$ and $c_t = a_c$ or $\sqrt{2}a_t$. In approximately stoichiometric LaOF, Zachariasen observed c/a = 1.43 rather than 1.414. In this structure, assigned to space group P4/nmm, the fluorine atoms are at 000 and $\frac{1}{2} \frac{1}{2} 0$, the metal atoms at $\frac{1}{2}$ Oz and $0\frac{1}{2}$ and the oxygen atoms at $00\frac{1}{2}$ and $\frac{1}{2} \frac{1}{2} \frac{1}{2}$. The value of z is 0.222 rather than 0.25. In this case the slight distortion from cubic symmetry results from the ordering of the oxygen and fluorine atoms into alternate layers normal to the 4-fold axis.

The fluorine-rich tetragonal phases must accomodate more than four anions per unit cell. This excess probably is located at the interstitial sites $\frac{1}{2}$ 0z and $0\frac{1}{2}$ z, z \simeq 0.75. For LaO.₇F_{1.6}, 1.4 0 and 0.6 F occupy the oxygen positions and 0.6 F are in the intersitial sites. Zachariasen noted that the intensity of the superstructure lines decreased in diffraction patterns of tetragonal samples as fluoride content increased. From this observation he concluded that z for the metal positions increased with increasing fluoride content. No consideration in the literature has been given to a cation vacancy structure.

The tetragonal and rhombohedral structures represent superlattices of the fluorite structure. The corresponding reflections listed in Table IX indicate the manner of splitting due to superstructure.

Table IX. Corresponding reflections in LnOF phases

Cubic	Tetragonal	Rhombohedral
111	101	110, 222
200	110, 002	211
220	200, 112	$10\overline{1}, 332$
311	103, 211	200, 321, 43
222	202	220, 444
400	220, 004	422
331	301, 213	$21\overline{1}$, 442 55
420	310, 222	310 , 5 43
422	312, 204	$2\overline{11}$, 431, 65

In Table X the structural data reported for cubic rhombohedral lanthanide oxide fluorides are tabulated. The rhombohedral parameters listed for the cubic phases were

Table X. Reported LnOF structural data

a) Rho	ombohedral	7			
Ln3+	Radius ¹ A	ar ² A	α deg.	V/Molc ³	Ref
La	1.061	7.132	33.01	47.87	46
La	1.061	7.111	33.12	47.75	54
Pr	1.013	7.016	32.99	45.66	5 3
Nd	0.995	6.953	33.04	44.43	5 3
Sm	0.964	6.865	33.07	42.85	5 3
Eu	0.950	6.827	33.05	42.09	53
Gd	0.938	6.800	33.05	41.57	5 3
Tb	0.923	6.758	33.02	40.74	53
Tb	0.923	6.751	33.09	40.80	51
Dy	0.908	6.716	33.07	40.12	54
Dy	0.908	6.685	33.10	39.39	56
НО	0.894	6.647	33.15	39.06	54
НО	0.894	6.637	33.16	38.67	56
Y	0.89	6.697	33.20	40.08	46
Er	0.881	6.628	33.14	38.7 3	54
Er	0.881	6.625	33.21	38.77	56
Yb	0.858	6.545	33.30	37.87	56
b) Cul	pic				
Ln ³⁺	Radius ¹	a o A	ar Ar	V/Molc ³	Ref
	8	Ä	Ä	Å3	
La	1.061	5.756	7.050	47.68	45
Ce	1.034	5.703	6.984	46.33	5 3
Pr	1.013	5.644	6.912	44.95	49
Nd	0.995	5.595	6.852	43.79	49
Sm	0.964	5.519	6.759	42.03	49
Но	0.894	5.523	6.764	42.12	50
Y	0.89	5.363	6.568	38.56	47

 $^{^1{\}rm Ln}^{3\,+}$ radii (Å) reported by Templeton and Dauben $^{5\,1}$, value for Y3 $^+$ estimated from relevant ${\rm Ln}_2{\rm O}_3$ and ${\rm LnF}_3$ crystal data.

²Reported errors range from $0.001~\text{\AA}$ to $0.005~\text{\AA}$.

 $^{^{3}}$ Volume per molecule LnOF.

 $^{^4\}text{a}_\text{r}$ = $\sqrt{1.5}$ $^{\text{a}}_\text{C}$ - for a rhombohedral cell with α = 33.560.

derived for a cell with $\alpha=33.56^{\circ}$ and $a_r=\sqrt{1.5}~a_c$. Also listed are the ${\rm Ln}^{3+}$ crystal radii and the calculated volume per molecule of LnOF. It is interesting to note that parameters observed for nominally identical phases often differ. In general the parameters decrease regularly with the size of the metal ion but the values listed for rhombohedral YOF seem too large on the basis of the given ion radius. Most of the molecular volumes of the cubic phases are less than those of the corresponding rhombohedral phases, as much as 3.7% in the case of YOF.

Purpose of this Research

The primary purpose of this research was to investigate phase transitions of lanthanide oxide fluorides at high temperatures. It was intended that the study would be confined principally to the rhombohedral phases, which reportedly exist only for the stoichiometric LnOF. Data such as transition temperatures were to be correlated to the crystal chemical properties of these systems.

Subsequently it was found desirable to make representative surveys of: the phases existing for various ${\rm LnO}_{1-x}{}^{\rm F}_{1+2x}$ stoichiometries, the effect of composition changes on the transitions and the nature of the decomposition of LnOF at high temperatures. These investigations provided much definitive data but also exposed several paths for future research.

VI. EXPERIMENTAL

Preparations

Lanthanide trifluorides were prepared by conversion of commercial oxide specimens with ammonium fluoride according to the following equation:

 $Ln_2O_3 + 6NH_4F \longrightarrow 2LnF_3 + 3H_2O^{\dagger} + 6NH_3^{\dagger}$ Mixtures of 99.9% Ln₂O₃ (Michigan Chemical Company) and a 50% excess of reagent NH₄F (J.T. Baker Chemical Company) were heated in platinum boats. The reaction was accomplished in a Vycor tube situated in a horizontal tube furnace. A flow of dried inert gas was maintained through the reaction vessel. The temperature was initially elevated slowly to $150-200^{\circ}$ during a 3-4 hour period, then increased to 350-5000 where it was maintained for 2-4 hours before being cooled to room temperature. The completeness of the conversion was established by the increase in weight of the lanthanide phase as well as by X-ray powder diffraction identification of the products. In most preparations, normally 4-6 grams of the trifluoride, the weight increases deviated less than 1% from the theoretical values after a single treatment. On occasion further heating with additional ammonium fluoride was required to produce the desired product.

Preparations of the lanthanide oxide fluorides, LnOF, were attempted by two techniques. In the first method the trifluorides of lanthanum, terbium and ytterbium were hydrolyzed in air at approximately 850, 500 and 900° respectively. In the second technique equimolar mixtures of the sesquioxide and trifluoride, thoroughly mixed and compacted in platinum boats, were heated in an inert gas atmosphere. In a typical preparation the temperature was increased from 25° to about 1050° during a 3 hour period, maintained there 4-5 hours, gradually lowered to 500-6000 in 2-3 hours and then to room temperature. The rhombohedral oxide fluorides of La, Nd, Sm-Gd, Dy-Er and Y were prepared by this technique. Identification of these phases was by comparison of the X-ray powder diffraction data to values found in the literature. The observed data are given in Tables XXII to XXIV in Appendix II. Weight loss during heating was invariably less than 0.5% for samples which varied from 2-10 grams.

Phases of the general stoichiometries $\operatorname{LnO}_{1-x}F_{1+2x}$, $\operatorname{Ln}=\operatorname{Nd}$, Gd , Dy and Er , were prepared from the sesquioxide and trifluoride in a manner identical to that described above. Eight gadolinium preparations $(-0.1 \stackrel{<}{\sim} x \stackrel{<}{\sim} 0.5)$, six neodymium and erbium preparations $(-0.1 \stackrel{<}{\sim} x \stackrel{<}{\sim} 0.4)$ and a dysprosium phase $(x \stackrel{\sim}{\sim} .25)$ were prepared.

Analytical

Two methods were employed for metal analysis: direct ignition to the oxide at approximately 850° or dissolution

in hot sulfuric acid, precipitation of the oxalate and subsequent ignition to the oxide. Precision and undoubtedly accuracy were best with the former method.

Both oxygen and fluorine contents were determined by neutron activation at the Dow Chemical Company, Midland, Michigan. The stoichiometries of the tetragonal phases were deduced from the metal and fluorine contents. Results of analyses are given in Table XI.

X-Ray Diffraction

X-Ray powder diffraction data were obtained by two techniques, both employing copper radiation. Most routine phase analyses were accomplished from Debye-Scherrer photographs prepared with 114.59 mm Norelco cameras. Data obtained on a Siemens diffractometer from samples mounted on glass plates were used for more accurate results and for the calculation of lattice parameters. Platinum powder (99.98% pure, J. Bishop and Co. Platinum Works) for which a = 3.9231 $^{8.9}$ was mixed with these samples. Lattice parameters were calculated using Vogel and Kempter's least-squares program. 18

High Temperature X-Ray Diffraction

High temperature X-ray diffraction data were obtained with a Materials Research Corporation high-vacuum diffractometer attachment, 60 model X86-G, mounted on a Siemens diffractometer. In this unit the sample was situated on a

Table XI. Analytical results

a) Metal Analyses in $LnO_{1-x}F_{1+2x}$

Ln	х	Ln(calcd)	Ln(found)	#Samples
La	~0	79.86	80.2 ± 0.3	2*
Nd	~0	80.43	80.45± 0.1	2 2*
Nd	~0	80.43	80.5 ± 0.3	2*
Sm	~0	81.13	81.13± 0.1	3
Eu	~0	81.28	81.08± 0.1	2
Gd	~0	81.79	81.79± 0.1	3
Tb	~0	81.98	81.4 ± 0.3	2*
Dy	~0	82.22	82.7 ± 0.3	2*
HO	~0	82.49	82.9 ± 0.1	2
Er	~0	82.69	82.54± 0.1	2
Y	~0	71.67	71.69± 0.1	4
Nd	0.27 ± 0.02	77.9	78.2 ± 0.3	2* 2*
Gđ	0.28 ± 0.02	79.3	79.1 ± 0.3	
Dy	0.23 ± 0.02	80.2	79.5 ± 0.3	2*
Er	0.20 ± 0.02	80.9	80.82± 0.1	2

^{*}Determined by oxalate precipitation. Probable errors based on variance found in all analyses.

b) Oxygen and Fluorine Analyses in LnO F 1+2x

Ln	x	O (calcd)	O (found)	$_{(calcd)}$	F (found)	F/Ln
Nd Nd Gd Dy Er	$egin{array}{l} 0.02 \pm 0.02 \\ 0.27 \pm 0.02 \\ 0.28 \pm 0.02 \\ 0.23 \pm 0.02 \\ 0.20 \pm 0.02 \\ \hline \end{array}$	8.7 6.3 5.8 6.1 6.2	6.7±0.6 7.8±0.7 5.8±0.5 5.7±0.5 5.2±0.5	11.1 15.8 14.9 13.7 13.0	14.9±0.3 13.6±0.3	1.05±0.04 1.54±0.04 1.56±0.04 1.46±0.04 1.41±0.04

metal ribbon resistance heater. Flat heaters of 5 mil platinum-40% rhodium or 5 mil platinum were used. Samples were ground to a fine powder in dry <u>n</u>-heptane and a few drops of this slurry were placed on the heater. The samples covered an area approximately 5 x 8 mm and were 0.1-0.4 mm thick. The heaters with mounted samples were connected to the electrical leads in the normal position for a horizontal diffractometer, <u>i.e.</u> sample surface is in a vertical position.

Temperature measurement proved to be a difficulty. The thermocouples provided by the manufacturer acted as a heat sink, caused the heater temperature to be lower at the point of attachment than at other areas. Also these thermocouples junctioned within the diffractometer attachment near the sample. Consequently the reference temperature was unknown and increased with heater temperature. Finally the temperature of the sample surface was lower than the heater temperature. The thermal gradient was particularly large, for specimens of the rhombohedral oxide fluoride -- as much as 100^{0} at a surface temperature of 500^{0} . The cause of the gradient was due to either poor sample-heater contact or to the low thermal conductivity of the samples. Temperature measurements required in this study were generally below the range of optical pyrometry. To circumvent the difficulties mentioned above, temperature measurements were made by internal calibration. Platinum powder was mixed with the samples and the temperature was determined from its

lattice parameter expansion using the data tabulated by Campbell⁶¹. The lattice parameter of platinum was calculated from the position of the (311) reflection after the sample had been aligned at temperature, as described below. The reflection was scanned , 1/8 degree per minute, two or three times and its 2θ position determined reproducibly to $\pm 0.01^{\circ}$. Assuming zero alignment error this precision corresponded to a temperature uncertainty of $\pm 10^{\circ}$ and the probable error may have been $\pm 20^{\circ}$. The accuracy of the measurements was confirmed by temperatures observed in thermal analyses, described in a later section.

Most high temperature experiments were run under vacuum conditions. A two inch oil diffusion pump was connected to the diffractometer attachment via two pieces of 9.5 mm bore Tygon-R vacuum tubing through two 6.4 mm diameter vacuum ports. Pressures measured in the vacuum main by an ionization gauge were generally 4-8 x 10⁻⁶ torr. However, small leaks occasionally present in the attachment raised the observed pressure to the 10⁻⁵ torr range. Undoubtedly the pressure was considerably higher within the camera because of the slow pumping speed through the small ports. In fact, at relatively low temperatures (900-1100°) hydrolysis of the lanthanide oxide fluorides was observed. The vacuum ports should be enlarged as the manufacturer has modified later models of the attachment.

Sample alignment was accomplished with controls for translation (sample horizontal displacement), azimuth rotation

and inclination rotation. In the initial alignment at room temperature these three controls were adjusted to produce maximum intensity for the platinum (111) reflection at 39.790 (2θ) . The most critical of the alignment controls was the translation adjustment. Fine adjustments of this control were made using the K_{C_1} peak of the platinum (311) reflection which occurs at 81.26° . The diffractometer itself had to be realigned if the values listed for (111) and (311) were not attainable simultaneously at room temperature. At high temperatures sample alignment was accomplished by adjusting the translation so that the (111) and (311) platinum reflection positions corresponded to identical lattice parameters. Unit cell measurements are much more sensitive to sample displacement at low than at high 2θ values. the parameter derived from the (311) reflection was used to adjust the (111) position. Repeated measurement-adjustment cycles produced the desired internal consistency, $\pm 0.01^{0}(2\theta)$.

Diffraction patterns were obtained over the temperature range $25\text{-}1000^{\circ}$ for most of the rhombohedral LnOF phases prepared. Initially scans were made for $2\theta = 25\text{-}50^{\circ}$ to find the phases present at a given temperature. With two phases present the fraction of each was estimated from the peak height of its most intense reflection relative to the height obtained with the corresponding pure phase. Lattice parameters of the high temperature phases were obtained in several instances. Attempts were made to quench observed high temperature modifications.

To obtain information regarding the nature of the phase transitions the thermal expansion of neodymium oxide fluoride, NdOF, was determined between 25 and 900° . Because of the poor quality of the diffraction lines at higher angles, the 2θ -range $25-60^{\circ}$ was generally examined, although some experiments were run to 120° . The rhombohedral-hexagonal lattice parameters were obtained by hand-fitting the five most intense isolated reflections. Cubic parameters were obtained by averaging all the observed diffraction data.

The effect of temperature on the structures of $LnO_{1-x}F_{1+2x}$ phases was also examined.

Differential Thermal Analysis

Differential thermal analysis (DTA) was used to determine transition temperatures in rhombohedral oxide fluorides, to study the effect of composition on the temperatures of these transitions and to discover any phase transitions in $LnO_{1-x}F_{1+2x}$, x>0.0.

A simple DTA apparatus was constructed. The sample holder was fabricated from 25 mm diameter 310 stainless steel rod. Two symmetrical 7.9 mm diameter, 12.2 mm deep, sample wells were drilled in the rod to accommodate sample and reference materials. These wells were lined with 5 mil platinum foil. One of the sesquioxides was used in each analysis as the inert reference. Both it and the sample were packed firmly in the appropriate well. A press-fit stainless steel cap covered the wells. The sample holder was enclosed in a

Vycor tube situated in a resistance tube furnace (type MK-70, Hevi-Duty Heating Equipment Company) and a dry inert gas was passed through the tube. A 36-gauge Iron-Constantan thermocouple enclosed in Inconel shields (Continental Sensing Company) was placed in each sample well through holes in the cap. The differential temperature was recorded on a Sargent Model SR recorder (1.0 millivolts full scale) while sample temperature was measured periodically with a Honeywell Model 2720 potentiometer. The sample temperature was calibrated at 99.4° with boiling water and at 583° with $K_2SO_4^{62}$. The observed temperatures were 100.4^0 and 589^0 . A correction of -1^0 per 100^0 was assumed over the temperature range of interest. Sample temperatures were read to \pm 0.5°. However, a probable error of \pm 2.0° seems more appropriate for temperatures obtained from DTA since these were obtained manually while the sample temperature was changing. Heating rates between 1 and 3^{0} per min. over the temperature range of interest were obtained by manual operation of a rheostat. In each run the differential temperature was measured in at least one heating and cooling cycle. The maximum temperature was in general less than 725° . However, in one run a temperature of 840° was attained and in another 1075°. Pt-Pt-10%Rh thermocouples were used in the latter experiment. The temperatures of any observed transitions were obtained from plots of the differential temperature(mv) versus sample temperature.

Thermal Decomposition of Neodymium Oxide Fluoride

A sample of NdO $_{1-x}F_{1+2x}$, $x\simeq 0.05$, was heated under high vacuum (less than 10^{-6} torr) in an out-gassed open tantalum crucible. The weighed sample was heated 52 hours at approximately 1475^{0} , 38 hours at approximately 1600^{0} and 10 hours at 1475^{0} to constant weight. Evolved products which had condensed on the glass chamber and final residual product were examined by X-ray powder diffraction.

VII. RESULTS

Preparations and Phase Analyses

Rhombohedral oxide fluorides specimens of La, Nd, and Sm-Er were prepared, however, X-ray diffraction and metal analyses indicated the presence of a slight excess of oxide in the DyOF and HoOF preparations. Several attempts to prepare rhombohedral YbOF were unsuccessful, yielding diffraction patterns with many unidentified reflections.

Four phases were identified by X-ray diffraction in the systems $LnO_{1-x}F_{1+2x}$, where x = -0.1 to +0.5 and Ln =Nd, Gd, and Er. Schematic illustrations of the X-ray results for $ErO_{1-x}F_{1+2x}$ are shown in Figure 10. For $x \simeq -0.1$, Ln_2O_3 and rhombohedral LnOF were present and at $x \simeq 0.0$ only the rhombohedral phase was observed. As the fluoride content was increased, x > 0.0, a tetragonal phase appeared together with the rhombohedral phase. The limits of the two phase region varied somewhat in the three systems studied. For the neodymium and erbium systems the tetragonal phase was in evidence for $x \simeq 0.05$ and was the dominant phase at $x \simeq 0.10$. In these systems, only the tetragonal phase was apparent for $x \simeq 0.15$. In the gadolinium system the strongest reflection of the rhombohedral phase was still present at $x \simeq 0.20$. The tetragonal phase existed with variable composition, $x \simeq 0.15$ to 0.25, for Nd and Er. The variations in stoichiometry were accompanied by changes

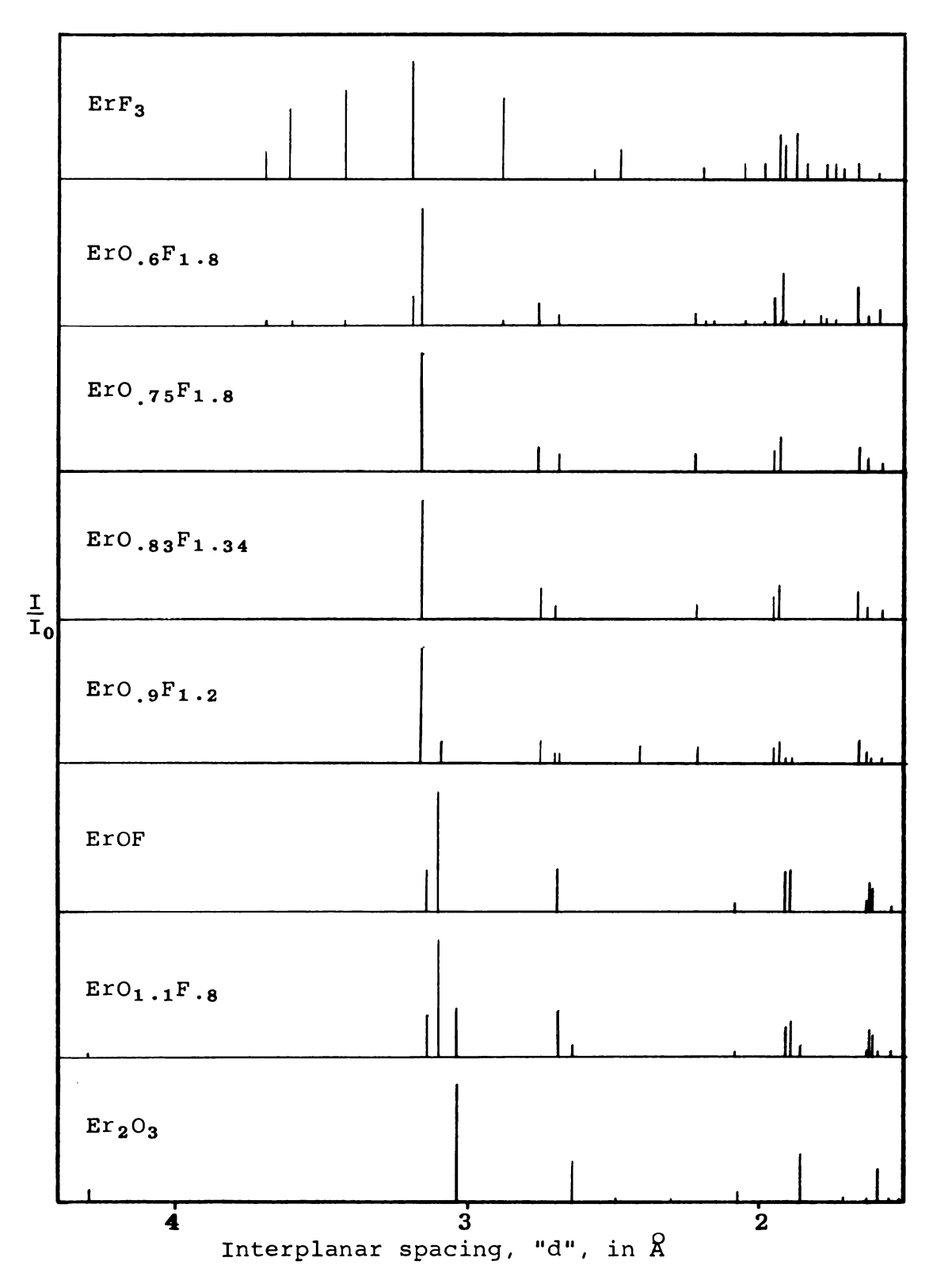


Figure 10. Schematics of X-ray diffraction patterns of Er-O-F phases.

in the lattice parameters. However for Gd the region of stability appeared to be much smaller, $x \simeq 0.25$. No change in the tetragonal reflection positions was perceptible in any gadolinium diffraction patterns in which the phase was a component. Table XII lists the structural data for tetragonal $LnO_{1-x}F_{1+2x}$ phases prepared in this study as well as those reported by Zachariasen. Diffraction data for the previously unreported phases are listed in Tables XVI to XXI in Appendix II. As the data in Tables XX and XXI indicate, diffraction patterns of the erbium phases contained several lines which could not be indexed. For greater than 0.25 the diffraction patterns exhibited lines of the trifluoride as well as those of the tetragonal oxide fluoride. The assignment of phases for the compositions $LnO_{1-x}F_{1+2x}$ is qualitatively supported by the thermal analysis results reported in the next section.

Phase Transitions

The existence of a rhombohedral to cubic structural transition was confirmed for the lanthanide oxide fluorides, LnOF. The transitions were observed for the Nd, Sm, Eu, Dy, Ho and Y phases using high temperature X-ray diffraction. Both the face-centered cubic and rhombohedral phases were perceptibly present over a 30° range about the transition temperature. It seems probable that the temperature gradient present in the sample accounted for part of this range. The temperature, determined by the platinum reflections, was

Table XII. Structural data for tetragonal $LnO_{1-x}F_{1+2x}$

Metal	x	a(Å)	c(Å)	c/a	$V/Molc(\mathring{A}^3)$
La*	0.0	4.083(1)**	5.825(1)	1.427(1)	48.55(2)
La*	0.3	4.098(2)	5.840(4)	1.425(2)	49.04(8)
Nd	~0.15	3. 999(2)	5.704(3)	1.426(2)	45.61(7)
Nd	0.27	4.014(3)	5.720(4)	1.425(2)	46.08(9)
Gđ	0.28	3.977(1)	5.528(1)	1.390(1)	43.72(2)
Dy	0.23	3.933(1)	5.451(1)	1.386(1)	42.16(2)
у*	0.0	3.910 (5)	5.43 (1)	1.389(4)	41.5 (2)
Y *	0.3	3.930 (5)	5.46 (1)	1.389(4)	42.2 (2)
Er	~0.15	3.893(1)	5.400(2)	1.387(1)	40.92(4)
Er	0.20	3.907(1)	5.385(1)	1.378(1)	41.10(2)

^{*}Parameters as given by Zachariasen

^{**}Standard deviation in last digit given in parentheses.

a mean value representative of the diffracting portion of the sample. At an observed mean temperature just below the transition temperature part of the sample will be above the transition-i.e., will produce the high temperature diffraction pattern. Analogously, above the transition temperature some of the sample will still exhibit a rhombohedral structure. Therefore the transition temperature is the temperature at which both phases are present in equal quantities. When samples were allowed to equilibrate for a few minutes no hysteresis effect was observed within the limits of error in temperature measurement. However at least partial quenching of the cubic phase was possible in the cases of neodymium, samarium and europium oxide fluorides. Attempts to quench other phases were unsuccessful. Some of the transition temperature and lattice parameter data obtained for the transitions were in error due to initial difficulties with temperature measurement. Transition temperatures and cubic lattice parameters considered reproducible are given in Tables XIII a and b.

Data for the thermal expansion of NdOF lattice parameters are given in Tables XIV a and b. It should be noted that α for the rhombohedral structure is constant within experimental error below the transition temperature. A plot of the NdOF volume per molecule <u>versus</u> temperature is illustrated in Figure 11. By linear extrapolation of the two volume-temperature lines to the transition temperature the

Table XIII. High temperature X-ray diffraction data for LnOF

a) Transition Temperature

Ln in LnOF	T(20% cubic)	T(50% cubic)	T(80% cubic)
Nd	504 ± 10°	519 ± 10°	534 ± 10°
Eu			<5 35
Gd	588	59 7	616
Dу	(558)	(573)	(588)
НО	579	59 3	607

b) Cubic Lattice Parameters

Sample	Temperature	$\mathtt{a}(\overset{\mathbf{O}}{\mathtt{A}})$
NdOF(quenched)	25 ± 10^{0}	5.631 ± .003
NdOF	648	5.685 ± .001
SmOF	539	5.606 ± .002
EuOF(quenched)	25	5.535 ± .002
EuOF	539	5.573 ± .002
GdOF	617	5.554 ± .005
DyOF	627	5.487 ± .005
H0 0F	620	5.466 ± .002

Table XIV. NdOF high temperature structural data

a) Rhombohedral

Run	т*	a _r *(Å)	* α	V/Molc*(83)
Ref. 25	25°	6.953	33.040	44.43
A1	2 5	6.949	33.06	44.43
D1	2 5	6.950	33.07	44.48
D 3 -H	152	6.963	33.05	44.66
A9-C	215	6.975	33.00	44.75
D4-H	215	6.976	33.00	44.82
A2-H	237	6.973	33.03	44.84
A0-C	265	6.983	33.03	44.92
D6-H	31 5	6.983	33.02	44.98
A7-C	3 66	6.993	32.98	45.06
D7-H	3 98	6.994	33.00	45.15
A3-H	418	6.997	32.98	45.18
A6-C	450	6.992	33.06	45.26
A5-C	480	6.992	33.07	45.29

^{*}Probable errors for T, a , α and V/Molc are 150, 0.004 Å, 0.030, and 0.04 Å3.

b) Cubic

Run	T*	a _C (A)	a _r (A)**	$V/molc(\hat{R}^3)$
D13-C	15 ⁰	5.6 31 (3)*	6.897	44.63(7)*
D 14- H	96	5.637(1)	6.904	44.77(2)
D15-H	258	5.647(2)	6.916	45.02(4)
B 1 -H	529	5.675(2)	6.950	45.70(4)
B 12-C	549	5.678(1)	6.954	45.76(2)
D16-H	559	5.675(1)	6.950	45.70(2)
в8 -с	569	5.678(2)	6.954	45.76(4)
D2 -H	569	5.678(1)	6.954	45.76(2)
B 7 -C	579	5.681(1)	6.958	${f 45.84(2)}$
B11-C	579	5.681(1)	6.958	45.84(3)
D17-H	588	5.679(2)	6.955	45.80(4)
в 2 -н	608	5.682(1)	6.959	45.85(2)
в9 -н	618	5.683(2)	6.960	45.89(4)
D 10- H	638	5.686(3)	6.963	45.96(7)
в 6 -с	648	5.685(1)	6.962	45.93(2)
C1 -H	648	5.685(1)	6.962	45.93(2)
в5 -с	668	5.688(1)	6.966	46.01(2)
B 10- H	697	5.690(1)	6.969	46.06(2)
D 11- H	697	5.688(3)	6.966	46.01(7)
B 4 -C	726	5.691(1)	6.970	46.08(2)
В 13- Н	736	5.693(1)	6.972	46.12(2)
в3 -н	756	5.692(1)	6.971	46.10(2)
C2 -H	786	5.696(1)	6.976	46.18(2)
B 14- H	878	5.703(1)	6.984	46.36(2)

^{*}Probable error in T is $15^{\rm o}$, standard deviations for a and V/Molc in parentheses.

^{**} $a_r = \sqrt{1.5} a_c$ for rhombohedral cell with $\alpha = 35.56^{\circ}$.

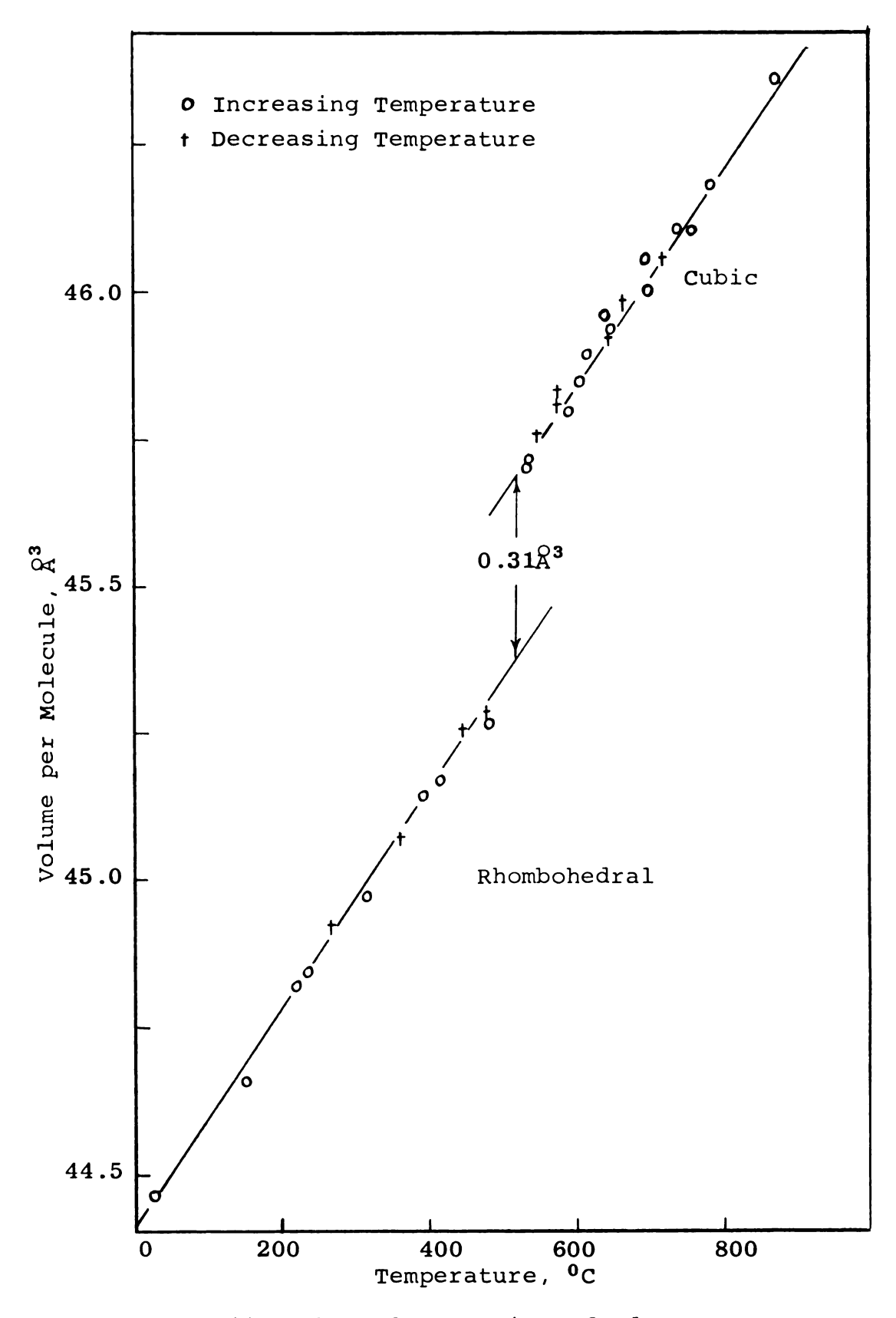


Figure 11. Thermal expansion of NdOF

volume change for the transition was estimated to be $0.31~\text{\AA}^3$. The change represents a small but significantly larger volume in the cubic structure. This is in marked contrast to the comparative results in the literature, Table X, which indicate the rhombohedral structure has the larger molecular volume. Also observed in the present study were the volumes per formula unit for rhombohedral HoOF at 25° and 571° (respectively 39.06 and $40.31~\text{\AA}^3$) and for cubic HoOF at 620° ($40.83~\text{\AA}^3$). Assuming a linear extrapolation of the rhombohedral data to 620° a volume difference of $0.41~\text{\AA}^3$ is calculated. The molecular volume of cubic EuOF quenched to 25° is $0.30~\text{\AA}^3$ greater than the analogous rhombohedral value. From these results a volume increase in the rhombohedral to cubic transitions of all the lanthanides is expected.

Differential thermal analyses confirmed the existence of the rhombohedral-cubic phase transitions in lanthanide oxide fluroides. The transitions observed for all LnOF preparations during both heating and cooling cycles are listed in Table XV. The temperatures at which the reaction commenced in heating and cooling cycles, T_1^0 and T_2^0 , generally agreed within T_1^0 and the temperatures of the peak maxima, T_1^1 and T_2^1 , agreed to within T_1^0 . However, the median values of reaction commencement and peak maxima, T_{med}^0 and T_{med}^1 , agreed to within T_{med}^0 0 or less and these were assumed to be the transition temperatures. The differences in T_1^0 and T_1^1 1 in heating and cooling cycles suggest hysteresis. Indeed, the evidence of hysteresis effects in the oxide fluoride

Table XV. Differential thermal analysis results

Stoich- iometry**	Heat- ing Rate o/min	T ₁ ⁰	T'i	Cool- ing Rate •/min	T ₂ ⁰	T ₂ ' 0	T _{med}	T'med
K_2SO_4 LaOF $NdO_{1.1}F8$	2 3.0 3.0	582.5 495 525	584 501 5 33	$\begin{array}{c} 2.0 \\ 2.0 \\ 2.0 \end{array}$	583.5 495 528	582 490 519	583 495 526	583 494 526
NdOF(1) NdOF(2) NdOF(3) NdO _{.93} F _{1.14}	3.0 2.5 3.0 3.0	526 530 528 522	535 535 534 533	2.0 2.0 2.0 2.0	507 507 520	500 497 514 (516)	517 517 524	518 516 524 524
NdO _{.85} F _{1.3} SmOF EuOF	2.0 5.0 2.0	- 527 5 13	- 535 518	3.0 2.0	- 521 513	- 515 509	- 524 513	- 525 513
GdO _{1.1} F.8 GdOF GdO.9F _{1.2}	3.0 3.0 3.0	602 611 612	610 615 617	2.0 3.0 2.5	606 605	602 595 599	604 608 608	606 605 608
GdO _{.8} F _{1.4} TbOF	3.0 2.0	- 549	- 556	- 2.0	- 554	- 545	- 552	- 550
DyOF YOF HOOF ErO _{1.1} F.8	2.0 2.5 3.0 3.0	560 569 588 588	563 578 594 593	1.5 2.0 2.5 3.0	557 570 590 585	552 567 582 579	558 570 589 586	558 572 588 586
ErOF ErO. ₉ F _{1.2} ErO. ₈₅ F _{1.3}	2.0 3.0 3.0	591 595 -	597 604 -	1.0 2.0	592 599 -	588 594 -	592 597 -	592 599 -

 $^{^{}st}$ The probable error in temperature measurements is 2^{0} .

 T_1^0 and T_2^0 are the temperatures at which the reaction commenced and T_1^i , T_2^i are the temperatures corresponding to the DTA peak in the heating and cooling cycles respectively.

^{**}Stoichiometries for $LnO_{1-x}F_{1+2x}$, x > 0.0, are approximate.

transition data is greater than that in the reversible transition data in K_2SO_4 also presented in Table XV. However, with the exceptions of the Nd and Sm cases the hysteresis effects are less than 10° . In general the transition temperatures are observed to increase from 4950 for LaOF to 5920 for ErOF. A noticeable exception to this trend is the 6060 transition temperature for GdOF. It was considered possible that the transition temperature varied significantly as a function of composition. The results listed in Table XV for $LnO_{1-x}F_{1+2x}$ suggest that composition does affect the transition temperature. However, over the range $-0.1 \lesssim x$ $\stackrel{<}{\sim} 0.1$ the change is small, about $10^{0}\,$, and would not account for the relatively high transition temperature of GdOF. Figure 12 illustrates the DTA results for $GdO_{1-x}F_{1+2x}$ which are typical. Notice that hysteresis increases with increasing fluoride content. The magnitude of the DTA peak also decreases as the proportion of rhombohedral phase decreases. Samples containing very little or no rhombohedral phase produce no DTA peaks in the temperature range examined. These analyses support the earlier conclusions based upon X-ray phase analysis.

The tetragonal phases, $\operatorname{LnO}_{1-x}F_{1+2x}$, were examined for a possible phase transition using both differential thermal analysis and high temperature X-ray diffraction. No endothermic DTA peaks were found in the temperature range studied for $\operatorname{GdO}_{.8}F_{1.4}$ below 725° , for $\operatorname{NdO}_{.85}F_{1.30}$ below 820° or for $\operatorname{ErO}_{.85}F_{1.30}$ below 1050° . In the latter two samples an

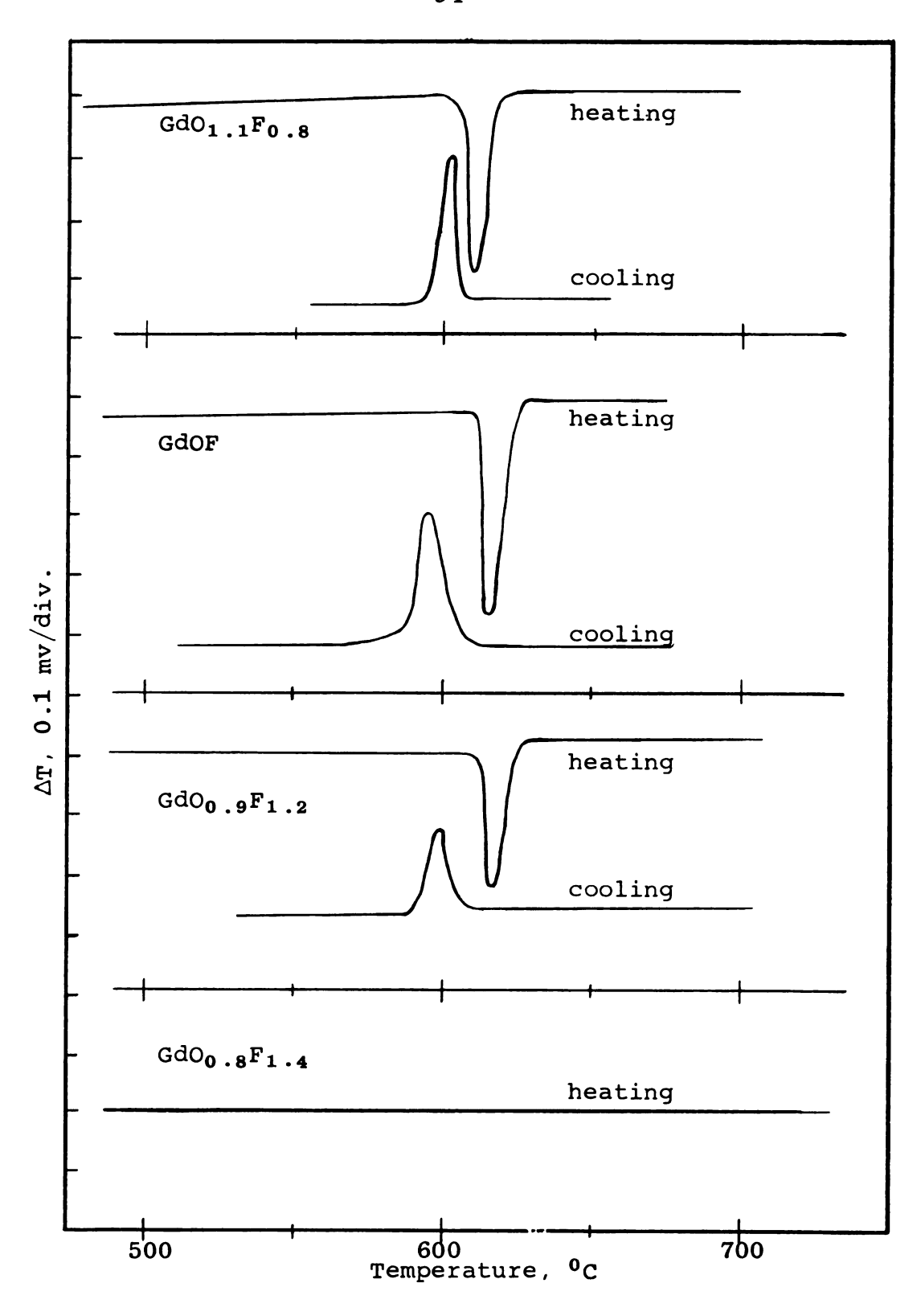


Figure 12. DTA curves for selected Gd-O-F stoichiometries.

exothermic trend which was observed above 8000 was assumed to result from hydrolysis of the sample. Above 1050° a sharp endothermic increase occurred for the ErO 85F1 3 case. This increase continued until heating was stopped at about 1075° . This endotherm probably resulted from sintering. Sintering was observed in all $LnO_{1-x}F_{1+2x}$ preparations (1050°) for x greater than 0.1. Examination of the tetragonal phases by high temperature X-ray diffraction was hampered by hydrolysis of the samples above 800° . No sharp structural transition was observed below 10000. Superstructure lines remained until the sample hydrolyzed to LnOF which was observed as a cubic phase at high temperature but reverted to the rhombohedral phase on cooling. However, changes in intensities of the tetragonal phases which were observed in these experiments could not be correlated with certainty to the hydrolysis reaction. A complete thermal analysis of the tetragonal phases will require further experimentation.

Decomposition of Neodymium Oxide Fluoride

In the thermal decomposition of neodymium oxide fluoride a dirty white product evolved which was examined by X-ray diffraction. The diffraction pattern was diffuse but was unmistakeably NdF_3 . The residue from the decomposition was a sintered mass of black-violet crystals. This dark crystalline mass became a lighter blue-gray when powdered. X-ray

diffraction of the residue indicated only $A-Nd_2O_3$. A 39% weight loss was observed in the decomposition. Assuming the following reaction:

$$3 \text{Ndof} \longrightarrow \text{Nd}_2 O_3 + \text{NdF}_3 \dagger$$
,

the calculated weight loss is 37.4%. However, fluorine analysis of the starting material indicated the stoichiometry was NdO $_{1-x}F_{1+2x}$, x=0.05. For this composition the calculated weight loss is 39.2%

VIII. DISCUSSION

The Phase Transition in Rhombohedral Oxide Fluorides

The transition of rhombohedral lanthanide fluorides to cubic symmetry at high temperature has been observed as predicted by Zachariasen. It would be desirable to describe the nature of these transitions structurally and thermodynamically. Such a description would require an exact structural knowledge of the rhombohedral and cubic phases. The ordered anion structure as given by Zachariasen for the rhombohedral phase appears well established, even though it was determined from powder data and the special anion positions were deduced from symmetry and size arguments. Zachariasen considered the cubic phase to have the CaF2 structure with a disordered anion arrangement. Little consideration has been given to a possible ordered cubic structure based on space group $F\overline{43}m$. Since the two alternatives would be indistinguishable a choice must be made on some other basis. If the disordered configuration has nearly the same internal energy as the ordered cubic structure, then the disordered structure should become increasingly stable with increasing temperature because of entropy-free energy arguments. That is, the disordered structure will be favored at high temperatures. Since transition from the ordered rhombohedral structure to another ordered structure would require complex anion migrations through intermediate configurations which are disordered, a transition

	١
I	
1	\langle
ĺ	\langle
	(
)
)
	l

to the disordered structure will be assumed in the following discussion. It will describe the general classification of phase transitions and will attempt to define the nature of the transitions in lanthanide oxide fluorides.

Polymorphism is the phenomenon of a chemical substance which crystallizes in more than one structure (called polymorphism or polymorphic modifications). Two types of polymorphic transitions may be differentiated. Enantiotropic transitions are reversible; when the substance is heated it transforms to the structure stable at high temperature but reverts to the original form on cooling. Monotropic transitions proceed in only one direction from a state metastable over the entire temperature range at a given pressure to a stable state. The transitions in LnOF are enantiotropic.

Solid state transitions may be classified in a number of ways. In a thermodynamic sense transitions may be of first-, second-, or higher order. A first-order transition is one for which there is a discontinuous change in energy and in all physical properties. These transitions are governed by the Gibbs phase rule. First-order transitions include normal polymorphic transformations and phase changes, such as melting, with which are associated a latent heat, a volume change and an entropy change. Transitions of the second order involve a discontinuity in the first derivative of the energy, <u>i.e.</u>, specific heat, but not in the energy, volume or entropy. Both ferromagnetic and order-disorder transitions in alloys are typical second order transitions,

often called λ points. Another characteristic of λ points is that the transition is spread over a large temperature interval up to the λ point where it ceases sharply.

Classification of the rhombohedral-cubic transitions in the oxide-fluorides on a thermodynamic basis is not clear-If order-disorder of anions is accepted then a secondorder transition is predicted. However, the transitions in question: appear to have volume changes of less than 1%, occur over a modest temperature range, are somewhat sluggish since the high temperature form may be quenched sometimes, and exhibit a relatively sharp thermal effect suggestive of a latent heat. These characteristics are not general for second-order transitions, but are not unknown. The alloy AuCu, undergoes a second-order transition involving disordering of the atoms. This transition has a latent heat, exhibits a 0.35% volume change which appears discontinuous, and orders so sluggishly that the disordered phase may be This is an example of an order-disorder transformation in which the order decreases gradually up to the critical temperature, but then the still partially-ordered phase rearranges quite abruptly with an associated latent Thus the transitions of the lanthanide oxide fluorides are very similar to a known order-disorder transition. may be questionable whether these transitions are strictly second-order or represent a superposition of first- and second-order processes. Such a possibility seems more likely with the oxide fluoride than with binary alloys. The oxygen and fluorine atoms could be disordering below the transition

without changing the metal structure. At the transition point the metal structure undergoes a distortional transformation which is probably first-order. Superimposed on this transition is the completion of the typically second-order process of anion disordering.

Buerger⁶³ has classified structural transitions on the basis of kinetics and the change of bonding and structure in the following manner. The change in internal energy during a polymorphic transition is essentially the change in bonding energy. The energy absorbed in a transformation during heating implies a reduction of net bonding. This reduction may occur by a decrease in interaction between first-nearest neighbors, second-nearest neighbors, or both. The kinetics of the transitions depend on the bonds disturbed and the intermediate configuration. Thus Buerger's classification of transformations are:

I Transformations of first coordination

Dilational (rapid)

Reconstructive (sluggish)

II Transformations of secondary coordination

Displacive (rapid)

Reconstructive (sluggish)

III Transformations of disorder

Rotational (rapid)

Substitutional (sluggish)

IV Transformation of bond type (usually sluggish)

How does the LnOF rhombohedral-cubic transtion fit into this categorization? If the conclusions of the preceding thermodynamic discussion are accepted the transformation should be considered as two superimposed processes, anion order-disorder and structural reorganization. Consider these processes with respect to the changes in first coordination of the metal. Four fluorine and four oxygen atoms are the nearest neighbors of the metals in both low and high temperature structures. At low temperature atoms of one type are ordered on one side of the coordination sphere and at different distances from the metal than the other anions. At high temperature the anions are disordered and at equal distances from the metal. The change in first coordination requires the breaking and making of bonds(a reconstruction process) and perhaps the transformation should be considered under that category. However, this change for LnOF is more appropriately classed as a transformation of disorder which is substitutional. For either category the transformation is expected to be sluggish. The disorder transformation will be discussed later in this section.

In both the high and low temperature modifications eight other metal atoms are the next nearest neighbors. The low temperature secondary coordination is a rhombohedral distortion of the high temperature arrangement. No breaking of bonds is required in the transformation between these arrangements and so the change should be regarded as displacive. Such transitions are usually rapid. Buerger

indicated a number of properties for this type of transformation. The high temperature form is always more open and thus has a larger molecular volume. It also has a larger heat capacity and entropy since the atoms in the open form are held in position with less force and are more capable of absorbing thermal energy. The low temperature form will have a lower symmetry and will in fact be a subgroup of the high temperature form. (The structures are sometimes referred to as derivative and basic structures.) As a consequence of this latter property the down-temperature modifications invariably produce twins. A transition of this type may occur in ScOF for which only twinned single crystals were obtained.⁵⁷

Disorder transformations are very similar to displacive ones and their speeds may vary from sluggish to rapid. In the substitutional disorder transformation of B' and B" among fixed A atoms the B' and B" become statistically equivalent. Again the symmetry of the low temperature phase is a subgroup of that of the high temperature one. Generally the volume is greater for the high temperature form due to the juxtaposition of identical atoms with an increase in repulsive energy. The ordering transformation is often sluggish because of the low probability that atoms will interchange locations to produce the ordered configuration rather than another disordered configuration.

I have suggested for the rhombohedral-cubic LnOF transitions the substitutional disorder and displacive secondary

coordination categories of Buerger's classification. Which more appropriately describes the transitions? Undoubtedly each applies to some degree. Both predict a larger volume and higher symmetry for the high temperature phase, as observed. With respect to speed of transitions the displacive transformation should be very fast while order-disorder is slower, particularly in the ordering process. The present transitions are relatively fast but some are sluggish enough to permit quenching of the disordered phase. In this latter respect the ordering of the anions must be the predominant criterion. Thus I conclude that both of the categories are useful for the description of these transitions.

The transition temperatures for the rhombohedral-cubic transitions increase in general with increasing atomic number, GdOF being a noticeable exception. The temperature trend should be related to the type of transition, If disorder is the important factor, migration of the ions to new sites should be considered. The fact that anions apparently occupy the large interstitial sites in tetragonal $\text{LnO}_{1-x}F_{1+2x}$ suggests that they can migrate through these holes. The ability of anions to diffuse should determine the temperature of the transition. It is reasonable to expect that the electrostatic attraction of the cation for the anion is an important energy consideration in this process, since it prevents the anion from leaving its site. In addition, the repulsive effect of the three anions which the migrating anion must pass also retards migration. As the atomic number

increases and cell size decreases the anions become more tightly packed. Qualitatively this decreases the hole size between anions making passage of the migrating ion more difficult. In other words, the repulsive force increases with increasing Z. Both the attractive and repulsive forces which are hindrances to anion migration increase with decreasing cation size. Thus the temperature of transition is expected to increase also. Unfortunately no explanation can be offered for the anomalous value obtained for gadolinium oxide fluoride.

Observations on the Tetragonal Phases, $LnO_{1-x}F_{1+2x}$

The tetragonal $\operatorname{LnO}_{1-x}F_{1+2x}$ has been observed in this study as a single component only for values of x greater than 0.1. This observation is contrary to previously reported results in which the pure phase was also observed for x=0.0 to 0.1. The structural data presented in Table XII for $\operatorname{LnO}_{1-x}F_{1+2x}$ have some interesting aspects. Immediately obvious is the change of cell volume with atomic number. Of greater interest is the variation of the c/a ratio which has two distinct value ranges, about 1.43 for lanthanum and neodymium and 1.39 for gadolinium to erbium. Recall that the ratio is expected to be 1.414 for the tetragonal cell derived from the fluorite arrangement.

How can this variation be explained on the basis of the tetragonal structure given by Zachariasen? In his structure the oxygen and fluorine atoms are ordered in layers normal to the c-axis. Because the oxygen atoms are effectively larger than fluorine atoms it might be expected that the alternating oxygen and fluorine layers would pack more tightly than oxygens within the layer. That is, c/ashould be less than 1.414 Å. However, this argument assumes anion-anion contact along both the [110] and [001] directions. The condition in fluorite structures for this anion contact is that the cation to anion radius ratio be less than about 0.73. Above this value the cation will be in contact with the eight surrounding anions preventing complete anion contact. Using the cation radii given by Templeton and Dauben⁵¹ and an anion radius equal 1.38 Å, calculated radius ratios are 0.769, 0.721, 0.680 and 0.638 respectively for La, Nd, Gd and Er. On this basis complete anion-anion contact is expected only for lanthanides smaller than neodymium. For the oxyfluorides Gd through Er, anion contact must be the determining factor since anion-anion distances are less than 2.81 and 2.77 Å along [110] and [001], respectively. For this condition the argument has been made above that the c/a ratio should be less than 1.414, which is as observed. In the case of the phases of La through Nd, anion contact is effective only in the oxygen layer, and the larger lanthanide ion separates the oxygen from the fluorine layers. In the lanthanum phase the anion-anion distances along [110], the distance of closest approach, are 2.90 Å, while along [001] they are 2.92 A. To summarize, because of the nature of the layered structure, as cation size decreases, shrinkage is less within the oxygen layer than between

the alternate oxygen and fluorine layers. Thus the c/a ratio changes markedly as Z increases.

The addition of excess fluoride ions, half of which go into interstitial sites and half of which replace oxygens, should have little effect on packing. Only a slight change in the c/a ratio is observed except in the case of erbium. Recall, however, that the diffraction patterns of the erbium phases contained extra lines.

A calculation of the size of the interstitial holes in $LnO_{1-x}F_{1+2x}$ was made using the distances between symmetrically opposite anions. For the lanthanum case this value is $4.85 \stackrel{\text{O}}{\text{A}}$ and for erbium $4.74 \stackrel{\text{O}}{\text{A}}$. Assuming that this distance is equal to four anion radii, then the average radius is about 1.2 A. This is much smaller than the normal fluoride and oxide radii and the assumption of anions in the interstitial sites would appear doubtful. However, it has been established that in solid solutions of YF3 in CaF2 (up to 55 mole per cent) anions are in the interstices and cation vacancies are insignificant 64. The size of these interstitial holes is of the same order of magnitude as those found in $LnO_{1-x}F_{1+2x}$. Apparently the anions are considerably distorted in both cases. In $LnO_{1-x}F_{1+2x}$ the stability of the tetragonal phase is expected to decrease with increasing atomic number because of the decreasing size of the interstice.

No tetragonal-cubic transition was observed in the temperature range of this study. Although a transition may

take place at higher temperatures, it is somewhat surprising that none was observed below 800° . The ions are mobile at these temperatures making disordering very likely. Perhaps a tetragonal-cubic transition is not favored because of a required decrease in volume. The molecular volume for tetragonal LaOF reported by Zachariasen. Was 48.55 $^{\circ}$ and that for cubic LaOF 45 was 47.68 $^{\circ}$. Although not impossible such a transition with volume decrease seems improbable, particularly for a disordering process. For molecular volumes in general it is very curious that the values deduced from the literature for cubic oxide fluorides are less than the corresponding rhombohedral volumes. In this study the opposite has been observed. Either the reports of cubic parameters are in error or they represent an ordered structure, such as F43m, which could have a smaller volume.

IX. SUGGESTIONS FOR FURTHER WORK

Knowledge of the La₂(CO₃)₃·8H₂O crystal structure serves as an aid in interpretation of lanthanide carbonate chemistry. However, a complete understanding of these carbonate systems will not be possible until all the related structures are known. The structures of both a $\operatorname{Ln_2(CO_3)_3 \cdot 2H_2O}$ phase and $\operatorname{Lu_2(CO_3)_3:5H_2O}$ should be determined if suitable single crystals can be prepared. The coordination number of the metal of these phases would be of great interest in light of the unusual coordination polyhedra in the lanthanum compound. Obviously the structure of the available $Nd_2(CO_3)_3 \cdot XH_2O$ crystals should be studied. Hopefully these crystals would exemplify the dihydrate. The possibility of obtaining single crystals of the anhydrous carbonates or oxycarbonates seems improbable. However, knowledge of their structures is required for complete interpretation of the interrelationships in the lanthanide carbonate systems.

The lanthanide-oxide-fluoride systems offer a number of interesting projects for further research. A neutron diffraction study of the rhombohedral and cubic LnOF phases should allow the verification of the anion positions presumed in the present work. An investigation of the high temperature decomposition of the rhombohedral phases by mass spectrometry would be profitable. The tetragonal $\text{LnO}_{1-x}F_{1+2x}$ phases offer several projects of interest. It is probable that complex crystal structures exist in some of these phases

and perhaps single crystal structure determinations could be undertaken. The possibility of transitions in these phases at high temperature also should be investigated more completely. Finally a study of the probable phase transition in ScOF would be very instructive with respect to the examination of order-disorder processes.

REFERENCES

- T. Moeller and E. P. Horwitz, J. Inorg. Nucl. Chem., <u>12</u>, 49 (1959).
- 2. L. Gordon, R. A. Brandt, L. L. Quill and M. Salutsky, Anal. Chem., 23, 1811 (1951).
- 3. Sr. M. Clarus Strouth, "Thermal Decomposition of Yttrium, Scandium, and Heavy Lanthanon Oxalates and Carbonates,"
 Thesis, Michigan State University, 1962.
- 4. M. L. Salutsky and L. L. Quill, J. Am. Chem. Soc., 72, 3306 (1950).
- 5. R. G. Charles, J. Inorg. Nucl. Chem., 27, 1489 (1965).
- 6. E. L. Head and C. E. Holley, Jr., "Rare Earth Research III," Gordon and Breach, New York, 1964, p. 51.
- 7. E. L. Head and C. E. Holley, Jr., "Rare Earth Research IV," Gordon and Breach, New York, 1965, p. 707.
- 8. R. L. N. Sastry, S. R. Yoganarisimhan, P. N. Mehrotra and C. N. R. Rao, J. Inorg. Nucl. Chem., 28, 1165 (1966).
- 9. E. L. Head, "Rare Earth Research VI," Gordon and Breach, New York, 1967, p. 366.
- 10. G. Pannetier, J. Nataf and A. Dereigne, Bull. Soc. Chim. Fr., 5, 318 (1965).
- 11. P. Caro and L. Eyring, personal communication.
- 12. S. D. Ross and J. Goldsmith, Spectrochim. Acta, 20, 781 (1964).
- J. Fujita, A. E. Martell and K. Nakamoto, J. Chem. Phys., 36, 339 (1962).
- 14. J. C. Barnes and H. Pincott, J. Chem. Soc., 1966, 842.
- 15. H. Brasseur, Bull. Soc. Roy. Sci. Liege, 18, 137 (1949).
- 16. D. Palache, H. Berman and C. Frondel, "Dana's System of Mineralogy", Vol II, 7th ed., John Wiley and Sons, New York (1944), p. 241.
- 17. H. E. Swanson and E. Tatge, Nat. Bur. Std. (U.S.), Circ. 539, Vol. I, p. 66.

- 18. R. E. Vogel and C. P. Kempter, Acta Cryst., <u>14</u>, 1130 (1961).
- 19. P. Coppens, L. Leiserowitz and D. Rabinovich, <u>ibid.</u>, <u>18</u>, 1035 (1965).
- 20. W. R. Busing and H. A. Levy, ibid., 10, 180 (1957).
- 21. D. T. Cromer and J. T. Waber, ibid., 18, 104 (1965).
- 22. M. Tokonami, ibid., 19, 486 (1965).
- 23. D. T. Cromer, ibid., 18, 17 (1965).
- 24. H. Lipson and W. Cochran, "The Determination of Crystal Structures", Vol. III in "The Crystalline State," L. Bragg, Ed., G. Bell and Sons Ltd., London, (1953), p. 207.
- 25. H. A. Levy, Acta Cryst., 9, 679 (1956).
- 26. P. Werner, Acta Chem. Scand., 18, 1851 (1964).
- 27. R. C. Srivistava and E. C. Lingafelter, Acta Cryst., 20, 918 (1966).
- 28. E. B. Hunt, Jr., R. E. Rundle and A. J. Stosick, <u>ibid.</u>, 7, 106 (1954).
- 29. F. Carter, "Rare Earth Research VI," Gordon and Breach, New York, 1967, p. 187.
- 30. J. L. Hoard, B. Lee, and M. D. Lind, J. Am. Chem. Soc., 87, 1612 (1965).
- 31. M. D. Lind, B. Lee and J. L. Hoard, ibid., 87, 1611 (1965).
- 32. E. L. Muetterties and C. M. Wright, Quart. Rev., <u>21</u>, 109 (1967).
- 33. L. Helmholz, J. Am. Chem. Soc., <u>61</u>, 1544 (1939).
- 34. R. Wang, R. Bodnar and H. Steinfink, Inorg. Chem., <u>5</u>, 1468 (1966).
- 35. A. Zalkin, J. D. Forrester and D. H. Templeton, J. Chem. Phys., 39, 2881 (1963).
- 36. I. Jelenic, D. Grdenic and A. Bezjak, Acta Cryst., 17, 758 (1964).
- 37. E. L. Muetterties, J. Am. Chem. Soc., <u>88</u>, 305 (1966).
- 38. I. I. Chernyaev, V. A. Golovnya and A. K. Molodkin, J. Inorg. Chem. (U.S.S.R.), 3, 100 (1958).

- 39. M. C. Steele, Austral. J. Chem., 10, 367 (1957).
- 40. J. L. Hoard and J. V. Silverton, Inorg. Chem., $\underline{2}$, 235 (1963).
- 41. T. Ueki, A. Zalkin and D. H. Templeton, Acta Cryst., 20, 836 (1966).
- 42. C. J. Brown, ibid., 2, 167 (1949).
- 43. F. E. Wickman, Arkiv Mineral. Geol., 1, 95 (1949).
- 44. R. L. Sass, R. Vidale and J. Donahue, Acta Cryst., 10, 567 (1957).
- 45. W. Klemm and H. A. Klein, Z. Anorg. Allgem. Chem., 248, 167 (1941).
- 46. W. H. Zachariasen, Acta Cryst., 4, 231 (1951).
- 47. F. Hund, Z. Anorg. Allgem. Chem., 265, 62 (1951).
- 48. F. Hund, <u>ibid</u>., <u>273</u>, 312 (1953).
- 49. L. Mazza and A. Iandelli, Atti accad. ligure sci. e lettere, 7, 44(1951); C. A., 47, 4194 (1953).
- 50. A. Zalkin and D. H. Templeton, J. Am. Chem. Soc., <u>75</u>, 2453 (1953).
- 51. D. H. Templeton and C. H. Dauben, ibid., 76, 5237 (1954).
- 52. A. I. Popov and G. E. Knudsen, ibid., p 3921.
- 53. N. C. Baenziger, J. R. Holden, G. E. Knudsen and A. I. Popov, <u>ibid</u>., p 4734.
- 54. K. S. Vorres and R. Riviello in "Rare Earth Research IV," Gordon and Breach, New York, 1964, p. 521.
- 55. L. R. Batsanova and G. N. Kustova, Russ. J. Inorg. Chem. (Eng. Transl.), 9, 181 (1964).
- 56. N. V. Podberezskaya, L. R. Batsanova and L. S. Egorova, J. Struct. Chem., (U.S.S.R.)(Engl. Transl.), 6, 815 (1965).
- 57. B. Holmberg, Acta Chem. Scand., 20, 1082 (1966).
- 58. F. Kutek, Russ. J. Inorg. Chem. (Eng. Transl.), 9, 1499 (1964).
- 59. H. E. Swanson and E. Tatge, Nat. Bur. Std. (U.S.), Circ. <u>539</u>, Vol. I, p. 31.

- 60. D. K. Smith, Norelco Reptr., 10, 19 (1963).
- 61. W. J. Campbell, U.S. Bur. Mines, Inform. Circ., 8107, (1962).
- 62. A. J. Majumdar and R. Roy, J. Phys. Chem., <u>69</u>, **1684** (1965).
- 63. M. J. Buerger, "Crystallographic Aspects of Phase Transformations," in "Phase Transformations in Solids," R. Smoluchowski, J. E. Mayer and W. A. Weyl, Eds., John Wiley and Sons, New York, 1951, p. 183.
- 64. J. M. Short and R. Roy, J. Phys. Chem., 67, 1860 (1963).
- 65. H. Lipson and W. Cochran, "The Determination of Crystal Structures," Vol. III in "The Crystalline State," L. Bragg, Ed., Cornell University Press, Ithaca, New York, 1966, p. 340.
- 66. J. S. Rollett, Ed., "Computing Methods in Crystallography," Pergamon Press, Oxford, (1965).
- 67. R. A. Sparks, R. J. Prosen, F. H. Kruse and K. N. Trueblood, Acta Cryst., 9, 350 (1956).

APPENDICES

APPENDIX I

Crystallographic Computer Programs

A. A. Zalkin's Incor Program

This program reduces raw intensities for input to the fourier or least-squares programs. Input parameters define the system under study. Goniostat or Weissenberg data are corrected for Lorentz and polarization or Lorentz, polarization and velocity effects respectively, after the computation of $\sin^2\theta$ and $\sin\theta/\lambda$ for each reflection from reciprocal lattice relations. The reciprocal of the Lorentz-polarization factor is calculated from,

$$1/LP = 2 \sin \theta \cos \theta/(1 + \cos^2 2\theta)$$

and the velocity correction from

$$V = (1 - (h\lambda/2a \sin \theta)^2]^{1/2}/(\sin \theta)$$

where a is the axis and h the corresponding index. Provisions are also available to scale the data and correct for \mathbf{K}_{α_1} and \mathbf{K}_{α_2} splitting in spectrometric data. The absolute value of the structure factor, \mathbf{F} , is calculated as the square root of the corrected intensity, $\left|\mathbf{F}\right|^2$.

B. Zalkin's Least-Squares Program

The method of least-squares is used to minimize with respect to atomic position, temperature parameters and over-all scale factor the function:

$$R = \sum_{h} w_{h} (|F_{0}|_{h} - 1/K |F_{c}|_{h})^{2} = \sum_{h} w_{h} (del)^{2}$$

where h is the index $hk\ell$, w_h is the weight of the observation, $|F_0|_h$ is the observed structure factor, $|F_c|_h$ the theoretical structure factor and 1/K is the scale factor. Discussions of the method appear in references 65-67. It may be shown that the s linear weighted observational equations of the form;

$$\sqrt{w}_{i} \sum_{j=1}^{m} a_{ij} p_{j} = \sqrt{w}_{i} g_{i},$$

which relate the m parameters p_j to the observation g_i , and w_i is the weight, may be reduced to m normal equations of the form;

It is common to express the observational and normal equations in matrix form as $\underline{A} \ \underline{P} = \underline{G}$ and $\underline{A}^T \underline{A} \ \underline{P} = \underline{A}^T \ \underline{G}$ respectively where the matrix $\underline{A}^T \underline{A}$ is symmetric and positive. The solution of the normal equations minimizes the $(\underline{G} - \underline{A} \ \underline{P})^T$ $(\underline{G} - \underline{A} \ \underline{P})$, the sum of squares of residuals.

The structure factor $|F_c|_h$ depends on parameters non-linearly. However, if an approximation of the parameters is known, linear observational equations may be formed of the type,

$$\sum_{j=1}^{m} \sqrt{w_{i}} \frac{d(|\mathbf{F}_{c}|_{h}/K)}{dp_{j}} \Delta p_{j} = \sqrt{w_{i}} (|\mathbf{F}_{0}|_{h} - 1/K|\mathbf{F}_{c}|_{h})$$

where Δp_j are the corrections to the parameters and may be represented by $\underline{A} \ \underline{P} = \underline{B}$. The normal equations are $\underline{A}^T \underline{A} \ \underline{P} = \underline{A}^T \underline{B}$ where element $(A^T A)_{jj}$, is

$$\sum_{h} w_{h} \frac{d|F_{c}|_{h}}{dp_{j}} \frac{d|F_{c}|_{h}}{dp_{j}}$$

and element $(A^TB)_{j}$ is

$$\sum_{h} w_{h}(K|F_{0}|_{h} - |F_{c}|_{h}) \frac{d|F_{c}|_{h}}{P_{j}}.$$

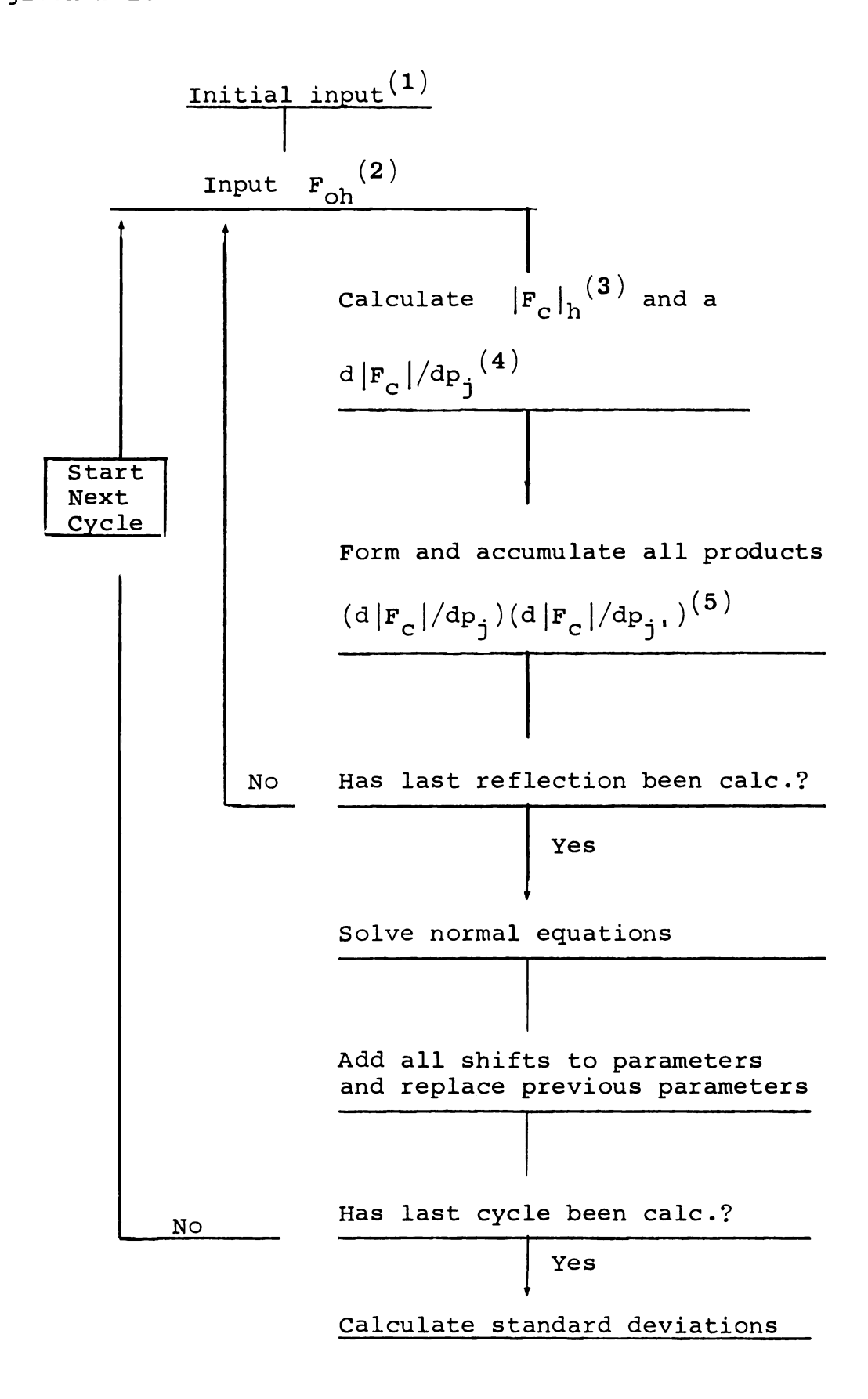
Solution to the normal equations for the corrections gives improved values for the parameters. More than one iteration is usually necessary since the initial observational equations are approximate. The standard deviations of the parameters are given by

$$\sigma^{2}(p_{j}) = N_{jj} \sum_{i=1}^{s} \frac{w_{i} \Delta_{i}^{2}}{s - m}$$

where N_{jj} is jth diagonal element of the matrix $(\underline{A}^T\underline{A})^{-1}$ and \triangle_i is $(K|F_0|_h - |F_c|_h)_i$.

	1	

A general flow chart for Zalkin's Least-Squares routine is given below.



- (1) Initial input data: Includes unit cell parameters, atomic scattering factors, equivalent positions of space group and parameters of atoms to be refined.
- (2) $|\mathbf{F_0}|_{\mathbf{h}}$; h,k, ℓ , $|\mathbf{F_0}|$, $1/\mathbf{w}$, and $\sin \theta/\lambda$.
- (3) $|\mathbf{F}_{c}|_{h} = \sqrt{\mathbf{A}_{h}^{2} + \mathbf{B}_{h}^{2}}$ where $\mathbf{A}_{h} = \sum_{i=1}^{m} \mathbf{f}_{i} e^{-\mathbf{T}_{i}} \cos 2\pi (\mathbf{h} \cdot \mathbf{r}_{i})$ and $\mathbf{B}_{h} = \sum_{i=1}^{m} \mathbf{f}_{i} e^{-\mathbf{T}_{i}} \sin 2\pi (\mathbf{h} \cdot \mathbf{r}_{i})$

where $T_i = h^2(b_{11})_i + k^2(b_{22})_i + \ell^2(b_{33})_i + 2hk(b_{12})_i + 2h\ell(b_{13})_i + 2k\ell(b_{23})_i$ or $= Bsin^2 \theta/\lambda^2$, m = total number of atoms per unit cell, $r_i = position of atom i$, $f_i = scattering factor of atom i$.

- $\begin{array}{lll} (4) & \text{d} \left| \mathbf{F_{C}} \right|_{h} / \text{d} (\mathbf{1} / \mathbf{K}) &= \left. \mathbf{w} \left| \mathbf{F_{C}} \right|_{h} \\ \\ & \text{d} \left| \mathbf{F_{C}} \right|_{h} / \text{d} \mathbf{p_{i}} &= \mathbf{w} \left. \left(\frac{\mathbf{A_{h}}}{\left| \mathbf{F_{C}} \right|_{h}} \right. \left. \frac{\text{d} \mathbf{A_{h}}}{\text{d} \mathbf{p_{i}}} \right. + \left. \frac{\mathbf{B_{h}}}{\left| \mathbf{F_{C}} \right|_{h}} \right. \left. \frac{\text{d} \mathbf{B_{h}}}{\text{d} \mathbf{p_{i}}} \right. \right\} \\ \\ & \text{the (NPAR + 1) term = } \mathbf{w} (\left| \mathbf{F_{0}} \right| 1 / \mathbf{K} \left| \mathbf{F_{C}} \right|) = \mathbf{w} (\text{del}) . \end{array}$
- (5) Terms of normal equations.

$$A(II JJ) = \sum_{i=1}^{s} (Deriv)_{j} (Deriv)_{j}$$

form lower triangular matrix of order (NPAR + 1)

$$A(1 \quad 1) = \sum w |F_C|^2$$

$$A\left[\frac{(NPAR + 1)(NPAR + 2)}{2}\right] = \sum_{i} w \operatorname{del}_{i}^{2}$$

APPENDIX II

 $X ext{-Ray Powder Diffraction Data}$

Table XVI. X-Ray powder diffraction data for NdO $_{.73}$ F $_{1.54}$

No.	hk <i>ℓ</i>	d calcd*	d obs	I/I ₀
1	001	5.720		_
2	101	3.286	3.283	100
3	002	2.860	2.858	20
4	110	2.838	2.835	3 5
5	111	2.543	2.545	1
6	102	2.322	2.328	7
7	-		2.228	1
8	112	2.015	2.012	66
9	200	2.007	1.998	15
10	003	1.907	1.904	1
11	201	1.894		_
12	103	1.722	1.717	24
13	211	1.713	1.709	13
14	202	1.643	1.645	
1 5	_		1.636	5
16	113	1.583	1.582	5 5 2 2
17	212	1.520	1.520	$\overline{2}$
18	004	1.430	1.429	$\overline{2}$
19	220	1.419	1.417	2 5
20	203	1.382	1.382	1
21	221	1.377		_
22	104	1.347	1.346	2
23	213	1.307	1.307	7
24	301	1.303	1.304	
25	_		1.296	9 2 3 4
26	114	1.277	1.276	3
27	222	1.271	1.270	4
28	310	1.269	1.266	1
29	311	1.239		
30	302	1.212		-
31	204	1.165	1.164	2
32	312	1.160	1.161	7
33	005	1.144		_ `
34	223	1.138	1.137	1
3 5	214	1.119	1.118	2
3 6	320	1.113	1.113	1
3 7	105	1.100,		
38	303	1.095	1.098	2
3 9	303 321	1.093	1.093	3

^{*}a = 4.014 Å and c = 5.720 Å.

Table XVII. X-Ray powder diffraction data for NdO $_{.85}F_{1.3}^{**}$

No.	hk ℓ	d calcd*	d obs	I/I _o
1	001	5.704		-
	101	3.275	3.270	100
2 3	002	2.852	2.848	13
4	110	2.828	2.824	22
5	111	2.534	2.529	2
6	102	2.322	2.320	5
7	112	2.008	2.005	41
8	200	2.000	1.996	18
9	003	1.901	1.899	2
10	201	1.887	1.886	1
11	103	1.717	1.717	13
12	211	1.707	1.705	24
13	202	1.637	1.635	5
14	113	1.578	1.577	2
15	212	1.515	1.513	2
16	004	1.426	1.425	1
17	220	1.414	1.412	4
18	203	1.378	1.377	2
19	221	1.373		_
20	104	1.343	1.342	2
21	213	1.303	1.302	6
22	301	1.298	1.296	4
23	114	1.273	1.272	1
24	222	1.267	1.266	1 3
25	310	1.265	1.262	3
26	311	1.235		-
27	302	1.208		***
28	204	1.161	1.160	2
29	312	1.156	1.156	5
30	005	1.141		_
31	223	1.135		-
32	214	1.115	1.115	2
33	321	1.089	1.088	5

^{*} a = 3.999 Å and c = 5.704 Å.

^{**}Stoichiometry approximate.

Table XVIII. X-Ray diffraction powder diffraction data for $$\tt GdO_{.72}F_{1.58}$$

No.	hk ℓ	d calcd*	d obs	I/I ₀
1	001	5.528	5.529	5
2	-		3.900	1
3	101	3.228	3.228	100
4	110	2.812	2.810	25
5	002	2.764	2.764	_
6	111	2.506	2.512	1
7	102	2.270	2.269	12
8	200	1.988	1.987	21
9	112	1.971	1.972	37
10	201	1.871	1.870	4
11	003	1.843	1.843	2
12	_		1.769	2 1
13	211	1.693	1.693	20
14	103	1.672	1.672	14
15	202	1.614	1.613	7
16	113	1.541	1.542	5
17	212	1.496	1.496	$\tilde{2}$
18	220	1.406	1.406	$\overline{2}$
19	004	1.382	1.382	5 2 2 3
20	221	1.363		
21	203	1.352	1.352	1
22	104	1.305	1.305	$ar{2}$
23	301	1.289	1.209	- 1 2 2 4
23 24	213	1.280	1.280	4
25 25	310	1.258	1.257	$\dot{\hat{2}}$
26	222	1.253	1.253	1
20 27	114	1.240	1.240	i
28	311	1.226	1.210	_
28 29	302	1.195	1.196	1
	312	1.145	1.146	5
30 31	204	1.135	1.135	5 2
31 32	204 223	1.118	1.100	_
32 33	005	1.116		-
				-
34	320	1.103	1.091	4
3 5	214	1.091	1.091	4

^{*}a = 3.977 Å and c = 5.528 Å.

Table XIX. X-Ray powder diffraction data for DyO .77F1.46

No.	hk 🛭	d calcd*	d obs	I/I ₀
1	001	5.451		-
2	101	3.190	3.191	100
3	110	2.781	2.782	27
3 4 5 6	002	2.726	2.727	9
5	111	2.477	2.479	1
	102	2.240	2.242	13
7	200	1.966	1.967	20
8	112	1.947	1.948	32
9	201	1.850	1.851	2
10	003	1.817	1.818	5
11	211	1.674	1.675	24
12	103	1.650	1.650	13
13	202	1.595	1.595	8
14	113	1.521	1.522	5
15	212	1.478	1.479	
16	220	1.391	1.391	4 4 1 1 1 5 4 7
17	004	1.363	1.364	1
18	221	1.347	1.348	1
19	203	1.335	1.33 5	1
20	104	1.288	1.288	5
21	301	1.275	1.275	4
22	213	1.264	1.265	7
23	310	1.244	1.245	2
24	222	1.239		_
25	114	1.224	1.226	- 1
26	311	1.213		
27	302	1.181		_
28	312	1.132	1.132	6
29	204	1.120	1.120	2

^{*}a = 3.933 Å and c = 5.451 Å.

		}
		'
		(
		;
		•

Table XX. X-Ray powder diffraction data for ErO $_{.85}F_{1.3}^{**}$

No.	hkℓ	d calcd*	d obs	I/I _o
1	001	5.400	5.405	5
2	-		3.834	2
3	101	3.158	3.161	100
4	110	2.753	2.753	26
5	002	2.700	2.701	9
6	111	2.453	2.454	1
7	102	2.219	2.218	13
8	_		2.180	1
9	200	1.947	1.950	19
10	112	1.928	1.928	27
11	201	1.831	1.832	2
12	003	1.800	1.800	2 2 1 2 22
13	-		1.787	1
14	-		1.734	2
15	211	1.657	1.657	22
16	103	1.634	1.634	10
17	202	1.580	1.579	7
18	113	1.507	1.506	7
19	212	1.463	1.463	7 1 2 1 1 2 3 4 3 2 2
20	220	1.377	1.37 5	2
21	004	1.350	1.349	1
22	221	1.334	1.336	1
23	203	1.322	1.322	2
24	104	1.276	1.276	3
25	301	1.262	1.262	4
26	213	1.251	1.251	3
27	310	1.231	1.230	2
28	222	1.226	1.225	2
29	114	1.212	1.212	1
30	311	1.200		_
31	302	1.170	1.170	1
32	312	1.120	1.120	3
33	204	1.109	1.110	1 3 1
34	223	1.093		_
35	005	1.080	1 000	4
36	320	1.080	1.080	1
37	214	1.067	1.067	3
38	321	1.059	1.060	2

^{*} a = 3.893 Å and c = 5.400 Å.

^{**}Stochiometry approximate.

Table XXI. X-Ray powder diffraction data for ErO.80F1.40

126

No.	hkℓ	d calcd*	d obs	I/I ₀
1	001	5 .3 85	5.385	8
2 3	-		3.818	8 2 1
3	_		3.754	1
4	101	3.162	3.163	100
5	110	2.762	2.764	22
5 6	002	2.692	2.694	15
7	_		2.515	
8	111	2.458	2.461	1 1 1
9	-		2.360	
10	102	2.217	2.218	13
11	_		2.161	1
12	200	1.953	1.954	18
13	112	1.928	1.928	30
14	201	1.836	1. 9 38	
15	003	1.795	1.795	2
16	003	1.795	1.775	1 3 2 2
	-			2
17	011	1 660	1.737	20
18	211	1.662	1.662	
19	103	1.631	1.631	12
20	202	1.581	1.581	7 1
21	-	1 505	1.519	Ţ
22	113	1.505	1.504	5
23	212	1.466	1.466	1
24	_		1.423	Ţ
25	220	1.381	1.382	5
26	004	1.346	1.346	1
27	221	1.338	1.340	2
28	203	1.322	1.322	2
29	104	1.273	1.273	3
3 0	301	1.266	1.265	2
31	213	1.252	1.252	3
32	31 0	1.235	1.235	5 1 1 5 1 2 2 3 1 2 1
33	222	1.229	1.230	2
34	114	1.210	1.210	1
3 5	311	1.204		_
36	302	1.172		-
37	312	1.123	1.123	2 1
38	204	1.108	1.109	1
39	223	1.095		_
40	005	1.077		_
41	214	1.066	1.067	2
42	321	1.062	1.063	$\frac{1}{2}$
				_

^{*}a = 3.907 Å and c = 5.385 Å.

Table XXII. X-Ray powder diffraction data for LaOF and NdOF

		LaOF			NdOF	
hk ℓ	d calcd*	d obs	I/I_0	d calcd*	d obs	I/I_0
111	6.737		_	6.567		_
100	3.456		-	3.373		_
222	3.368	3.3 65	34	3.283	3.274	36
110	3.314	3.316	100	3.234	4.234	100
211	2.882	2.883	34	2.811	2.810	36
221	2.650	2.650	3	2.584	2.583	3
333	2.246	2.246	2	2.189	2.187	3
322	2.229	2.230	4	2.174	2.174	4
332	2.050	2.051	37	1.999	1.997	32
$10\overline{1}$	2.026	2.026	38	1.976	1.978	3 5
210	1.940	1.941	1	1.893		_
433	1.751	1.751	13	1.708	1.706	11
111	1.748			1.705	_,,,,,,,,,,,,,,,,,,,,,,,,,,,,,,,,,,,,,,	
321	1.736	1.735	27	1.693	1.694	26
200	1.728	1.730	20	1.686	1.689	25
444	1.684	1.684	1	1.641	1.642	2
220	1.657	1.657	6	1.617	1.618	6
443	1.628	1.628	2	1.587	1.587	2
311	1.609		-	1.570		-
432	1.504	1.505	3	1.467	1.466	3
331	1.499	1.501	3	1.462		_
422	1.441	1.441	6	1.405	1.405	8
544	1.421	1.423	1	1.386	1.386	
555	1.347	i.349	1	1.313	1.313	1
554	1.335	1.334	2	1.302	1.301	2
442	1.325	1.324	4	1.292	1.291	2
$20\overline{1}$	1.323		-	1.291		_
211	1.315	1.315	9	1.283	1.284	

^{*} $a = 7.132 \text{ Å} \text{ and } \alpha = 33.01^{\circ}.$

^{**} a = 6.953 Å and α = 33.04° .

Table XXIII. X-Ray powder diffraction data for SmOF and EuOF SmOF EuOF

hk L	d calcd*	d obs	I/I_{0}	\mathtt{d} calcd *	* d obs	I/I_0
111	6.483		_	6.450		_
100	3.334		_	3.312		_
222	3.242	3.247	31	3.225	3.228	32
110	3.196	3.201	100	3.176	3.182	100
211	2.777	2.782	40	2.761	2.764	3 5
221	2.553	2.556	3	2.538	2.538	4
333	2.161	2.163	3	2.150	2.151	4
322	2.147	2.151	5	2.135	2.136	6
332	1.974	1.976	31	1.963	1.964	3 5
$10\overline{1}$	1.954	1.956	38	1.941	1.943	3 9
210	1.870	1.872	1	1.859	1.861	1
433	1.686	1.685	12	1.677	1.677	12
$11\overline{1}$	1.685	1.000		1.675	1.675	7
321	1.673	1.674	25	1.663	1.665	26
200	1.667	1.668	21	1.656	1.659	21
444	1.621	1.623	1	1.612	1.613	1
220	1.598	1.599	6	1.588	1.589	6
443	1.567	1.568	2	1.559	1.559	4
311	1.551	1.551	1	1.542	1.543	2
432	1.449	1.451	2	1.441	1.441	4
331	1.445	1.446	2	1.436	1.435	1
422	1.389	1.386	10	1.380	1.381	7
544	1.368	1.369	1	1.361	1.362	2
555	1.297		-	1.290	1.290	1
554	1.285	1.286	2	1.278	1.279	4
442	1.276	1.281	2	1.268	1.268	2
$20\overline{1}$	1.276	1 070	6	1.268	1.268	2
$21\overline{1}$	1.268	1.272	U	1.260	1.260	7

^{*} a = 6.865 Å and α = 33.07° .

^{**} a = 6.827 Å and α = 33.05°.

Table XXIV. X-Ray powder diffraction data for GdOF and TbOF

GdOF TbOF

hk £	d calcd*	d obs	I/I_0	d calcd*	* d obs	I/Io
111	6.420		-	6.383		_
100	3.299		-	3.276		_
222	3.212	3.210	34	3.192	3.188	31
110	3.163	3.161	100	3.141	3.142	100
211	2.749	2.748	39	2.731	2.731	34
221	2.528	2.527	4	2.511	2.510	2
333	2.141	2.140	3	2.128	2.126	2
322	2.126	2.126	3	2.112	2.113	2
332	1.955	1.954	46	1.943	1.943	31
101	1.933	1.934	37	1.920	1.921	34
210	1.810	1.850	1	1.838	1.841	1
433	1.670	1.671	6	1.659	1.658	10
111	1.668	1.669	12	1.656	1.000	10
321	1.656	1.656	24	1.645	1.645	22
200	1.649	1.649	21	1.638	1.640	20
444	1.606	1.604	1	1.596	1.593	1
220	1.581	1.581	6	1.570	1.572	5
443	1.552	1.551	3	1.542	1.542	2
311	1.535		-	1.525		_
432	1.435	1.435	4	1.425	1.426	3
331	1.430	1.431	3	1.421	1.422	2
422	1.375	1.375	7	1.365	1.366	8
544	1.3 55	1.355	1	1.347	1.347	3
555	1.285	1.286	1	1.277		_
554	1.273	1.273	3	1.265	1.266	2
442	1.264	1.265	3	1.255	1.256	2
$20\overline{1}$	1.263	1.261	1	1.254		_
211	1.255	1.255	9	1.246	1.248	7

^{*}a = 6.800 Å and α = 33.05°.

^{**} a = 6.758 Å and α = 33.02° .

Table XXV. X-Ray powder diffraction data for DyOF and YOF

DyOF YOF

hk ℓ	d calcd*	d obs	I/I _o	d calcd*	* d obs	I/I ₀
111	6.343		_	6.323		-
100	3.261		-	3.265		-
222	3.172	3.166	33	3.162	3.148	25
110	3.126	3.125	100	3.129	3.110	68
211	2.717	2.718	3 9	2.717	2.701	15
221	2.498	2.496	5	2.496	2.482	2
333	2.114	2.120	6	2.108	2.100	2
322	2.101	2.100	11	2.098	2.088	4
332	1.932	1.931	51	1.929	1.918	25
101	1.911	1.911	52	1.914	1.900	28
210	1.830		-	1.832		_
433	1.650	1.651	13	1.646	1.638	7
$11\overline{1}$	1.649	1.646	11	1.651		•
321	1.637	1.636	42	1.637	1.622	15
200	1.631	1.631	36	1.632	1.621	14
444	1.586	1.583	4	1.581	1.574	1
220	1.563	1.564	13	1.564	1.555	3
443	1.533	1.5 32	8	1.530	1.523	1
311	1.518		-	1.519		-
432	1.418	1.418	8	1.417	1.408	2
331	1.414	1.412	4	1.414		_
422	1.359	1.358	16	1.358	1.356	5
544	1.339	1.338	4	1.336	1.330	1
555	1.269	1.271	2	1.265	1.260	1
554	1.257	1.258	2	1.254		_
442	1.249	1.250	10	1.248	4 0 10	
$20\overline{1}$	1.248	1.248	6	1.250	1.249	1
211	1.240	1.240	8	1.242	1.241	1

^{*}a = 6.716 $^{\circ}$ and α = 33.07°.

^{**} a = 6.697 Å and α = 33.20° .

Table XXVI. X-Ray powder diffraction data for HoOF and ErOF HoOF

	HOOF			EIOr		
hk &	d calcd*	d obs	I/I ₀	d calcd*	* d obs	I/I ₀
111	6.278		-	6.258		-
100	3.234		-	3.224		-
222	3.139	3.148	34	3.129	3.139	3 5
110	3.100	3.108	100	3.091	3.097	100
211	2.693	2.704	32	2.685	2.691	36
221	2.475	2.485	3	2.467	2.481	3
333	2.093	2.090	6	2.086	2.094	3
322	2.081	2.030	· ·	2.075	2.080	5
332	1.913	1.920	32	1.907	1.912	32
$10\overline{1}$	1.895	1.901	38	1.890	1.893	36
210	1.814	1.820	1	1.809	1.814	1
111	1.635			1.630		
433	1.634	1.640	9	1.629	1.633	10
321	1.622	1.626	22	1.618	1.620	23
200	1.617	1.622	20	1.612	1.612	21
444	1.570	1.5 7 6	1	1.565	1.570	1
220	1.550	1.555	5	1.545	1.548	5
443	1.518	1.525	1	1.513	1.517	2
311	1.505		-	1.500	1.503	1
432	1.405	1.409	2	1.400	1.404	3
331	1.401		-	1.397	1.401	2
422	1.346	1.351	7	1.342	1.346	7
544	1.326	1.332	2	1.321	1.325	2
555	1.256		-	1.252	1.255	1
554	1.245	1.250	1	1.241	1.244	2
$20\overline{1}$	1.238		_	1.234		_
442	1.237	1.243	2	1.234	1.236	3
$21\overline{1}$	1.230	1.235	6	1.226	1.228	6

^{*} a = 6.647 $^{\circ}$ and α = 33.15°.

^{**} a = 6.628 Å and α = 33.14° .

		1
		:
		•
		1
		•
		1
		1
		1
		`
		1

